PSU-IRL-SCI-455

THE PENNSYLVANIA
STATE UNIVERSITY

IONOSPHERIC RESEARCH

Scientific Report 455

DENSITIES AND TEMPERATURES IN THE POLAR THERMOSPHERE

by
Larry J. Gardner
June 30, 1977

The research reported in this document has been supported by The National Aeronautics and Space Admnistration under Grant No. NGL 39-009-003.

IONOSPHERE RESEARCH LABORATORY

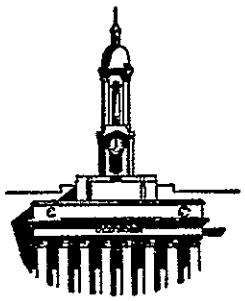

University Park, Pennsylvania

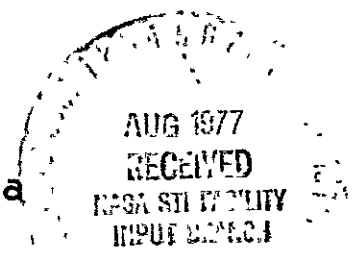

REPORT DOCUMENTATION PAGE		READ INSTRUCTIONS BEFORE COMPLETING FORM
1 REPORT NUMBER 455	2 GOVT ACCESSION NO	3 RECIPIENT'S CATALOG NUMBER
4 TITLE (and Subtitle) Densities and Temperatures in the Polar Thermosphere		5 TYPE OF REPORT & PERIOD COVERED Scientific Report 6 PERFORMING ORG REPORT NUMBER PSU-IRL-SCI-455
7 AUTHOR(s) Larry J. Gardner		8. CONTRACT OR GRANT NUMBER(s) NASA NGL 39-009-003
9 PERFORMING ORGANIZATION NAME AND ADDRESS The Ionosphere Research Laboratory 318 Electrical Engineering East Building University Park, Pennsylvania 16802		10 PROGRAM ELEMENT, PROJECT, TASK AREA & WORK UNIT NUMBERS
11 CONTROLLING OFFICE NAME AND ADDRESS National Aeronautics and Space Administration Washington, D. C. 20546		12 REPORT DATE June, 1977 13 NUMBER OF PAGES 135
14 MONITORING AGENCY NAME & ADDRESS(if different from Controlling Office)		15 SECURITY CLASS (of this report) NONE 15a DECLASSIFICATION/DOWNGRADING SCHEDULE
16 DISTRIBUTION STATEMENT (of this Report)		
17 DISTRIBUTION STATEMENT (of the abstract entered in Block 20, if different from Report)		
18 SUPPLEMENTARY NOTES		
19 KEY WORDS (Continue on reverse side if necessary and identify by block number) Heterosphere		

20 ABSTRACT (Continue on reverse side if necessary and identify by block number)

The importance of the polar thermosphere has been well documented. For the first time, data from the OGO-6 satellite has made it possible to separate a number of temperature effects from those based on density and thus the morphology of the high-latitude thermosphere can be studied in some detail. Specifically, the atomic oxygen density at 120 km, the 630 nm airglow temperature, the helium density at 300 km and the molecular nitrogen density near 400 km have been examined as functions of geomagentic latitude, geomagnetic time, season and magnetic activity level. The long-term averages of these

quantities have been examined so as to provide a baseline of these thermospheric parameters from which future studies may be made for comparison.

The hours around magnetic noon are characterized by low temperatures, high O and He densities, and median nitrogen densities. The pre-midnight hours exhibit high temperatures, high He density, low nitrogen density and median O densities. The post-midnight sector shows low O and He densities, median temperatures and high nitrogen densities. These results are compared to recent models and observations and are discussed with respect to their causes due to divergence of the wind field and energy deposition in the thermosphere.

PSU-IRL-SCI-455

Scientific Report 455

Densities and Temperatures in the Polar Thermosphere

by

Larry J. Gardner

June 30, 1977

The research reported in this document has been supported by The National Aeronautics and Space Administration under Grant No. NGL 39-009-003.

Submitted by:

John J. Olivero
Associate Professor of
Meteorology

Approved by:

J. S. Nisbet, Director
Ionosphere Research Laboratory

Ionosphere Research Laboratory

The Pennsylvania State University

University Park, Pennsylvania 16802

ACKNOWLEDGEMENTS

The author wishes to express his appreciation to Dr. John S. Nisbet and Dr. John J. Olivero for their guidance and advice during the course of this work. He also wishes to thank Robert Divany and Beverly Beiswenger for computer programming, Bruno Krause and Steve Prutzman for their art work and Linda Shapira, Brenda Grenoble and Elaine Gardner for help in preparing the data for publication.

The mass spectrometer data were supplied by Goddard Space Flight Center and discussions with Dr. C. A. Reber are gratefully acknowledged. Dr. J. E. Blamont of the Service d'Aeronomie of CNRS supplied the 630 nm temperatures. This work was supported in part by the National Aeronautics and Space Administration under grant NGL 39-009-003.

TABLE OF CONTENTS

LIST OF TABLES

LIST OF FIGURES

ABSTRACT

The importance of the polar thermosphere has been well documented. For the first time, data from the OGO-6 satellite has made it possible to separate a number of temperature effects from those based on density and thus the morphology of the high-latitude thermosphere can be studied in some detail. Specifically, the atomic oxygen density at 120 km, the 630 nm airglow temperature, the helium density at 300 km and the molecular nitrogen density near 400 km have been examined as functions of geomagnetic latitude, geomagnetic time, season and magnetic activity level. The long-term averages of these quantities have been examined so as to provide a baseline of these thermospheric parameters from which future studies may be made for comparison.

The hours around magnetic noon are characterized by low temperatures, high O and He densities, and median nitrogen densities. The pre-midnight hours exhibit high temperatures, high He density, low nitrogen density and median O densities. The post-midnight sector shows low O and He densities, median temperatures and high nitrogen densities. These results are compared to recent models and observations and are discussed with respect to their causes due to divergence of the wind field and energy deposition in the thermosphere.

CHAPTER I

INTRODUCTION

1.1 General Statement of the Problem

The high latitude thermosphere is of primary importance because it is the site of major energy inputs to the upper atmosphere. This energy causes ionization and dissociation of atmospheric constituents and controls the circulation cells that produce meridional winds. The winds redistribute the energy to lower latitudes and also carry the constituents with them. They greatly modify the F region of the ionosphere by raising the layer to heights where recombination is low and by transporting atomic oxygen to low latitudes which changes the O to N_2 density ratio. Since the major ion is O^+ and the major loss mechanism is $O^+ + N_2 \rightarrow NO^+ + N$, the O to N_2 ratio affects the electron density.

It has been difficult to determine thermospheric densities because satellites generally make measurements at only one height. The OGO-6 satellite mass spectrometer data, as well as the 630 nm airglow temperatures, have been made available to us and the purpose of this study is to separate a number of temperature effects from those based on density so that the morphology of the high latitude thermosphere can be studied in some detail.

1.2 Introduction to Thermospheric Models

From early satellite drag measurements, it has been shown that geomagnetic activity affects thermospheric density and temperature (Nicolet, 1961; Jacchia, 1959a,b). However even recent models and

observations have failed to explain adequately how these parameters are affected by the observed thermospheric circulation.

Recent findings and theories (see reviews by von Zahn, 1974; Rishbeth, 1974; Carignan, 1975; and Champion, 1975) indicate that the magnetic storm acts as an energy source which generates electric fields and currents in the polar thermosphere. These currents in turn, heat the neutral atmospheric constituents and the resulting pressure gradients and the electric fields produce horizontal winds which lead to upwelling of gases from below (Mayr and Volland, 1972). The upwelling changes the boundary conditions and in particular the atomic oxygen density at 120 km in the lower thermosphere. Thus energy is transported into and out of the polar regions by horizontal winds (Hays et al., 1973). Observational support for these concepts is discussed in section 1.3.

Various models have been developed recently using different assumptions. For example, some models use fixed boundary temperatures and density (Jacchia, 1971) or they fix the temperature and vary the density (Hedin et al., 1974). Mayr and Volland (1972) have, however, delineated the inputs required for a successful model based on Joule heating and variable density and temperature. All of the models also assume diffusive equilibrium for all constituents in the lower thermosphere, an assumption recently attacked by Kasprzak and Newton (1976) and Zimmerman and Keneshea (1976).

1.3 Theoretical Models

Nicolet (1961) examined satellite drag results and initiated a model of the thermosphere in which cooling of the atmosphere took

place. The theoretical results showed consistent temperature and density profiles, which were nearly independent of the assumed initial conditions.

Other early models of the thermosphere were made by Jacchia (1964, 1965) based on earlier satellite drag data (Jacchia, 1959a,b). He was able to construct a global model of temperature and density with respect to diurnal, seasonal, latitudinal and longitudinal changes. He has updated his work (Jacchia, 1970, 1971, 1974) and one of his latest models is included in the CIRA Standard Upper Atmosphere tables (CIRA 1972). His models have been based on constant temperature and density at the base of the thermosphere. He also assumes diffusive equilibrium throughout the thermosphere.

Other polar and global models have appeared recently. Mayr and Volland (1972, 1974) have attempted to model magnetic storm characteristics of the thermosphere by allowing both temperature and density to vary by a small amount. They then used spherical harmonic analysis of the perturbations of these two parameters using Joule heating as the energy source. Their results imply that molecular nitrogen expansion in the auroral zone generates meridional winds that are everywhere equatorward. Their model also depicts the decrease of helium and atomic oxygen with increased magnetic activity as well as the delay time of magnetic effects. The results have been compared favorably with the OGO-6 mass spectrometer data of Hedin et al., (1974) which were for middle and low latitudes and high magnetic activity. In a later work Mayr and Volland (1974) concluded that the OGO-6 data could be explained by diffusive mass transport which arises from the thermospheric circulation.

Moffett (1973) has offered a critique of Mayr and Volland's work in which he pointed out that their neglect of the higher-order harmonics of temperature and use of an incorrect zeroth-order harmonic produced significant errors. He also felt that variations in number density and temperature at 120 km may influence the phases of both mass and number density relative to the phase of the temperature. This situation can only complicate the results. He concluded by adding that a three-dimensional, time dependent model has not yet been successfully developed.

Bailey and Moffett (1972) have developed a global theoretical model using fixed density and temperature in the lower thermosphere. Their results show that vertical velocity has important effects on density and temperature at 120 km, the lower boundary of static diffusion models.

Hays et al., (1973) have modeled the auroral region and have shown that as a magnetic storm begins, the helium and atomic oxygen densities are decreased relative to the molecular nitrogen density. They conclude that this decrease of density is due to cellular upwelling in which gases rich in molecular nitrogen and poor in helium and atomic oxygen are carried upward. This vertical motion leads to horizontal flow. They also conclude that there is enough energy available in the auroral electric fields to generate this flow by heating the neutral atmosphere.

Cole (1975) has also argued that the dissipation of electric fields is a major source of energy for the thermosphere. He also presents the theory that energy from tropospheric weather systems may

propagate upward to the thermosphere to produce winds. Then electrostatic fields are produced by dynamo action which leads to trapping of solar wind plasma in the magnetosphere which, in turn, leads to a magnetic storm. Thus, there may be a connection between tropospheric weather and thermospheric motions.

Reber et al., (1971) argue that the helium concentrations are indicators of the thermospheric winds. Thus observations and models of helium should give clues to thermospheric dynamics. Continuing this reasoning, Reber and Hays (1973) have attempted to model helium in the global thermosphere. They show helium upwelling in the summer hemisphere flowing toward and descending into the winter hemisphere.

Blum and Harris (1975a, b) have presented a model of the global thermospheric wind system where they integrated the horizontal equations of motion, including all non-linear terms. They used the thermospheric model of Jacchia (1971) and the ionospheric model of Nisbet (1970). Their results show a wind field at 300 km that blows from the dayside to nightside over the poles. Their main conclusion, however, was that the equations of motion cannot be simplified without considerable loss of accuracy.

Creekmore et al., (1975) took the Jacchia (1971) model with constant lower boundary conditions and derived a model based on conservation of mass and energy. They, too, included all non-linear terms in the equations of motion. They concluded that the major shortcoming of this approach and those of previous models was the neglect of vertical motions on the energy balance. Strauss et al., (1975) took the model of Creekmore et al., (1975) and added solar EUV

heating. Their conclusion was that there is a necessity for an additional heat source at high latitudes, even during magnetically quiet periods.

1.4 Observations and Empirical Models

Newton (1970) used satellite density gauge data to infer a permanent heating source above 40^{o} latitude. He felt this source may be influenced by increased magnetic activity.

Taeusch et al., (1971) presented results from the neutral atmospheric experiment on board the OGO-6 satellite. These results indicate that the major portion of the energy from a magnetic storm is deposited at high latitudes causing enhancements in molecular nitrogen densities. The results also suggest dynamic processes that cause a thermospheric circulation that is upward at the pole with subsidence at the equator. Carignan and Reber (1971) presented similar results from a study of the large magnetic storm of 8 March 1970.

Reber et al., (1971), present data from OGO-6 showing the horizontal distribution of helium at high altitudes and latitudes. They show a one order of magnitude higher concentration in winter than in summer with the maximum concentration at -53^{o} magnetic latitude. They reiterate the point that helium concentrations are indicators of thermospheric winds.

Blamont and Luton (1972) presented 630 nm airglow temperature from OGO-6 and concluded that high latitude behavior is largely determined by geomagnetic activity. They also showed unexpected temperature maxima in the polar regions during quiet magnetic periods.

DeVries (1972) used accelerometer data to show that most of the energy associated with geomagnetic activity is deposited in the auroral region and is then transported toward the equator by atmospheric waves and convective circulation.

Hedin and Reber (1972) presented OGO-6 data that showed the helium concentrations varying inversely to the nitrogen concentrations. Maximum nitrogen densities at 450 km occur above 65^{o} latitude and a maximum also occurs near 0800 UT. Their conclusion was that the polar heat input is magnetically controlled.

Johnson and Gottlieb (1973) have attempted to explain observed atomic oxygen density variations as resulting from photodissociation of molecular oxygen at the subsolar point. Winds then carry the densities toward the poles at equinox and toward the winter pole at solstice. Kohl and King (1967) and Blum and Harris (1973) have shown similar results.

Reber et al., (1973) have taken the OGO-6 data and concluded that dynamics play a significant role in the thermosphere. Geomagnetic disturbances create circulation cells which decrease the atomic oxygen at low altitudes.

Forbes and Marcos (1973) have used accelerometer data from a satellite to show that density enhancements occur in conjunction with electrojet currents. These density variations are what would be expected from Joule heating. Therefore, they point out that future models should include electric fields, Joule heating and dynamics. Support for the electric field inclusion came from Truttse (1969) who showed a linear relation between density variations and the AE indices.

Burge et al., (1973) used work by Roemer (1971) to show that the preferential heating of the high latitude during magnetic storms is sufficient to reverse the normal poleward daytime wind. Similarly, Johnson (1974) analyzed data from various sources and concluded that during magnetic storms the heat input in the auroral region may actually equal or exceed that at the low latitudes so that there can be large-scale winds away from the auroral zones.

Reber and Hedin (1974), again using OGO-6 data, showed that heat inputs exist in both hemispheres at mid to high latitudes that corotate with the magnetic poles. The heat source showed maxima at 0900 and at 2100 UT. They conclude that the observed variation of peak concentration of helium in winter is also a manifestation of this heating.

Brekke et al., (1974) used rocket data to show that the neutral wind over the poles at altitudes of 110-115 km flowed in a mainly antisolar direction during a magnetic storm due to a heat source in the auroral oval.

Barlier et al., (1974) used several different types of data and came to the conclusion that there is more energy deposited in the southern hemisphere than in the northern hemisphere. This asymmetry may be due to geomagnetic field asymmetry and tidal dissipation from asymmetrical ozone distribution.

Philbrick (1974) used a satellite mass spectrometer to show that molecular nitrogen has a large variability in the polar regions. The variations are much larger than those used in static diffusion models with constant boundary densities and temperatures at 120 km.

Wydra (1975) analyzed OGO-6 data and showed that atomic oxygen observations indicate that particularly under disturbed magnetic conditions the atomic oxygen vertical velocity is upward in the polar cap and downward at low latitudes. He also concluded that the thermospheric pressure induces winds which are nongeostrophic due to ion drag such that the pressure gradients are minimized. He also compared airglow temperature and the temperature derived from the density of a single gas constituent. He concluded that the density-derived temperatures had, at times, significant errors due to changes in the lower thermospheric boundary conditions of atomic oxygen.

Taeusch and Hinton (1975) have analyzed the OGO-6 data which show that the molecular nitrogen density at 400 km at polar latitudes peaks near local magnetic noon and has a minimum around 1800 local magnetic time. They conclude that these variations are magnetically controlled and are associated with localized heating effects such as electrodynamic and particle heating sources. This last conclusion, however, is different from the results of Wydra (1975) who showed that the 630 nm airglow temperature peaks in the pre-midnight sector and has a minimum in the noon sector regardless of the magnetic activity level. The data used by Taeusch and Hinton (1975) and those used by Wydra (1975) are included in the data base used in the present paper and this point is a major item for the present study.

Kasprzak and Newton (1976) have compared San Marcos 3 data with OGO-6 data and have shown that non-diffusive equilibrium exists below 170 km, especially for helium, at low and middle latitudes.

Prölss and von Zahn (1976) have presented results from the ESRO 4 gas analyzer which shows that atomic oxygen decreases and molecular nitrogen increases with increasing magnetic activity. Under disturbed conditions, small-scale fluctuations were dominant.

Nisbet and Glenar (1977) have taken the analysis of atomic oxygen discussed in section 3.3 and shown that the atomic oxygen variations are related to vertical velocities in the 95 km to 120 km altitude region and to the meridional fluxes at 70^{o} geomagnetic latitude. These fluxes are compared to fluxes derived from high latitude rocket vapor trail wind measurements. It is shown that the poleward fluxes are well correlated with the derived oxygen densities. The average upward vertical velocity in the region poleward of 70^{o} geomagnetic latitude is calculated to be of the order of 0.3 m/sec. The energy transported by the winds out of the region poleward of 70^{o} geomagnetic latitude is calculated to be of the order of 3×10^{10} watts for Kp levels of 2.

Other reviews of models and observations, especially for lower latitudes may be found in Carignan (1975), Champion (1975) and Wydra (1975).

1.5 General Comments on the Models

All of the models above have admitted shortcomings. Some of these are pointed out by Kasprzak and Newton (1976). They have presented satellite data which they compared to the Hedin et al., (1974) OGO-6 model to show that conditions are not really in diffusive equilibrium below 170 km.

Also, Zimmerman and Keneshea (1976) have presented theoretical arguments against the assumption of diffusive equilibrium which cast doubt on such practices as:

1) Using satellite drag densities to model the thermosphere.
2) Determining thermospheric densities from incoherent backscatter radar.
3) Determining temperature from single-species measurements.
4) Deriving flow diagrams from meridional differences in lower-thermospheric heating and species production.

They argue that their rocket data show that the lower thermosphere is not in an equilibrium state.

As already stated, Moffett (1973) as well as Johnson (1973) argued against the use of constant boundary conditions in the lower thermosphere.

Another primary deficiency in these models has been insufficient data, especially in the polar regions. This paper includes extensive data analysis which will demonstrate that the density and temperature distributions over the polar thermosphere are much more complex than has been shown previously or included in theoretical or empirical thermospheric models.

1.6 Specific Statement of the Problem

It is the purpose of this study to,

1) Determine the distributions of the densities of O, He and N_2 and temperature as a function of magnetic time.
2) Present mathematical models of these distributions which will reproduce the observations as functions of three seasons and three levels of magnetic activity.

3) Qualitatively explain the reasons for the observed distributions.

CHAPTER II

DATA ACQUISITION

2.1 OGO-6 Satellite Measurements

The OGO-6 satellite was launched 5 June 1969 into a polar orbit of inclination 82^{o} with a perigee of 398 km and an apogee of about 1100 km. The orbital period was about 100 minutes.

The 630 nm oxygen airglow emission was determined by the use of a spherical Fabry-Perot interferometer aimed towards the horizon. Blamont and Luton (1972) discuss this instrument and its data in detail. The accuracy of the measurement of the neutral temperatures determined from the profile of this emission line was calculated to be $\pm$ 65^{o} K for each individual measurement. The spatial resolution of the measurement was approximately 1^{o} longitude, 6^{o} latitude, and 30 km altitude at the equator. The measurements were made at altitudes in the range of 240 to 300 km.

The OGO-6 quadrupole mass spectrometer used to measure the concentration of O, He and N_2 is described by Carignan and Pinkus (1968) and Hedin et al., (1974). The uncertainty of these measurements were determined by these authors to vary with constituent and to increase with increasing altitude. The uncertainties were generally less than 10 to 15 per cent near perigee, however, there is an additional calibration uncertainty of 10 to 15 per cent in the absolute value of all measurements. No data were used where the estimated statistical uncertainty was greater than 25 per cent for N_2 and O and 50 per cent

for He. The spatial resolution of the measurement is less than $1/2^{o}$ in latitude and longitude and less than 5 km in altitude.

CHAPTER III

DATA ANALYSIS

3.1 General Description of the Data

The measurements of polar thermospheric densities and temperatures have been made available by observations from the OGO-6 satellite as described in Chapter II. These observations cover the period of June 1969 to August 1971.

Since the purpose of this study is to investigate the long-term averages of the atomic oxygen, helium and molecular nitrogen densities and 630 nm airglow temperatures and since the short term fluctuations of these observations are subject to large variations, they were averaged over a period of 45 days before and after the solstices and equinoxes. In addition, they were averaged over both hemispheres, i.e., June in the northern hemisphere was averaged with December in the southern hemisphere. The equinox values were also averaged together. This averaging over the hemispheres and equinoxes also minimized the amount of missing data.

Since geophysical effects at high latitudes are known to be influenced mainly by geomagnetic variations, the data are displayed in geomagnetic coordinates. The method used to calculate these coordinates is the method of Agy (1965) as adapted by Nisbet (1976).

The data were then subdivided into "bins" of geomagnetic latitude at 5 degree intervals from 60^{o} to 90^{o} and in intervals of one hour in geomagnetic time (longitude). They were further divided into ranges of the Kp index from 0.0 to 1.3, from 1.3 to 4.0 and > 4.0. The

average of each "bin" and the number of observations used in calculating the averages of the data are shown in tables in sections 3.2 through 3.5.

To quantify the variations of these averages and to also allow for future comparisons, a Fourier analysis was done for each latitude band. This Fourier analysis uses an equation of the form:

$$F(t) = A_o + \sum_{n=1}^{\infty} \left\{ A_n \cos \frac{2\pi nt}{T} + B_n \sin \frac{2\pi nt}{T} \right\}$$

where A_o is the average for the latitude band and A_n and B_n are coefficients of the sine and cosine components for the fundamental and harmonics. T is 24 hours and t is the magnetic local time. The values of A_o and first five coefficients of each sine and cosine term for each latitude band are shown in sections 3.2 through 3.5. Some of the tables for winter and summer are not shown due to insufficient data.

In order to show the results graphically, the tables of averages were converted to a 25 by 25 matrix using standard linear interpolation techniques; the result being displayed in polar coordinates. Missing data were also estimated where possible by the use of linear interpolation.

The matrix was then analyzed (in a synoptic sense) by drawing simple isopleths (contours) in polar geomagnetic coordinates. These results are shown in the figures in sections 3.2 through 3.5. The concentric circles are geomagnetic latitude and the radial lines indicate local geomagnetic time.

It should be pointed out that for the high Kp level, there are less data than for the lower levels. There are also less data for helium than for oxygen, airglow temperature or nitrogen, except at the equinoxes. Also, any areas on the matrix used for the contour analysis having fewer than five observations have been indicated by cross-hatching. The number of observations for each point ranged from five to over 800.

The quantitative aspects and general, persistent features of the results are discussed in the following sections. The possible physical causes for the results are discussed in Chapter IV.

3.2 630 nm Airglow Temperature

The 630 nm airglow temperature is shown as a function of geomagnetic time and latitude in Figures 1 through 9 and Tables 2 through 16. Table 1 provides a convenient index to this data.

The dependence of this temperature on latitude is seen in the Fourier coefficient tables. The A_o (average) term peaks near the pole during winter. During summer this peak moves to lower latitudes. The contributions of the fundamental and harmonic terms are small, being two to three orders of magnitude smaller than the A_o term.

The geomagnetic local time effect is evident in Figures 1 through 9. There are persistent maxima at 1800-2200 LMT and 0500-0800 LMT. There are minima at 1200 LMT and 1400 to 1600 LMT.

The effect of magnetic activity on these temperatures is also easily seen in Figures 1 through 9. The temperatures increase markedly with increasing magnetic activity. The A_o Fourier coefficient shows the temperature at equinox is 70^o higher for Kp = 1.3 to 4.0 and 250^o higher for Kp > 4.0 than for Kp = 0.0 to 1.3.

A seasonal effect is also observed, being 100° warmer at equinox and 180° warmer in summer than in winter for Kp = 1.3 to 4.0. The seasonal effect is larger for the low Kp level than for the high Kp level.

It should also be mentioned that these temperatures were used as the isothermal thermospheric temperature, T_∞, in the following sections.

Thuillier (1976) has reexamined the data base used here for the 630 nm temperatures and discovered that under certain conditions of background radiation, range and altitude quite large errors can occur. Based on these analyses he has edited the data base so that these erroneous points are not included. We have, unfortunately, not been able to obtain tapes of the edited data, nor have we edited the data ourselves as we do not have the raw data tapes. We have done all that we can to eliminate the problem by removing data points that are more than 2.5 σ from the average value in each data bin and then reaveraging. Care should be taken, however, in accepting the temperatures from this source too literally.

3.3 Atomic Oxygen Density at 120 km

The atomic oxygen density measurements were extrapolated from satellite altitudes down to 120 km, the height of the lower boundary of static diffusion models. This extrapolation requires the assumption of diffusive equilibrium. Nisbet and Glenar (1976) have presented a similar extrapolation which is outlined below.

The vertical distribution of atomic oxygen under diffusive equilibrium with no vertical diffusion velocities is given by:

$$\frac{1}{n(O)} \frac{dn(O)}{dZ} = - \frac{m(O)g}{kT} - \frac{1}{T} \frac{dT}{dZ} \qquad (1)$$

where n(O) is the density of atomic oxygen, T is temperature, Z is altitude, m(O) is the mass of an atomic oxygen atom, k is the Boltzmann constant, and g is the gravitational acceleration of height Z. The $\frac{1}{T} \frac{dT}{dZ}$ term is difficult to evaluate but it can be eliminated by noting that:

$$\frac{1}{n(N_2)} \frac{dn(N_2)}{dz} = - \frac{m(N_2)g}{kT} - \frac{1}{T} \frac{dT}{dZ} \qquad (2)$$

Integrating equations (1) and (2) from 120 km to height Z and combining them to eliminate the first term on the right hand side of each equation gives:

$$\log_e n(O)_{120} = \log_e n(O)_z + \frac{4}{7} (\log_e n(N_2)_{120} - \log_e n(N_2)_z) + \frac{3}{7} \log_e \frac{T_z}{T_{120}} \qquad (3)$$

In this way the oxygen density at 120 km can be derived using the measured temperature, oxygen and nitrogen densities at the satellite altitude providing $n(N_2)_{120}$ and T_{120} can be taken as constant values of 3.8×10^{11} cm^{-3} and $350^{o}K$, respectively from the CIRA (1972) model. T_z is taken as the 630 nm airglow temperature, since the satellite measurements of the densities were taken in the isothermal region of the thermosphere.

The results of this extrapolation are shown in Figures 10 through 18 and Tables 16 through 30.

A latitudinal variation is apparent from the A_o Fourier components. For Kp = 1.3 to 4.0 the density decreases with increasing latitude, the pole densities being 40 per cent lower than 60^o-65^o latitude in summer, 20 per cent lower in winter and 15 per cent lower at equinox.

There is also a strong seasonal variation; the density is 46 per cent lower in summer and 14 per cent higher in winter than at equinox for Kp = 1.3 to 4.0.

There is a marked decrease in $n(O)_{120}$ with magnetic activity and the densities are 20 per cent higher for Kp = 0.0 to 1.3 and 27 per cent lower for Kp > 4.0 than for Kp = 1.3 to 4.0 at equinox.

The variation of atomic oxygen with geomagnetic time shows the most impressive result of all. There is a persistent area of low density (about 25 to 50 per cent lower than at other times) in the 0000 to 0800 LMT sector. This sector of low density is present in all seasons at all Kp levels. In addition, the densities are consistently high in the noon sector. The possible physical significance of these results will be discussed in Chapter IV.

As stated earlier, vertical velocities were neglected in the extrapolation of the atomic oxygen densities to 120 km. The work of Nisbet and Glenar (1976) and the atomic oxygen observations at 95 km by Donahue et al., (1974) allows one to estimate these velocities and then to estimate the error in the extrapolated densities due to the assumption of diffusive equilibrium.

Examples of the comparison between the results of this section and Donahue's data are shown in Tables 31 and 32. Table 31 shows the comparison for mid-latitudes and Table 32 shows the comparison for high latitudes. There is a suggestion that the density difference between the two altitudes increases over the poles. Nisbet and Glenar (1976) attribute this observation to increased upward diffusion velocity over the poles.

This diffusion velocity may be estimated, as shown by Nisbet and Glenar (1976), by the equation:

$$\log_{10} n(O)^{*}_{120} = -10.14\, V_{d\ 120} + \log_{10} n(O)_{95} - 1.52 \qquad (4)$$

where $n(O)^{*}_{120}$ is the extrapolated atomic oxygen density at 120 km (no vertical velocity), $V_{d\ 120}$ is the vertical diffusion velocity at 120 km and $n(O)_{95}$ is the measured atomic oxygen density at 95 km. This equation gives vertical diffusion velocities of $-.15$ m s^{-1} at low latitudes and $-.10$ m s^{-1} at high latitudes based on the information in Tables 31 and 32. Nisbet and Glenar (1976) also show that the difference between extrapolated densities and true densities is a function of the vertical diffusion velocity only, i.e.:

$$\log_{e} n(O)^{*}_{120} + 6.74\, V_{d\ 120} = \log_{e} n(O)_{120} \qquad (5)$$

where $n(O)_{120}$ is the actual atomic oxygen density at 120 km. The above-mentioned vertical velocities give actual densities at 120 km of around 50 to 60 per cent lower than the extrapolated values for the same season and magnetic activity. The actual values of density at

120 km, then, are nearly one order of magnitude smaller than the actual density at 95 km. This difference is close to that reported by Donahue et al., (1974).

3.4 Temperature Derived from Molecular Nitrogen Densities

The nitrogen densities are presented here in the form of equivalent temperatures for comparison with the airglow temperatures as has been done previously by Wydra (1975) and Nisbet et al., (1977). These values are merely the temperature, T, of the CIRA (1972) model that would give the same N_2 density at the satellite altitude. They are not real temperatures but depend greatly on the temperature gradients in the 95 to 150 km region. These values will be called NT. A regression equation was used to fit the CIRA (1972) densities of N_2 to the exospheric temperature. The resulting equation was:

$$NT = \frac{1521.5 - 12.0697\ Z}{\log_{10} n(N_2)} - 15.9523 - 2.4356 \times 10^{-4}\ Z \qquad (6)$$

where Z is the satellite altitude in kilometers and $n(N_2)$ is the molecular nitrogen density (m^{-3}) at altitude Z.

The results are shown in Figures 19 through 29 and Tables 31 through 45.

The latitudinal variation of these NT values is such that the peak occurs near the pole in winter with higher values at lower latitudes in summer. The difference between the pole and lower latitudes is greater in winter than in summer.

The variation with magnetic activity is shown by the NT value being 100°K lower at Kp = 0.0 to 1.3 and 200°K higher at Kp > 4.0 than at Kp = 1.3 to 4.0 for equinox. These NT differences correspond to the density being 8 times smaller at Kp = 0.0 to 1.3 and 15 times larger at Kp > 4.0 than at Kp = 1.3 to 4.0 for equinox at an altitude of about 400 km.

There is a strong seasonal variation as well; the NT value is 275 K higher in summer and 120 K lower in winter than at equinox for Kp = 1.3 to 4.0. These differences correspond to the N_2 density being 14 times larger in summer and 8 times smaller in winter than at equinox at 400 km. This represents a change of two orders of magnitude in the molecular nitrogen density not included in the CIRA 1972 model.

The variation with geomagnetic time indicates that there is a persistent maximum near the 0800 to 1200 LMT sector and a minimum in the 1600 to 2000 LMT sector. This is in close agreement with Taeusch and Hinton (1975) and Hedin and Reber (1972). However, Tauesch and Hinton (1975) show a second maximum around 0000-0300 LMT which does not appear in the data presented here. This difference may be due to different averaging techniques and the fact that the data presented here were averaged over a much longer time. Also, their results were presented relative to the OGO-6 model of Hedin et al., (1974).

The comparison of these NT values with the airglow temperatures shows that the average NT values are higher at all Kp levels and all

seasons. At equinox the NT values are higher by 67 K at Kp = 0.0 to 1.3, 87 K at Kp = 1.3 to 4.0 and 106 K at Kp > 4.0. In summer, the difference is nearly 200° at all Kp levels. Nisbet et al., (1977) show average differences of about 75°K at low Kp and about 100°K at high Kp at geomagnetic latitudes above 60°.

The differences in horizontal distributions of these two temperatures are obviously large at all Kp levels and all seasons as seen by comparing corresponding figures. Nisbet et al., (1977) point out that it is not surprising that the two temperatures do not correspond on a one-to-one basis since it is known that large changes in temperature profile occur with magnetic activity. It should be emphasized, therefore, that the NT values presented here should be interpreted as the distribution of a parameter indicative of both the temperature gradients in the 95 to 150 km region and the exospheric temperature.

3.5 Helium Densities at 300 km

The helium densities measured at satellite altitudes were extrapolated to a constant height of 300 km using the isothermal diffusive equilibrium equation:

$$n(He)_{300} = n(He)_Z \exp\left[(Z-300)\, M(He)g/RT\right] \qquad (7).$$

where $n(He)_Z$ is the helium density measured at satellite altitude Z; T is airglow temperature; M(He) is atomic mass of He; g is acceleration of gravity; R is the universal gas constant.

There were less helium density data than for the other constituents, except at equinox. Also, the mass spectrometer on the satellite had a much lower signal-to-noise ratio for the helium data than for the rest of the data. Therefore, the quantitative aspects of the summer and winter data should be regarded with caution.

The results are shown in Figures 28 through 36 and Tables 46 through 61. There does not appear to be any persistent latitudinal dependence of He density in the data presented here. The dependence on magnetic activity shows the average density is 8 per cent higher at Kp = 0.0 to 1.3 and 20 per cent lower at Kp > 4.0 than at Kp = 1.3 to 4.0 at equinox. There is also a seasonal dependence; the average density is 19 per cent lower in winter and 21 per cent lower in summer than at equinox for Kp = 1.3 to 4.0. The variation with magnetic time indicates there is a persistent maximum around 2000-2300 LMT at latitudes 70°-80°. There is a persistent minimum in the pre-dawn hours at latitudes 60°-70° similar to the low density sector observed for atomic oxygen at 120 km.

The distribution of helium density appears to be more complex than expected, but this could be due to fewer data.

The maximum average density over the poles appears to occur at equinox. This observation does not agree with theory which suggests that the maximum should occur in winter as shown by Reber et al., (1971). The work of Reber et al., (1971), however, shows only low and middle latitudes. No previous observations of helium at high latitudes could be found. The work of Hedin and Reber (1972) also shows

averages of helium density over several orbits over the North Pole. They show helium densities on the order of 4.5×10^6 cm^{-3} near equinox at low magnetic activity at 450 km altitude. The difference between the highest and lowest density values is about 2.5×10^6 cm^{-3}. These observations compare favorably with Figure 31.

The pertinent details of the results presented here along with possible physical mechanisms will be discussed in the next chapter.

Table 1: Data index for airglow temperature.

	Summer	Equinox	Winter
$0 < Kp < 1.3$	Tabulated Values: Table 2, p. 37	Tabulated Values: Table 7, p. 42	Tabulated Values Table 13, p. 48
	Graphical Analysis: Figure 1, p. 28	Graphical Analysis: Figure 4, p. 31	Graphical Analysis: Figure 7, p. 34
	Fourier Analysis: Table 3, p. 38	Fourier Analysis: Table 8, p. 43	Fourier Analysis: Insufficient Data
$1.3 < Kp < 4.0$	Tabulated Values: Table 4, p. 39	Tabulated Values: Table 9, p. 44	Tabulated Values: Table 14, p. 49
	Graphical Analysis: Figure 2, p. 29	Graphical Analysis: Figure 5, p. 32	Graphical Analysis: Figure 8, p. 35
	Fourier Analysis: Table 5, p. 40	Fourier Analysis: Table 10, p. 45	Fourier Analysis: Table 15, p. 50
$Kp > 4.0$	Tabulated Values: Table 6, p. 41	Tabulated Values: Table 11, p.46	Tabulated Values: Table 16, p. 51
	Graphical Analysis: Figure 3, p. 30	Graphical Analysis: Figure 6, p. 33	Graphical Analysis: Figure 9, p. 36
	Fourier Analysis: Insufficient Data	Fourier Analysis: Table 12, p. 47	Fourier Analysis: Insufficient Data

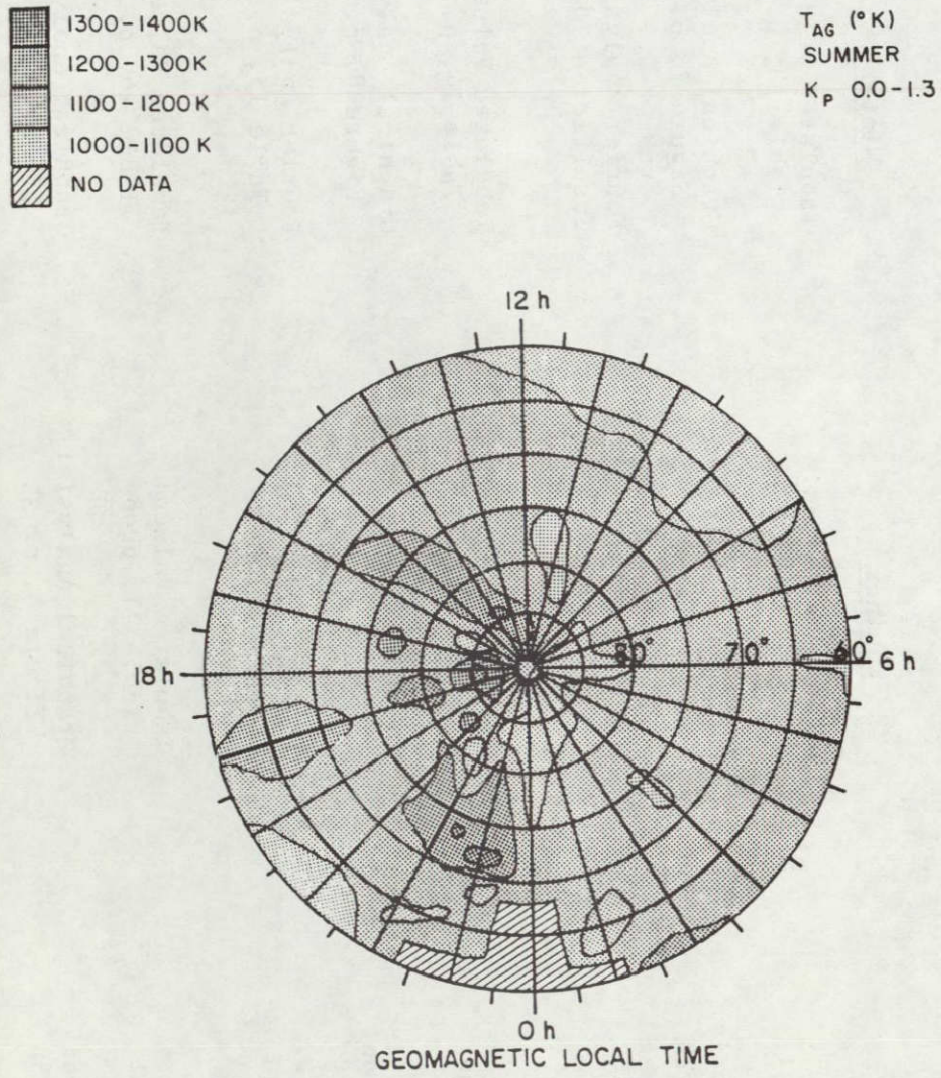

Figure 1: 630 nm airglow temperature as a function of geomagnetic time and geomagnetic latitude for Kp range 0.0 to 1.3 for summer.

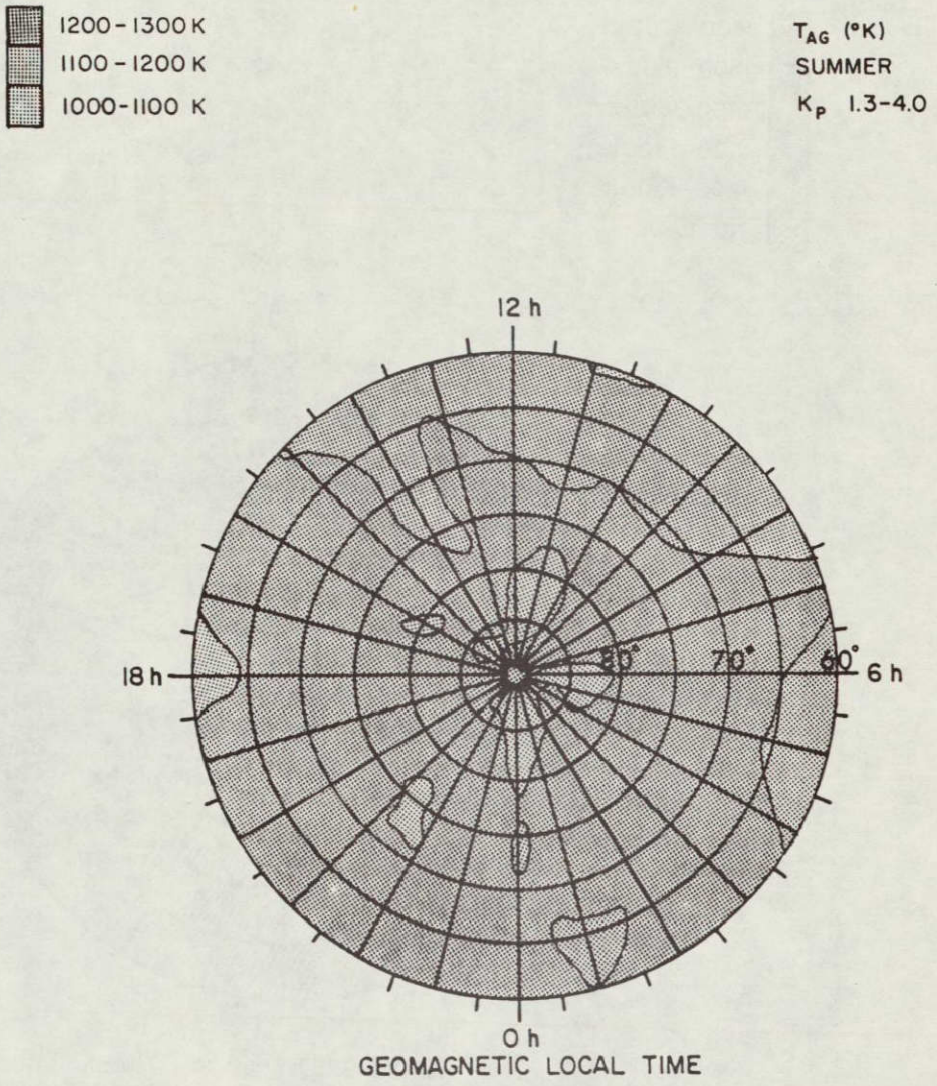

Figure 2: 630 nm airglow temperature as a function of geomagnetic time and geomagnetic latitude for Kp range 1.3 to 4.0 for summer.

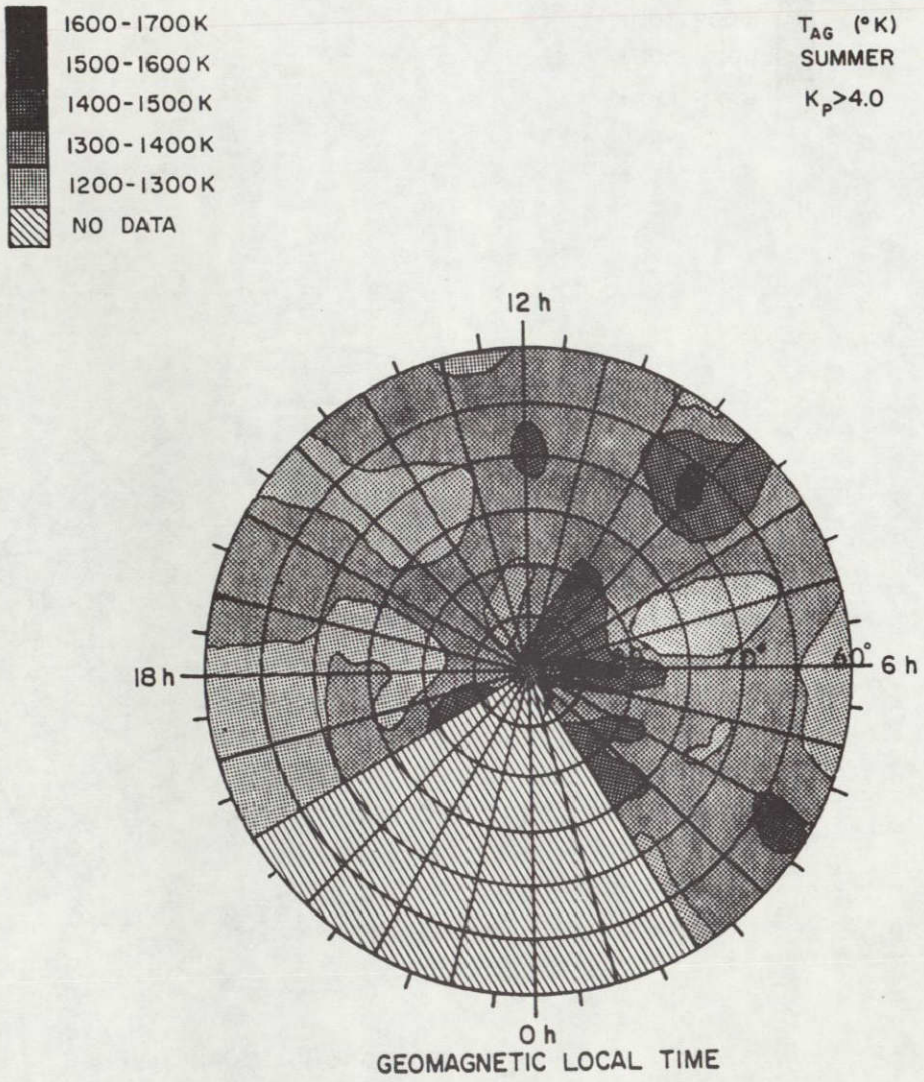

Figure 3: 630 nm airglow temperature as a function of geomagnetic time and geomagnetic latitude for Kp range > 4.0 for summer.

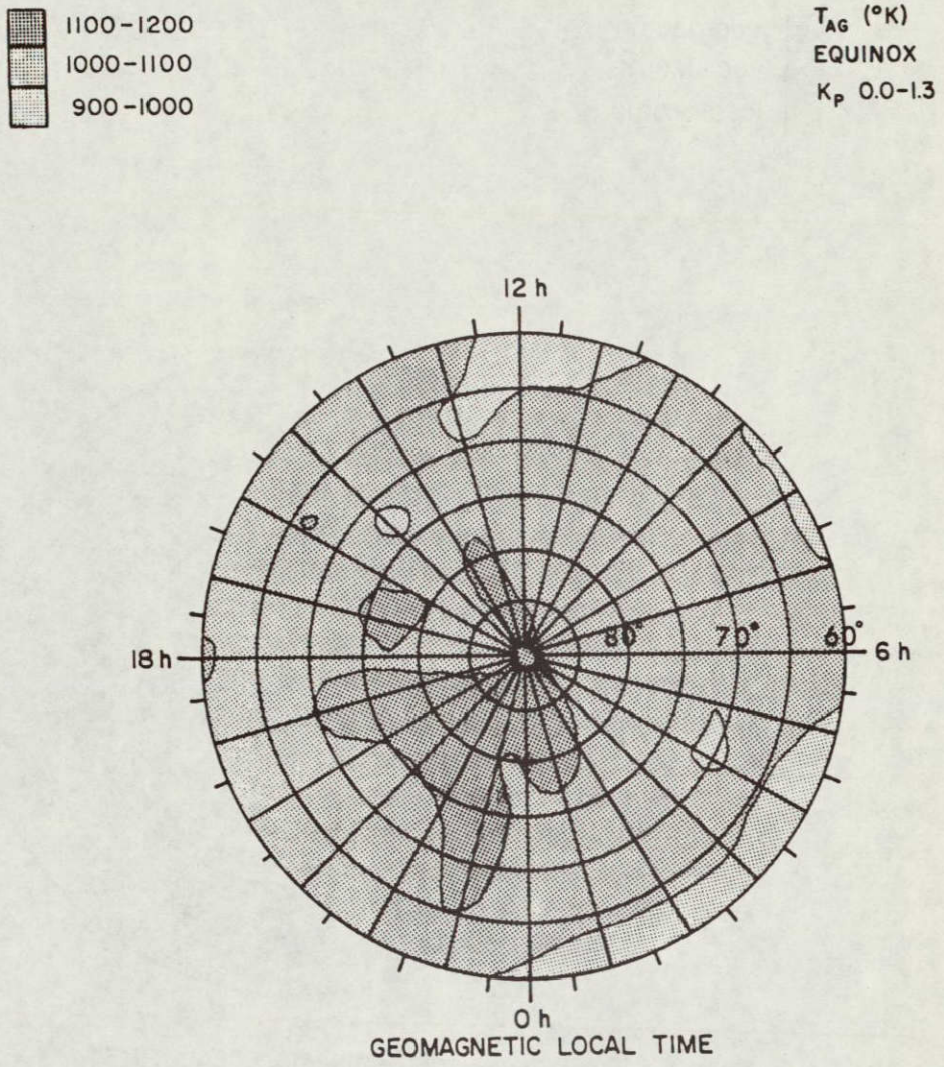

Figure 4: 630 nm airglow temperature as a function of geomagnetic time and geomagnetic latitude for Kp range 0.0 to 1.3 for equinox.

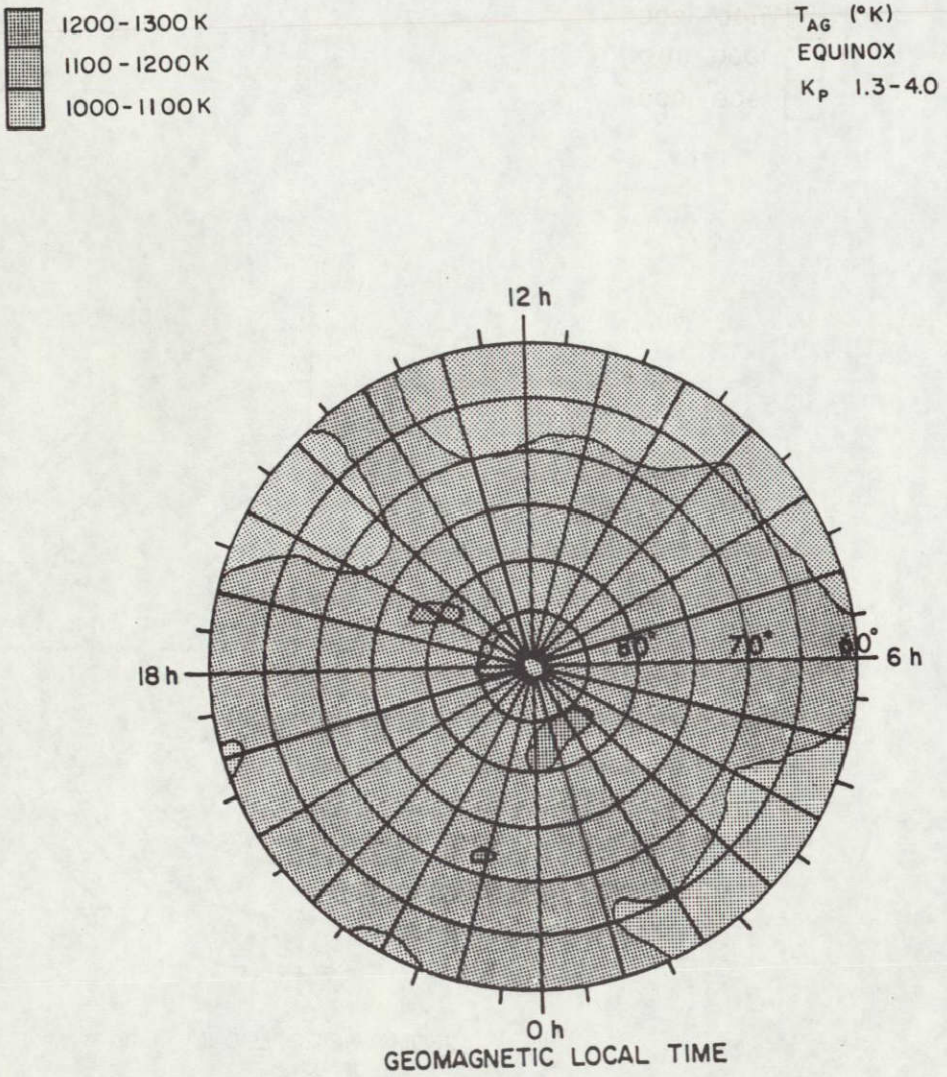

Figure 5: 630 nm airglow temperature as a function of geomagnetic time and geomagnetic latitude for Kp range 1.3 to 4.0 for equinox.

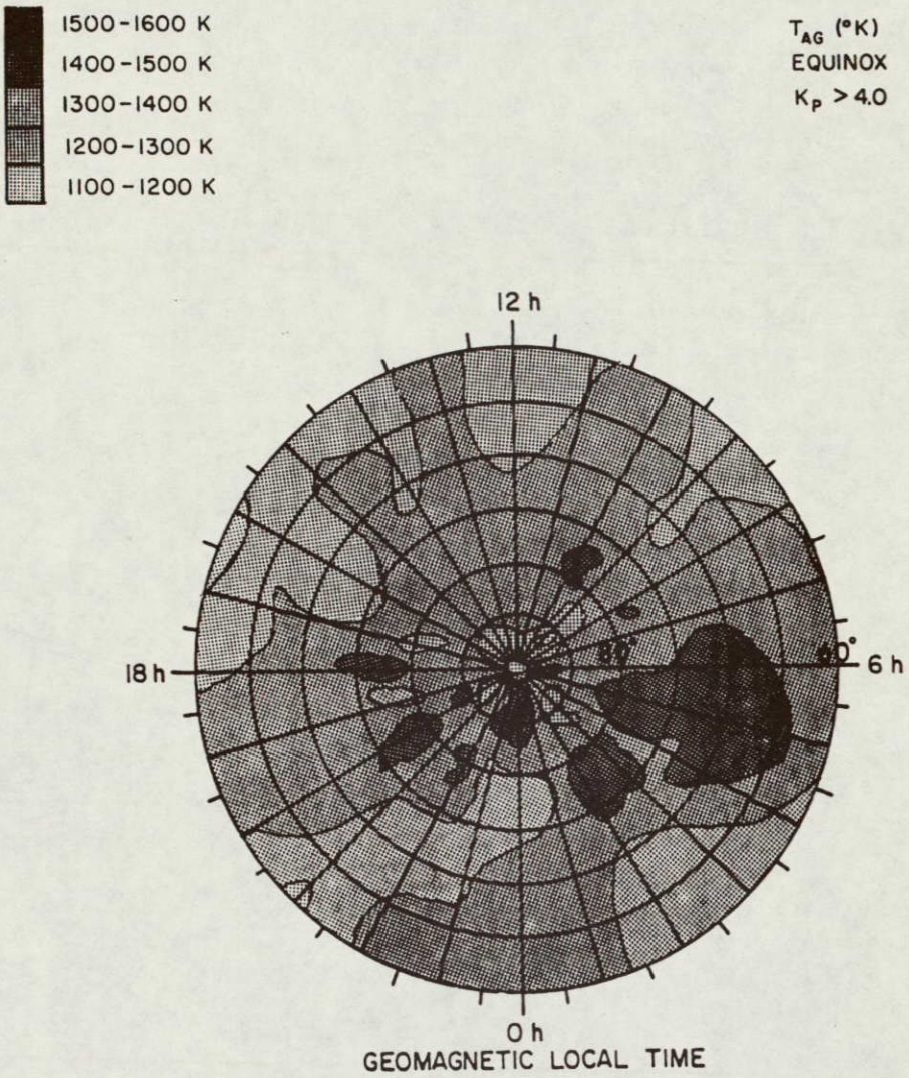

Figure 6: 630 nm airglow temperature as a function of geomagnetic time and geomagnetic latitude for Kp range > 4.0 for equinox.

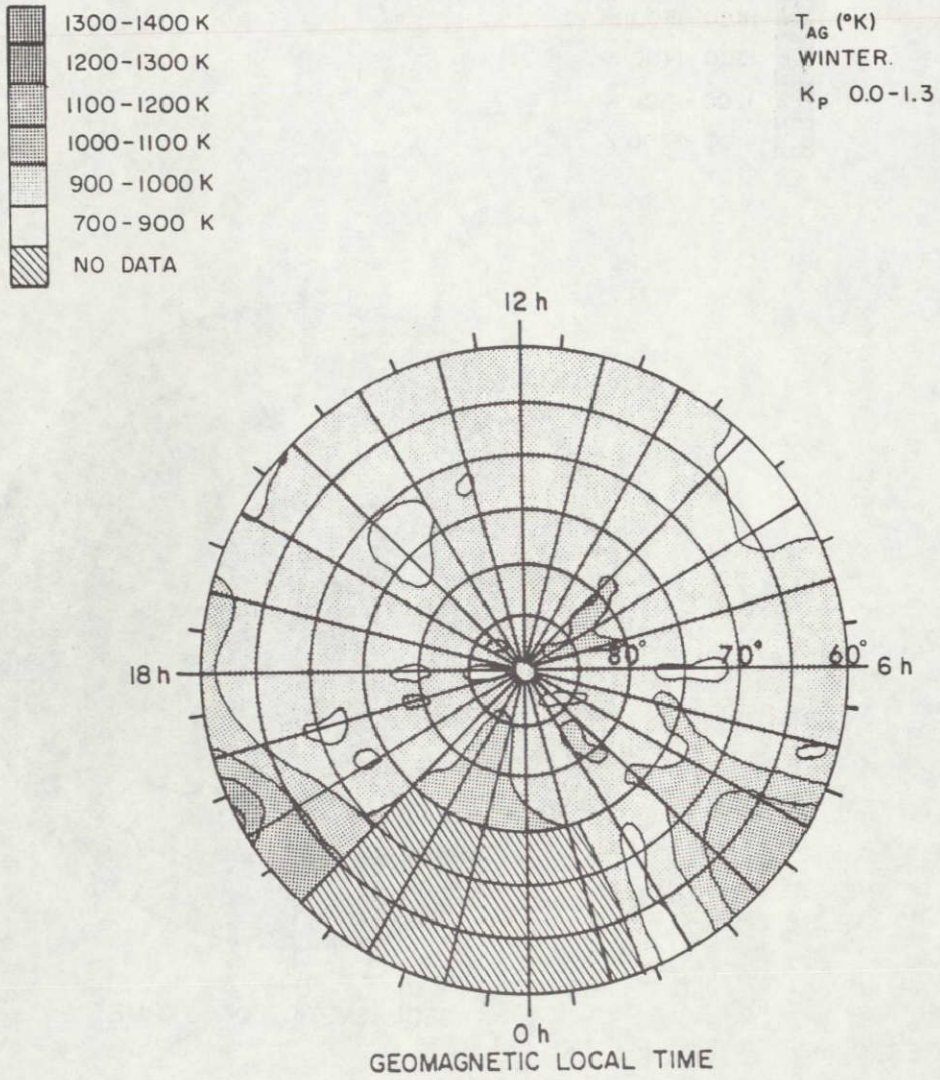

Figure 7: 630 nm airglow temperature as a function of geomagnetic time and geomagnetic latitude for Kp range 0.0 to 1.3 for winter.

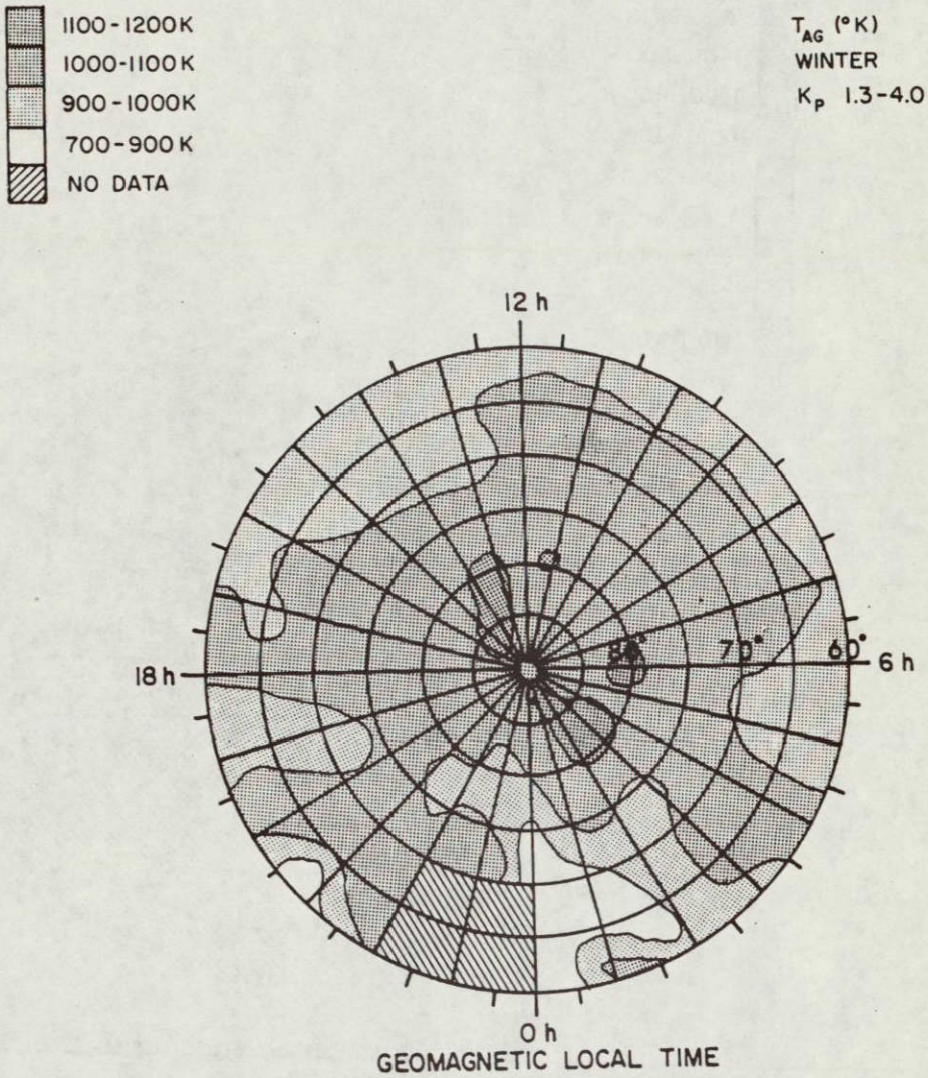

Figure 8: 630 nm airglow temperature as a function of geomagnetic latitude for Kp range 1.3 to 4.0 for winter.

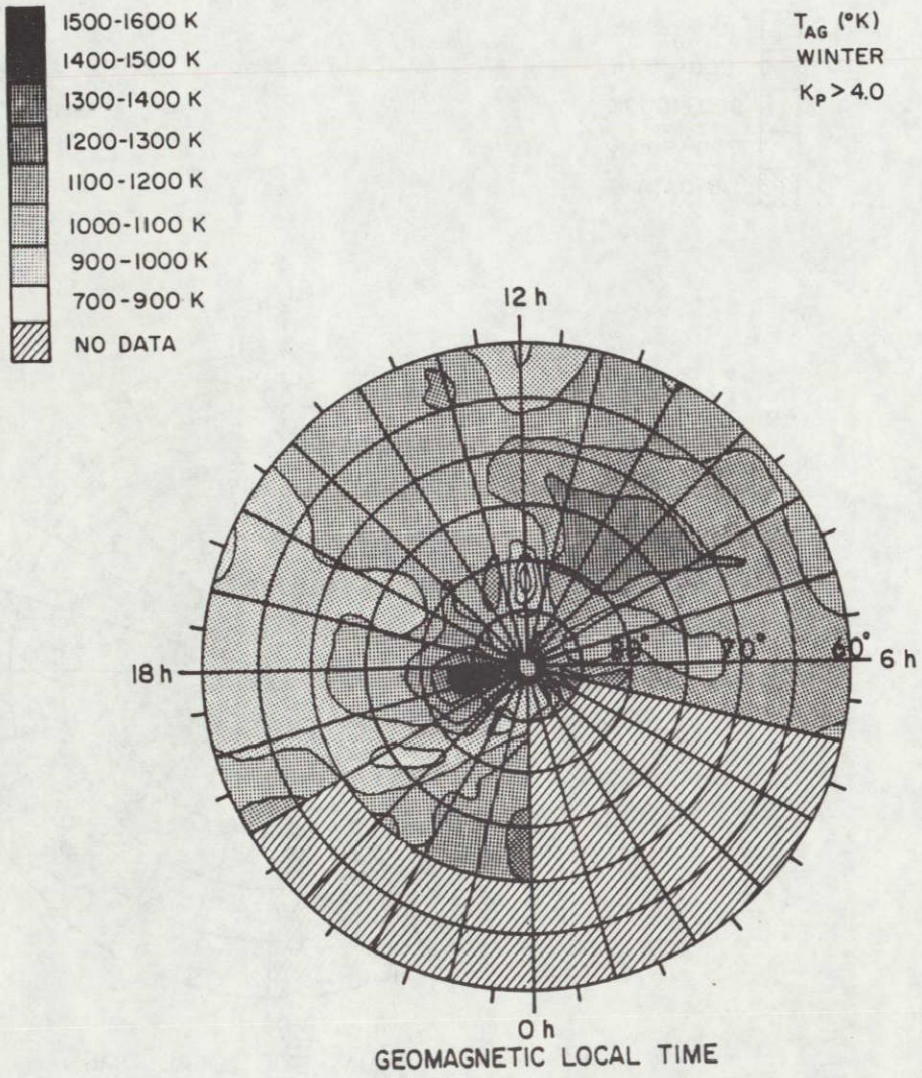

Figure 9: 630 nm airglow temperature as a function of geomagnetic time and geomagnetic latitude for Kp range > 4.0 for winter.

T_{AG} (K)

SUMMER

Kp = 0.0 - 1.3

Local Geomagnetic Time in Hours

Geomagnetic Latitude	1	2	3	4	5	6	7	8	9	10	11	12	13	14	15	16	17	18	19	20	21	22	23	24
85 - 90	1150	1098	920	1133	1113	1094	1028	1124	1228	1087	1185	1124	1234	1026	1177	946	910	959	1232	1165	1155	1148	987	1194
	1	3	3	5	1	2	6	2	3	4	4	2	3	2	3	1	2	3	2	2	1	2	3	2
80 - 85	1085	1037	1130	1081	1232	1064	1130	1109	1025	1126	1090	1098	1224	1144	1313	1176	1091	1135	1247	1219	1130	1262	971	1245
	7	6	8	10	6	8	3	12	3	11	11	13	7	6	5	3	5	7	2	2	5	5	4	4
75 - 80	1054	1159	1153	1125	1117	1195	1089	1226	1158	1109	1157	1092	1074	1181	1195	1233	1172	1236	1181	1224	1156	1194	1250	1314
	5	10	9	8	5	13	11	8	10	10	16	18	13	14	14	12	10	4	11	9	6	9	1	6
70 - 75	1180	1139	1207	1079	1159	1140	1176	1157	1157	1102	1156	1083	1168	1139	1195	1192	1220	1157	1153	1173	1172	1196	1227	1200
	1	7	18	15	13	18	12	13	19	12	19	22	17	13	15	12	11	5	12	6	8	2	1	1
65 - 70	1253	1029	1135	1175	1107	1143	1129	1108	1103	1005	1100	1107	1119	1152	1184	1170	1172	1189	1148	1286	1138	1121	1060	1118
	1	1	12	23	19	13	14	17	21	7	16	37	17	18	13	17	11	14	14	8	11	7	1	2
60 - 65	0	0	1296	1154	1153	1127	1087	1137	1084	1080	1053	1056	1079	1108	1100	1147	1156	1179	1172	1192	1091	1043	1185	0
	0	0	4	21	23	23	40	32	16	16	20	26	21	23	13	12	20	22	17	10	11	10	1	0

Table 2: 630 nm airglow temperatures and numbers of samples of averaged data tabulated by geomagnetic latitude and geomagnetic time for Kp range 0.0 to 1.3 for summer.

T_{AG} (K)

SUMMER

Kp = 0.0-1.3

Coefficient		Geomagnetic Latitude 60-65	65-70	70-75	75-80	80-85	85-90
A_o			1136	1164	1167	1137	1099
A_1	INSUFFICIENT DATA		15.12	19.23	19.08	-10.15	-12.24
B_1			-33.83	-19.30	-32.32	-46.10	14.15
A_2			-27.23	- 0.20	-14.02	-17.56	37.72
B_2			16.12	1.04	-12.24	12.49	-47.26
A_3			- 3.88	26.23	29.10	-19.61	-37.48
B_3			- 5.18	- 7.71	- 6.22	-33.05	-13.27
A_4			2.61	- 1.31	- 3.15	-12.64	- 7.33
B_4			22.99	- 3.34	-12.48	12.43	40.14
A_5			8.82	- 7.03	13.07	25.30	47.18
B_5			16.61	- 1.56	-10.44	15.00	21.79

Table 3: Fourier coefficients for the 630 nm airglow temperatures tabulated by geomagnetic latitude for Kp range 0.0 to 1.3 for summer.

$$T_{AG}(K) = A_O + \sum_{n=1}^{\infty} \left(A_n \cos \frac{2\pi nt}{T} + B_n \sin \frac{2\pi nt}{T}\right)$$

T_{AG}(K)

SUMMER

Kp = 1.3 - 4 0

Local Geomagnetic Time in Hours

Geomagnetic Latitude	1	2	3	4	5	6	7	8	9	10	11	12	13	14	15	16	17	18	19	20	21	22	23	24
85 - 90	1112	1220	1060	1242	1033	1335	1203	1234	1156	1193	1188	1284	1229	1315	1185	1050	1241	1190	1168	1199	1162	1215	1211	1279
	2	5	6	6	2	6	8	4	5	6	4	7	5	2	3	2	3	6	1	2	2	2	4	8
80 - 85	1175	1192	1228	1216	1231	1200	1185	1178	1257	1247	1220	1137	1182	1254	1238	1262	1166	1269	1279	1282	1177	1218	1328	1250
	16	9	14	14	9	8	7	12	11	9	23	12	10	17	8	10	11	9	6	9	5	8	11	12
75 - 80	1184	1272	1228	1234	1220	1208	1219	1250	1265	1217	1195	1210	1199	1209	1188	1260	1185	1253	1198	1259	1239	1329	1271	1305
	14	15	21	19	12	14	15	16	15	25	24	30	23	19	19	19	16	23	11	12	16	10	13	10
70 - 75	1211	1277	1222	1235	1241	1210	1240	1191	1252	1202	1233	1189	1241	1214	1186	1205	1259	1201	1312	1186	1267	1288	1315	1242
	8	8	26	26	23	26	18	22	41	31	35	40	21	29	31	23	30	14	23	12	14	20	13	7
65 - 70	1236	1157	1207	1278	1212	1201	1209	1230	1191	1096	1172	1166	1151	1230	1179	1230	1260	1247	1205	1270	1218	1279	1266	1297
	2	5	23	31	40	34	27	53	44	26	18	33	33	26	33	28	35	31	25	26	21	21	21	7
60 - 65	1298	1171	1333	1229	1198	1165	1173	1213	1185	1115	1115	1079	1144	1164	1158	1198	1216	1203	1178	1229	1221	1258	1210	1266
	2	2	3	43	41	55	67	108	39	20	32	32	36	39	34	37	42	43	39	38	43	22	5	5

Table 4: 630 nm airglow temperatures and numbers of samples of averaged data tabulated by geomagnetic latitude and geomagnetic time for Kp range 1.3 to 4.0 for summer.

T_{AG} (K)

SUMMER

Kp = 1.3-4.0

Geomagnetic Latitude

Coefficient	60-65	65-70	70-75	75-80	80-85	85-90
A_o	1197	1216	1234	1232	1224	1195
A_1	60.66	38.31	24.86	23.65	11.62	-21.76
B_1	- 0.17	-17.81	- 6.37	- 1.82	-18.83	- 1.19
A_2	- 8.61	-14.01	5.12	5.30	- 4.83	16.31
B_2	11.12	0.00	-10.96	-17.11	- 8.42	-13.74
A_3	14.65	13.32	- 0.46	9.33	6.47	- 0.23
B_3	5.07	-15.21	- 2.88	- 5.34	1.59	-27.68
A_4	-16.93	6.59	3.74	-11.91	- 6.86	29.02
B_4	2.68	- 7.32	- 7.95	- 8.83	-11.91	21.39
A_5	- 1.36	2.46	- 2.61	- 5.29	37.07	- 5.24
B_5	-12.68	-16.09	-14.63	-13.04	-10.37	-16.13

Table 5: Fourier coefficients for the 630 nm airglow temperatures tabulated by geomagnetic latitude for Kp range 1.3 to 4.0 for summer.

$$T_{AG}(K) = A_0 + \sum_{n=1}^{\infty} \left(A_n \cos \frac{2\pi nt}{T} + B_n \sin \frac{2\pi nt}{T}\right)$$

T_{AG} (K)

SUMMER

Kp > 4.0

Local Geomagnetic Time in Hours

Geomagnetic Latitude	1	2	3	4	5	6	7	8	9	10	11	12	13	14	15	16	17	18	19	20	21	22	23	24
85 - 90	0	1246	0	0	1567	1404	0	0	0	1514	1338	1528	1563	1725	1113	0	0	0	0	0	1399	0	0	0
	0	1	0	0	1	2	0	0	0	1	1	1	1	1	2	0	0	0	0	0	2	0	0	0
80 - 85	1419	1333	1485	1276	1373	1253	1559	0	1439	0	1452	1401	1291	1252	1295	1362	1408	1302	1334	1427	1552	0	1648	1170
	3	3	2	1	2	1	1	0	4	0	2	3	1	1	2	2	2	3	1	1	1	0	1	1
75 - 80	1177	0	1487	1447	0	1372	1411	1251	1280	1368	0	1360	1290	1328	1344	1290	1371	1225	0	1277	0	0	0	0
	1	0	6	1	0	7	2	1	5	3	0	5	3	6	3	4	5	3	0	2	0	0	0	0
70 - 75	0	1415	1282	1354	1274	1343	1360	1192	1354	1364	1364	1374	1434	1315	1211	1296	1321	1259	1332	1315	1334	1412	0	0
	0	1	1	4	3	2	1	7	6	5	7	7	3	2	4	3	2	3	4	1	2	2	0	0
65 - 70	0	0	1254	1364	1432	1314	1350	1328	1290	1705	1398	1369	1392	1366	1361	1269	1358	1358	1192	1232	1210	1256	0	0
	0	0	1	5	4	5	4	7	6	1	5	5	8	10	3	7	6	4	1	3	1	1	0	0
60 - 65	0	0	0	1375	1401	1262	1211	1323	1487	1276	1289	1371	1281	1562	1277	1267	1313	1309	1314	1212	1268	1237	1326	0
	0	0	0	3	5	6	5	16	2	2	5	2	7	3	4	3	8	2	3	5	2	3	1	0

Table 6: 630 nm airglow temperatures and numbers of samples of averaged data tabulated by geomagnetic latitude and geomagnetic time for Kp range > 4.0 for summer.

$T_{AG}(K)$

EQUINOX

Kp = 0 0 - 1.3

Local Geomagnetic Time in Hours

Geomagnetic Latitude	1	2	3	4	5	6	7	8	9	10	11	12	13	14	15	16	17	18	19	20	21	22	23	24
85 - 90	1179	1115	1098	1157	1131	1080	1132	1052	1131	1038	1066	1207	1191	1009	1059	1080	1087	1031	1036	1120	969	1171	976	1126
	3	8	7	11	6	32	8	12	6	4	6	8	5	5	5	7	8	5	4	8	6	10	3	9
80 - 85	1151	1190	1136	1063	1108	1049	1049	1033	1102	1054	1067	1102	1066	1091	1139	1098	1074	1035	1024	1143	1157	1106	1152	1093
	15	8	17	16	17	26	27	21	29	29	35	31	24	16	23	18	20	16	19	14	9	10	16	16
75 - 80	1097	1113	1087	1070	1042	1043	1046	1079	1037	1089	1070	1048	1054	1129	1096	1009	1110	1122	1087	1122	1096	1131	1136	1098
	22	26	20	37	31	37	48	45	29	30	45	47	40	27	37	27	35	18	25	19	17	20	24	25
70 - 75	1068	1081	1031	1030	987	1003	1046	1051	1052	1055	1022	1077	1029	1024	1043	993	1084	1090	1102	1111	1099	1062	1083	1138
	20	20	14	20	23	44	75	65	47	50	58	69	62	56	68	33	37	33	19	30	20	19	26	20
65 - 70	1034	1047	1033	1039	1016	1018	1070	1023	1068	1016	1039	1013	1011	969	1060	1098	1078	1017	1038	1086	1038	1089	1071	1121
	16	20	15	26	26	27	86	74	53	59	73	85	86	73	68	46	31	32	24	22	14	20	24	15
60 - 65	1179	1145	1101	1124	947	992	1055	1039	946	1026	1004	999	955	1063	1142	1131	1076	1060	1084	1157	1045	1140	1064	1132
	3	4	4	8	10	12	52	59	55	47	59	68	51	30	21	18	22	24	17	13	7	8	1	6

Table 7: 630 nm airglow temperature and numbers of samples of averaged data tabulated by geomagnetic latitude and geomagnetic time for Kp range 0.0 to 1.3 for equinox.

$T_{AG}(K)$

EQUINOX

Kp = 0.0 - 1.3

Coefficient	Geomagnetic Latitude 60-65	65-70	70-75	75-80	80-85	85-90
A_o	1067	1045	1056	1084	1096	1093
A_1	53.70	17.71	21.70	21.83	31.60	- 1.40
B_1	-33.47	-11.03	-23.24	-21.01	- 6.05	28.52
A_2	5.95	- 1.79	9.21	11.53	27.91	15.79
B_2	26.44	- 8.76	-20.78	- 4.52	13.29	19.45
A_3	20.60	19.18	2.13	0.84	0.70	-15.63
B_3	14.00	1.70	15.47	2.70	- 4.08	2.46
A_4	-23.31	- 4.30	6.35	- 4.30	-23.47	16.36
B_4	12.23	-11.98	13.84	4.81	1.67	9.88
A_5	- 3.89	- 5.72	0.31	3.90	- 5.91	-17.49
B_5	19.62	7.07	- 5.06	-10.01	17.39	0.75

Table 8: Fourier coefficients for the 630 nm airglow temperatures tabulated by geomagnetic latitude for Kp range 0.0 to 1.3 for equinox.

$$T_{AG}(K) = A_0 + \sum_{n=1}^{\infty} \left(A_n \cos \frac{2\pi nt}{T} + B_n \sin \frac{2\pi nt}{T}\right)$$

T_{AG}(K)

EQUINOX

Kp = 1.3 - 4.0

Local Geomagnetic Time in Hours

Geomagnetic Latitude	1	2	3	4	5	6	7	8	9	10	11	12	13	14	15	16	17	18	19	20	21	22	23	24
85 - 90	1014	1174	1147	1180	1173	1119	1185	1112	1166	1166	1121	1224	1167	1156	1126	1259	1322	1183	1191	1143	1230	1202	1210	1089
	7	13	9	12	13	10	12	10	8	6	9	6	9	11	13	6	8	7	3	7	12	2	14	12
80 - 85	1243	1215	1221	1184	1190	1192	1172	1138	1132	1181	1146	1180	1139	1225	1115	1185	1182	1087	1212	1127	1164	1103	1145	1147
	34	22	29	27	30	30	35	36	38	44	50	42	46	24	31	25	22	25	18	23	31	22	25	23
75 - 80	1177	1170	1065	1170	1159	1171	1165	1138	1170	1150	1156	1142	1159	1172	1189	1147	1223	1144	1144	1136	1167	1174	1174	1141
	37	33	29	33	43	66	73	46	58	58	63	73	72	61	54	50	40	53	38	32	44	39	35	33
70 - 75	1151	1157	1192	1116	1110	1167	1169	1156	1139	1136	1121	1112	1122	1100	1141	1095	1087	1150	1133	1167	1157	1170	1194	1201
	36	26	31	37	35	68	111	94	78	73	113	110	101	80	73	81	66	49	48	47	45	41	49	43
65 - 70	1164	1086	1089	1105	1079	1115	1177	1148	1108	1115	1083	1100	1083	1091	1108	1096	1090	1147	1091	1134	1174	1192	1134	1156
	28	24	30	36	50	53	132	116	116	114	145	129	140	143	132	85	81	64	56	46	33	55	50	50
60 - 65	1185	1155	1069	1046	1089	1092	1131	1065	1052	1070	1060	1049	1061	1063	1131	1085	1073	1103	1159	1081	1152	1122	1083	1113
	2	5	18	31	42	66	135	125	125	155	216	147	115	103	149	122	92	70	60	50	43	63	41	19

Table 9: 630 nm airglow temperature and numbers of samples of averaged data tabulated by geomagnetic latitude and geomagnetic time for Kp range 1.3 to 4.0 for equinox.

$T_{AG}(K)$

EQUINOX

Kp = 1.3 - 4.0

Geomagnetic Latitude

Coefficient	60-65	65-70	70-75	75-80	80-85	85-90
A_o	1095	1119	1143	1159	1168	1169
A_1	30.19	20.84	26.70	- 3.36	9.24	-12.72
B_1	-11.42	- 2.62	8.66	- 7.38	16.33	-34.41
A_2	- 1.31	1.35	6.68	- 0.63	3.10	-24.82
B_2	- 0.50	-25.03	-14.74	0.83	25.40	- 1.39
A_3	11.41	15.71	6.78	13.47	- 5.48	- 7.63
B_3	1.65	-11.49	- 3.68	- 8.86	9.29	- 4.25
A_4	2.89	0.46	- 0.87	5.37	1.95	- 4.78
B_4	19.65	5.89	8.70	- 6.65	11.17	-35.36
A_5	- 1.34	- 8.06	- 1.22	1.06	1.79	-33.68
B_5	21.53	1.61	- 2.54	5.38	13.86	- 18.42

Table 10: Fourier coefficients for the 630 nm airglow temperatures tabulated by geomagnetic latitude for Kp range 1.3 to 4.0 for equinox.

$$T_{AG}(K) = A_0 + \sum_{n=1}^{\infty} \left(A_n \cos \frac{2\pi nt}{T} + B_n \sin \frac{2\pi nt}{T}\right)$$

T_{AG} (K)

EQUINOX

Kp > 4.0

Local Geomagnetic Time in Hours

Geomagnetic Latitude	1	2	3	4	5	6	7	8	9	10	11	12	13	14	15	16	17	18	19	20	21	22	23	24
85 - 90	0	1813	1335	0	1227	1151	0	1342	1397	1303	0	1203	1346	0	1261	1195	1348	0	1296	0	0	1142	0	1364
	0	1	1	0	1	2	0	2	2	2	0	2	1	0	1	2	1	0	1	0	0	2	0	2
80 - 85	1483	1356	1334	1267	1421	1287	1366	1303	1345	1137	1416	1465	1297	1317	1313	1232	1402	1248	1333	1369	1357	1292	1439	1313
	2	1	3	4	7	3	7	6	2	2	6	3	2	6	4	5	1	3	3	2	4	4	7	4
75 - 80	1205	1282	1528	1458	1313	1525	1375	1326	1432	1379	1457	1326	1315	1411	1310	1467	1338	1299	1232	1267	1512	1340	1511	1139
	3	3	3	2	3	7	14	3	3	10	10	12	10	4	7	4	3	4	1	5	4	9	2	3
70 - 75	1350	1371	1297	1355	1439	1414	1449	1336	1297	1308	1318	1388	1302	1338	1304	1293	1249	1282	1397	1321	1375	1307	1229	1317
	4	5	4	3	2	7	11	31	10	7	11	7	18	16	14	11	4	6	2	5	6	4	5	2
65 - 70	1339	1337	1237	1226	1394	1437	1404	1357	1374	1266	1377	1295	1231	1323	1284	1343	1270	1324	1280	1333	1412	1230	1329	1280
	4	4	3	5	4	6	21	15	12	12	11	9	14	19	16	11	12	5	6	4	6	7	8	4
60 - 65	1310	1290	1270	1252	1231	1340	1311	1317	1281	1234	1322	1308	1232	1344	1252	1261	1177	1165	1315	1399	1270	1184	1332	1331
	1	1	1	3	7	10	25	12	19	14	16	11	13	12	25	16	6	10	4	4	9	7	6	5

Table 11: 630 nm airglow temperatures and numbers of samples of averaged data tabulated by geomagnetic altitude and geomagnetic time for Kp range > 4.0 for equinox.

$T_{AG}(K)$

EQUINOX

Kp > 4.0

Coefficient	Geomagnetic Latitude 60-65	65-70	70-75	75-80	80-85	85-90
A_o	1280	1321	1334	1369	1339	INSUFFICIENT DATA
A_1	6.65	- 3.79	1.27	-19.45	28.02	
B_1	15.01	23.27	35.67	31.81	4.48	
A_2	15.73	-22.68	-23.50	-10.13	29.39	
B_2	-15.32	-25.98	- 1.84	- 2.41	2.66	
A_3	- 2.39	15.07	-25.19	-18.58	- 6.13	
B_3	-12.22	-15.06	-19.12	-37.78	- 5.79	
A_4	4.01	12.69	14.00	-42.17	36.68	
B_4	36.91	11.10	26.34	-58.34	15.62	
A_5	18.24	- 2.72	- 0.91	-34.03	-17.11	
B_5	24.43	40.03	27.30	-11.26	13.73	

Table 12: Fourier coefficients for the 630 nm airglow temperatures tabulated by geomagnetic latitude for Kp range > 4.0 for equinox.

$$T_{AG}(K) = A_0 + \sum_{n=1}^{\infty} \left(A_n \cos \frac{2\pi nt}{T} + B_n \sin \frac{2\pi nt}{T}\right)$$

T_{AG}(K)

WINTER

Kp = 0.0 - 1.3

Local Geomagnetic Time in Hours

Geomagnetic Latitude	1	2	3	4	5	6	7	8	9	10	11	12	13	14	15	16	17	18	19	20	21	22	23	24
85 - 90	974	1053	773	787	953	1029	903	975	998	989	1016	0	946	863	999	927	899	910	923	1081	1103	1075	0	992
	2	4	2	3	2	4	1	4	1	4	5	0	2	3	2	4	2	4	1	1	3	3	0	1
80 - 85	892	899	1039	992	930	877	958	1063	973	1032	876	994	962	931	973	1026	953	983	908	922	915	914	1083	1005
	3	3	6	6	5	5	9	2	7	7	4	8	11	13	21	12	16	3	11	5	7	5	4	7
75 - 80	1020	911	939	1026	906	1057	909	955	970	1010	937	905	932	896	940	883	925	932	921	1069	918	1016	1020	1001
	1	5	4	9	7	9	6	11	12	18	15	17	15	16	19	18	13	10	15	4	12	8	2	4
70 - 75	0	1091	858	995	1045	984	890	924	916	970	903	973	979	915	896	861	937	944	917	893	926	0	0	0
	0	1	4	6	8	9	8	10	21	24	18	22	21	28	22	10	11	13	20	17	3	0	0	0
65 - 70	0	976	858	1168	1146	854	976	952	917	922	938	925	948	899	973	961	948	990	893	943	1111	0	0	706
	0	1	2	4	3	7	12	21	22	19	18	28	26	25	26	14	13	19	19	9	3	0	0	1
60 - 65	0	0	0	1200	1158	914	982	983	842	862	966	900	911	925	939	908	883	1061	992	1178	0	0	0	0
	0	0	0	3	5	11	8	12	21	21	33	42	43	41	21	26	19	15	22	3	0	0	0	0

Table 13: 630 nm airglow temperatures and numbers of samples of averaged data tabulated by geomagnetic latitude and geomagnetic time for Kp range 0.0 to 1.3 for winter.

T_{AG} (K)

WINTER

Kp = 1.3 - 4.0

Local Geomagnetic Time in Hours

Geomagnetic Latitude	1	2	3	4	5	6	7	8	9	10	11	12	13	14	15	16	17	18	19	20	21	22	23	24
85 - 90	1053	1098	1039	982	1118	1099	1025	1205	1062	1014	1071	1134	1072	1152	1095	1084	955	1024	1039	1009	1075	1015	1158	1229
	7	7	6	8	5	4	5	6	8	4	7	5	9	8	4	7	5	6	3	3	5	7	3	5
80 - 85	1044	1063	993	1199	1127	1103	1072	1021	1059	1035	1083	1043	1170	1122	1061	1067	1047	1089	1073	1060	1019	1002	1000	1051
	6	14	13	15	11	5	12	18	16	17	11	17	18	20	23	27	12	22	19	19	20	6	13	12
75 - 80	871	990	1147	1048	1129	1075	1117	1104	1061	1031	1115	1106	1076	1100	1058	1063	1047	1055	1047	1031	1007	1030	980	1001
	3	10	8	19	11	18	22	21	25	26	36	27	31	22	32	19	35	33	37	29	19	11	4	5
70 - 75	1010	857	1044	944	1012	1092	1039	1024	1035	1025	1013	1045	996	987	993	993	1058	998	1036	962	979	1103	986	1182
	1	5	7	11	20	15	30	34	34	44	48	44	48	47	33	23	21	30	57	46	13	6	3	2
65 - 70	760	839	787	1022	1096	944	976	1097	1002	1024	1024	1038	1005	983	960	957	997	996	1007	962	1064	969	1157	693
	1	1	3	16	16	31	42	34	47	54	55	54	50	45	29	32	25	36	52	36	7	2	1	1
60 - 65	0	0	975	971	1039	973	999	981	997	987	974	979	994	998	1003	977	947	1014	1001	945	1056	729	0	0
	0	0	1	6	8	23	34	50	59	61	70	66	59	48	44	44	55	46	72	23	4	3	0	0

Table 14: 530 nm airglow temperature and numbers of samples of averaged data tabulated by geomagnetic latitude and geomagnetic time for Kp range 1.3 to 4.0 for winter.

T_{AG} (K)

WINTER

Kp = 1.3-4.0

Coefficient		Geomagnetic Latitude 60-65	65-70	70-75	75-80	80-85	85-90
A_o	INSUFFICIENT DATA		976	1015	1052	1066	1074
A_1			-52.89	- 3.07	-47.67	-20.92	- 3.72
B_1			-10.34	3.91	20.28	10.59	16.21
A_2			-30.42	- 0.28	-29.46	-15.59	33.42
B_2			-58.02	-21.81	5.92	28.74	0.72
A_3			-25.02	19.52	-26.04	-24.98	26.61
B_3			-43.84	-13.48	-15.51	-12.13	-30.21
A_4			0.17	29.10	- 5.40	13.96	12.99
B_4			-44.80	-15.36	- 7.81	4.62	17.62
A_5			1.82	3.56	-14.04	21.21	15.02
B_5			-37.43	- 4.84	-17.63	- 6.43	- 4.31

Table 15: Fourier coefficients for the 630 nm airglow temperatures tabulated by geomagnetic latitude for Kp range 1.3 to 4.0 for winter.

$$T_{AG}(K) = A_0 + \sum_{n=1}^{\infty} \left(A_n \cos \frac{2\pi nt}{T} + B_n \sin \frac{2\pi nt}{T}\right)$$

T_{AG} (K)

WINTER

Kp > 4 0

Local Geomagnetic Time in Hours

Geomagnetic Latitude	1	2	3	4	5	6	7	8	9	10	11	12	13	14	15	16	17	18	19	20	21	22	23	24
85 - 90	1071	1438	0	1076	0	1177	0	936	0	1307	1269	0	0	1168	0	1217	0	1177	0	0	0	0	1202	0
	1	1	0	2	0	2	0	1	0	1	1	0	0	2	0	1	0	1	0	0	0	0	1	0
80 - 85	1096	0	0	0	0	1236	1417	1233	1031	1281	1180	1164	0	1283	1141	0	1313	1313	1546	1275	1348	987	884	1287
	3	0	0	0	0	1	1	1	2	1	1	4	0	4	1	0	2	3	1	2	2	2	1	1
75 - 80	1348	0	0	0	1179	1189	1202	1196	1202	1291	1341	1407	971	1235	1157	1215	948	1158	1135	1163	860	1104	1223	1250
	3	0	0	0	2	4	2	2	6	3	5	1	2	4	1	1	4	3	2	4	1	3	1	2
70 - 75	0	1311	942	1151	1549	1294	1197	1182	1285	1388	1307	1295	1351	1123	1196	1097	1110	1102	1122	1087	1037	1195	0	0
	0	3	2	1	1	3	2	2	6		3	3	4	4	5	4	3	3	4	6	2	4	0	0
65 - 70	0	977	1255	1051	0	1196	1294	1308	1311	1212	1188	1153	1106	1211	1162	1138	1081	1063	1003	1079	1241	0	0	1270
	0	1	3	4	0	3	5	4	4	13	2	5	5	5	5	5	1	1	7	5	2	0	0	1
60 - 65	0	0	1053	1247	1187	1177	1270	1142	1126	1240	1079	1148	945	1216	1141	1152	1006	0	1056	1104	0	0	0	0
	0	0	2	3	3	6	5	7	4	8	12	10	7	4	7	9	8	0	12	4	0	0	0	0

Table 16: 630 nm airglow temperatures and numbers of samples of averaged data tabulated by geomagnetic time for Kp range > 4.0 for winter.

Table 17: Data index for atomic oxygen density.

	Summer	Equinox	Winter
0 < Kp < 1.3	Tabulated Values: Table 18, p. 62	Tabulated Values: Table 23, p. 67	Tabulated Values: Table 29, p. 73
	Graphical Analysis: Figure 10, p. 53	Graphical Analysis: Figure 13, p. 56	Graphical Analysis: Figure 16, p. 59
	Fourier Analysis: Table 19, p. 63	Fourier Analysis: Table 24, p. 68	Fourier Analysis: Insufficient Data
1.3 < Kp < 4.0	Tabulated Values: Table 20, p. 64	Tabulated Values: Table 25, p. 69	Tabulated Values: Table 30, p. 74
	Graphical Analysis: Figure 11, p. 54	Graphical Analysis: Figure 14, p. 57	Graphical Analysis: Figure 17, p. 60
	Fourier Analysis: Table 21, p. 65	Fourier Analysis: Table 26, p. 70	Fourier Analysis: Table 31, p. 75
Kp > 4.0	Tabulated Values: Table 22, p. 66	Tabulated Values: Table 27, p. 71	Tabulated Values: Table 32, p. 76
	Graphical Analysis: Figure 12, p. 55	Graphical Analysis: Figure 15, p. 58	Graphical Analysis: Figure 18, p. 61
	Fourier Analysis: Insufficient Data	Fourier Analysis: Table 28, p. 72	Fourier Analysis: Insufficient Data

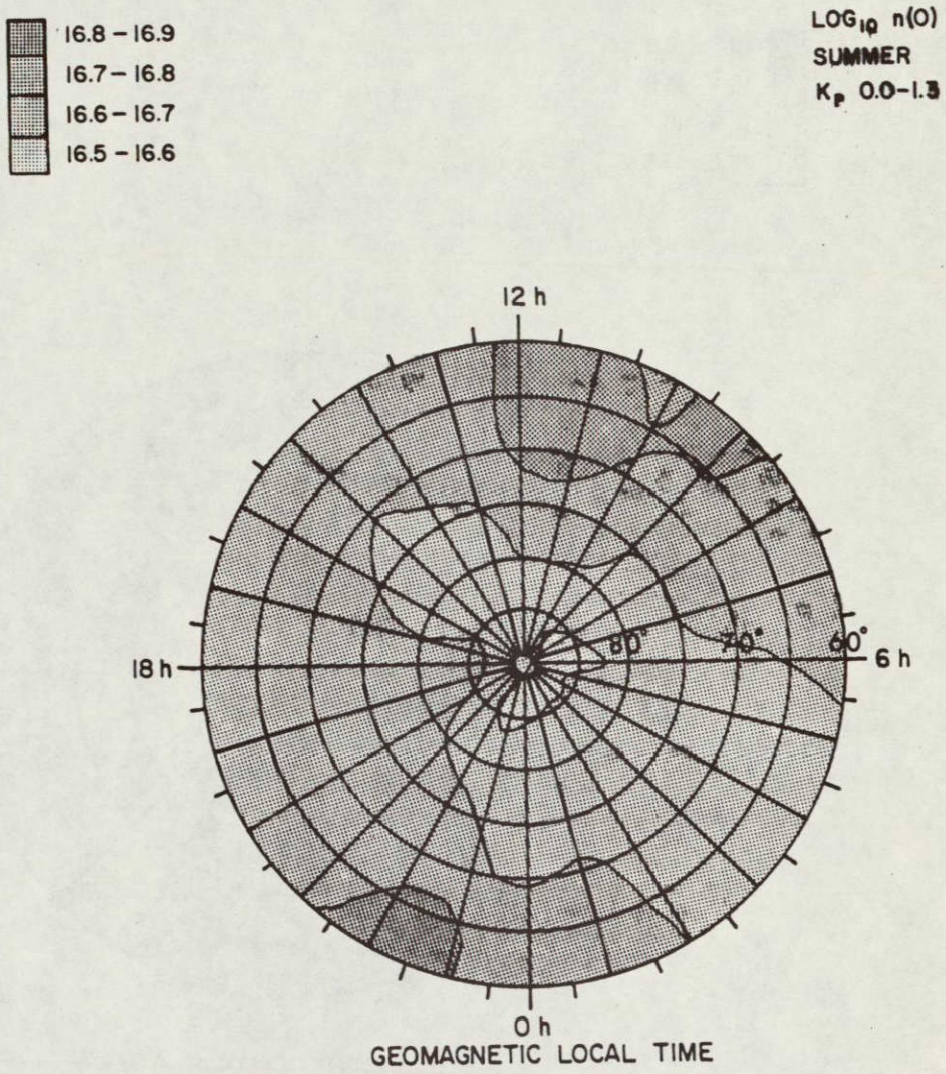

Figure 10: Atomic oxygen density at 120 km as a function of geomagnetic time and geomagnetic latitude for Kp range 0.0 to 1.3 for summer.

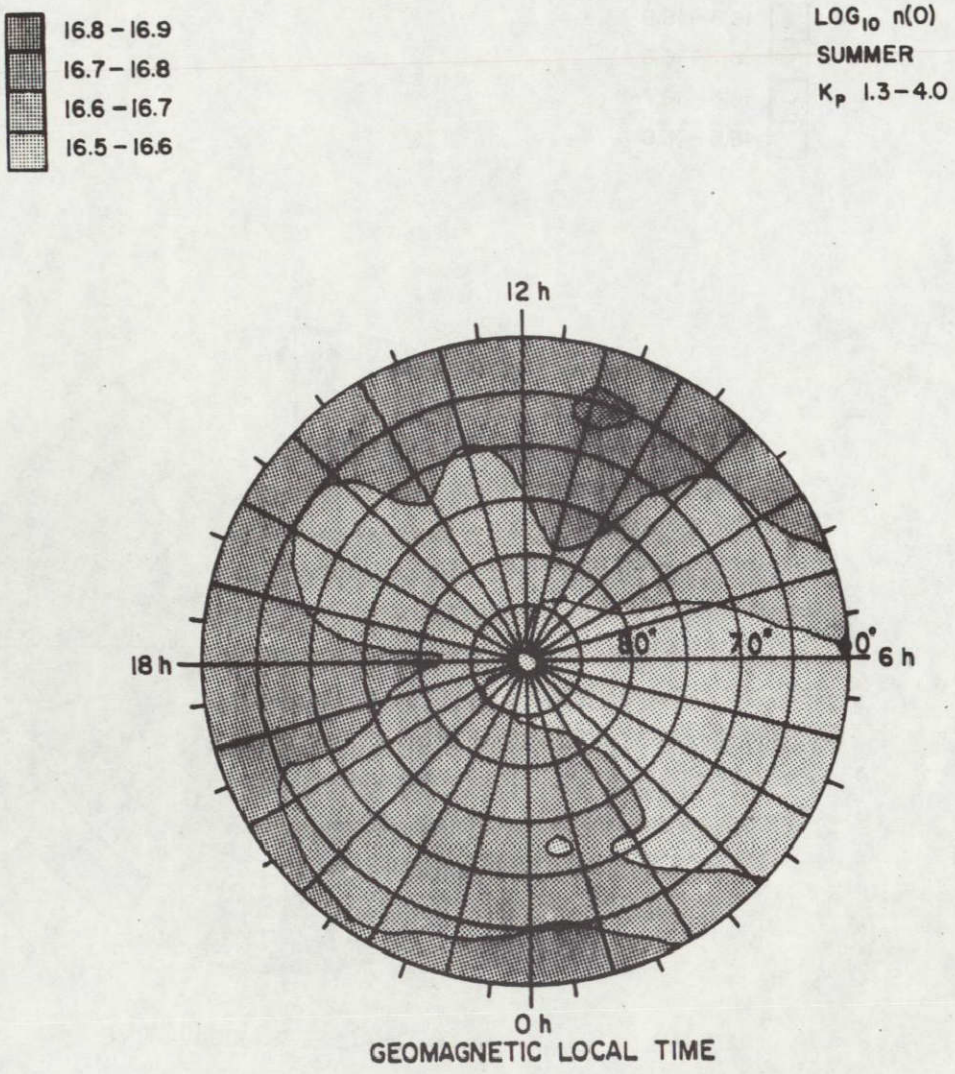

Figure 11: Atomic oxygen density at 120 km as a function of geomagnetic time and geomagnetic latitude for Kp range 1.3 to 4.0 for summer.

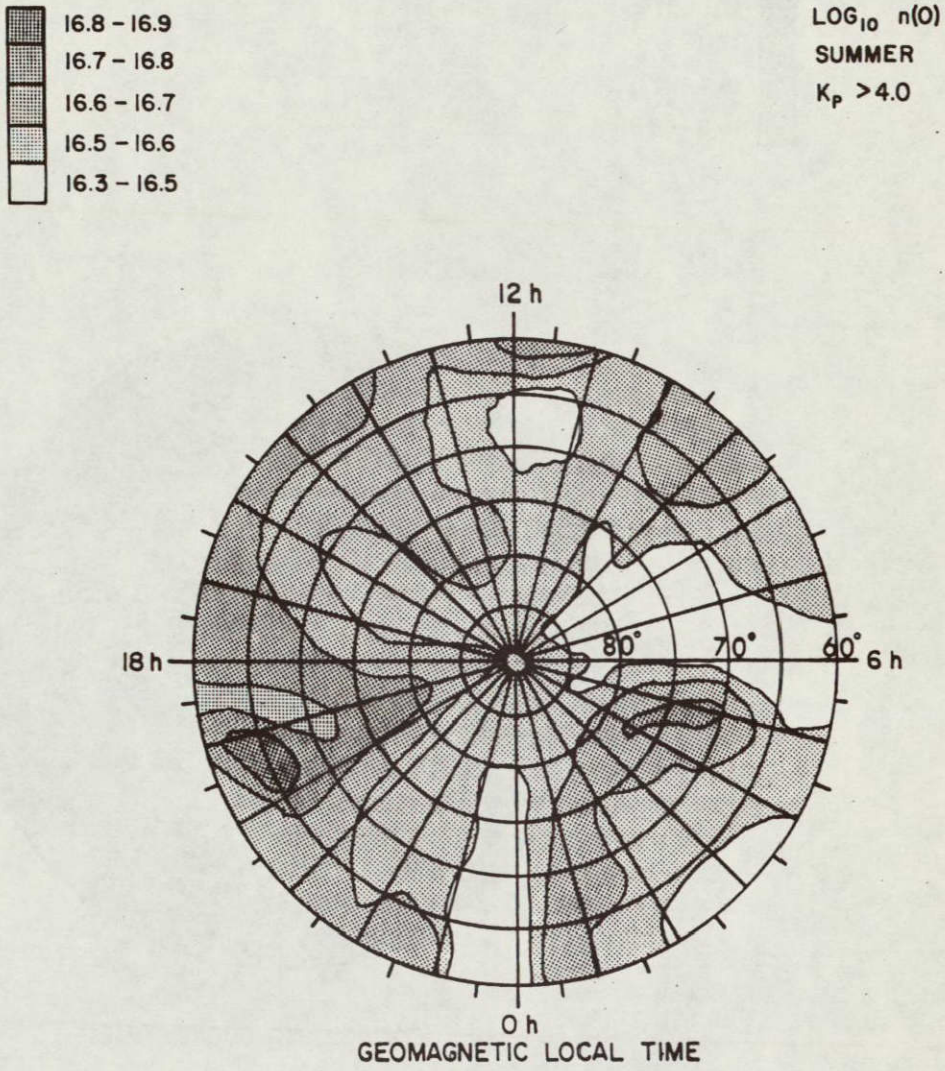

Figure 12: Atomic oxygen density at 120 km as a function of geomagnetic time and geomagnetic latitude for Kp range > 4.0 for summer.

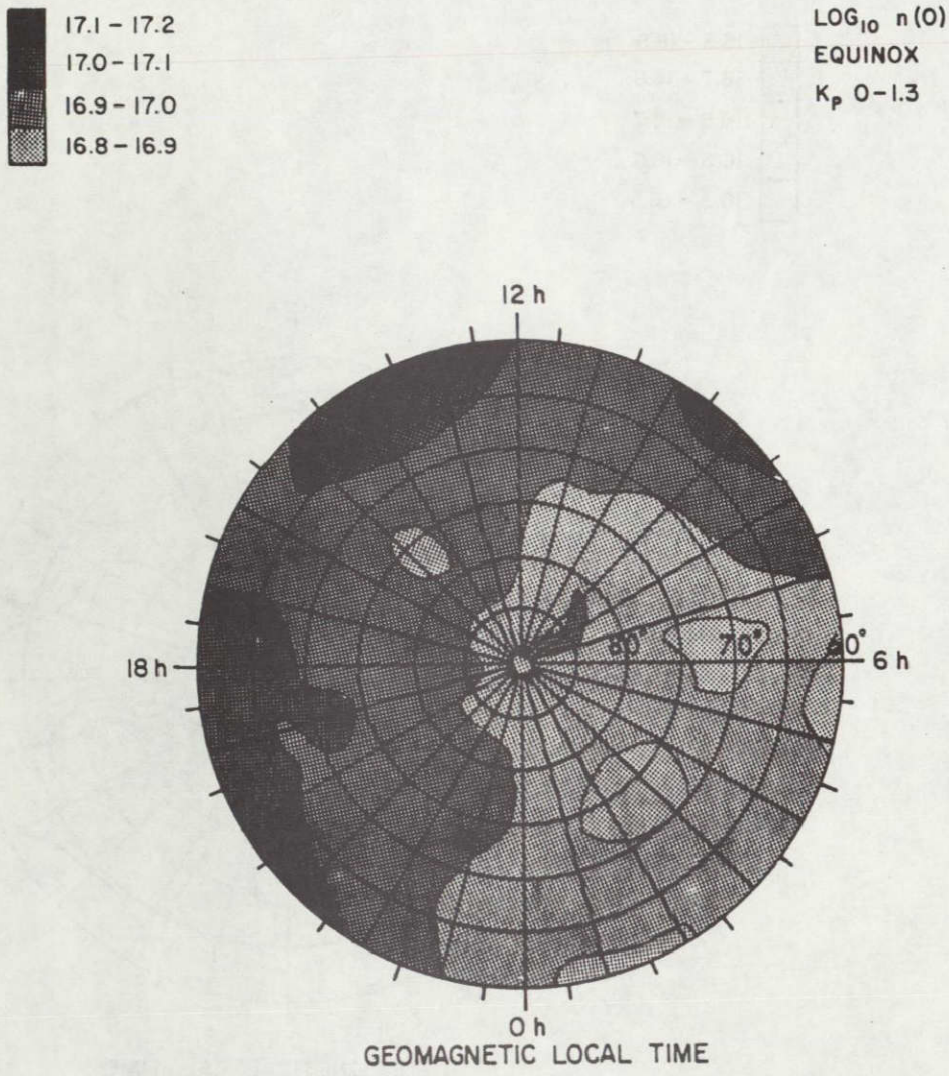

Figure 13: Atomic oxygen density at 120 km as a function of geomagnetic latitude for Kp range 0.0 to 1.3 for equinox.

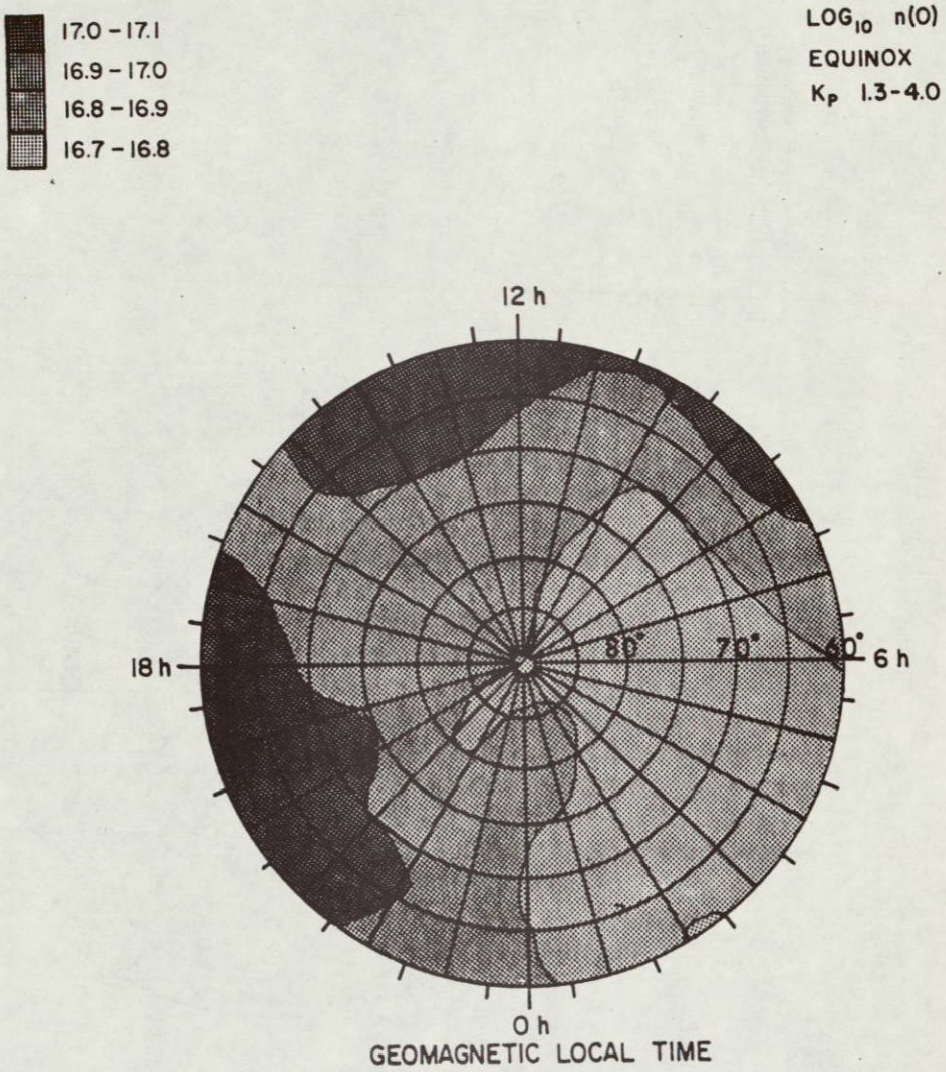

Figure 14: Atomic oxygen density at 120 km as a function of geomagnetic time and geomagnetic latitude for Kp range 1.3 to 4.0 for equinox.

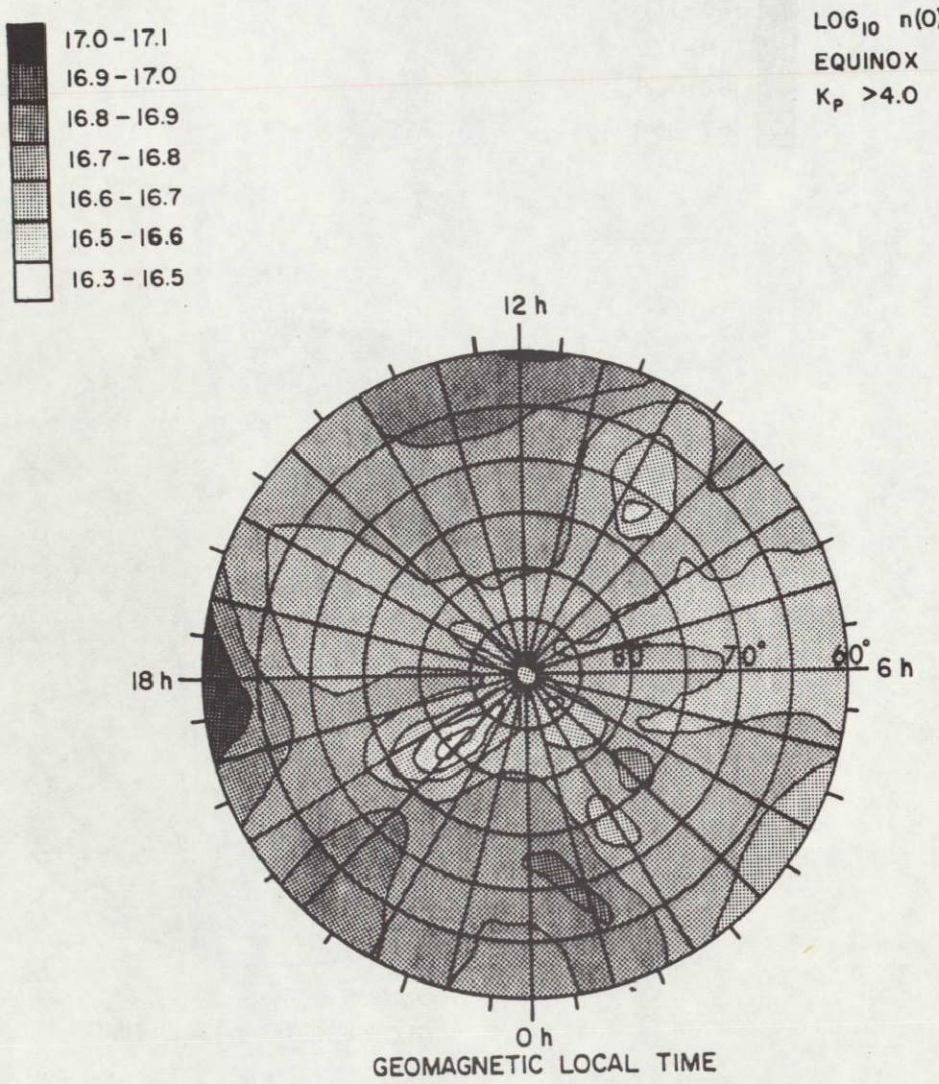

Figure 15: Atomic oxygen density at 120 km as a function of geomagnetic time and geomagnetic latitude for Kp range > 4.0 for equinox.

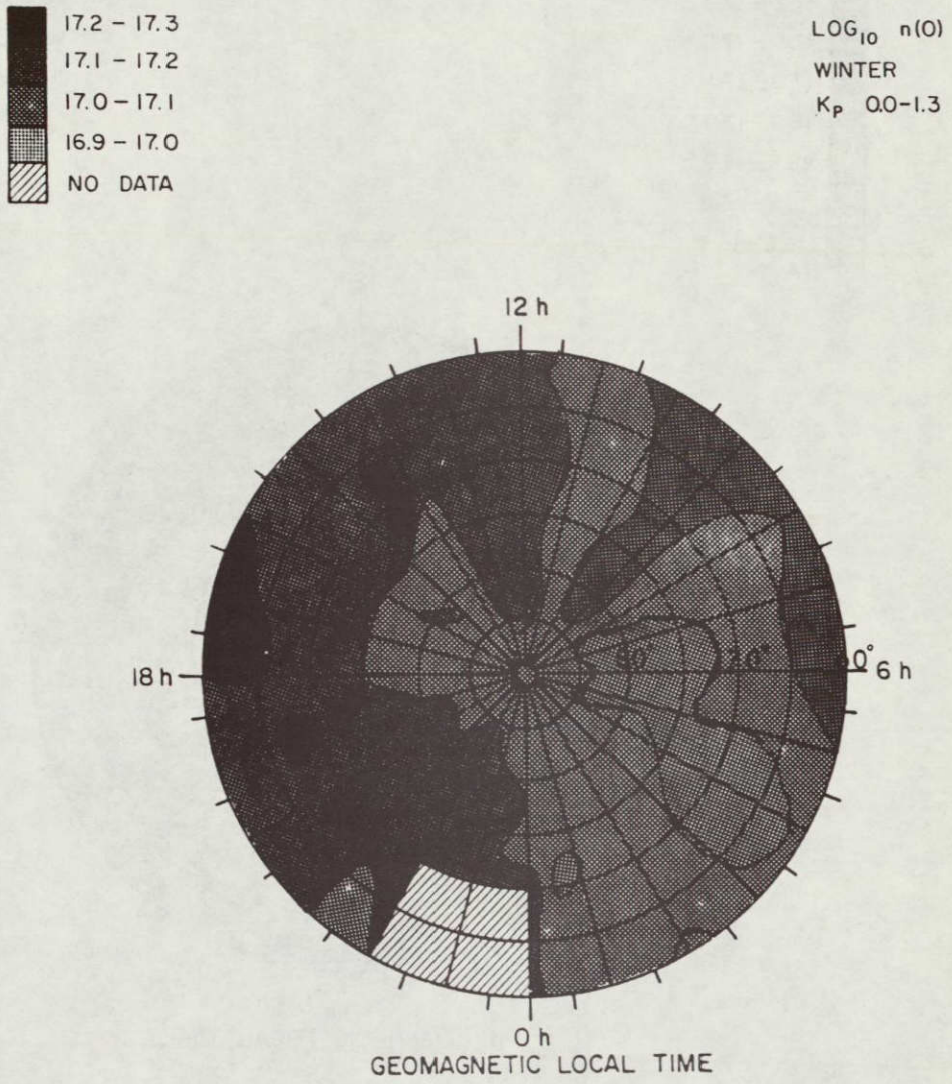

Figure 16: Atomix oxygen density at 120 km as a function of geomagnetic time and geomagnetic latitude for Kp range 0.0 to 1.3 for winter.

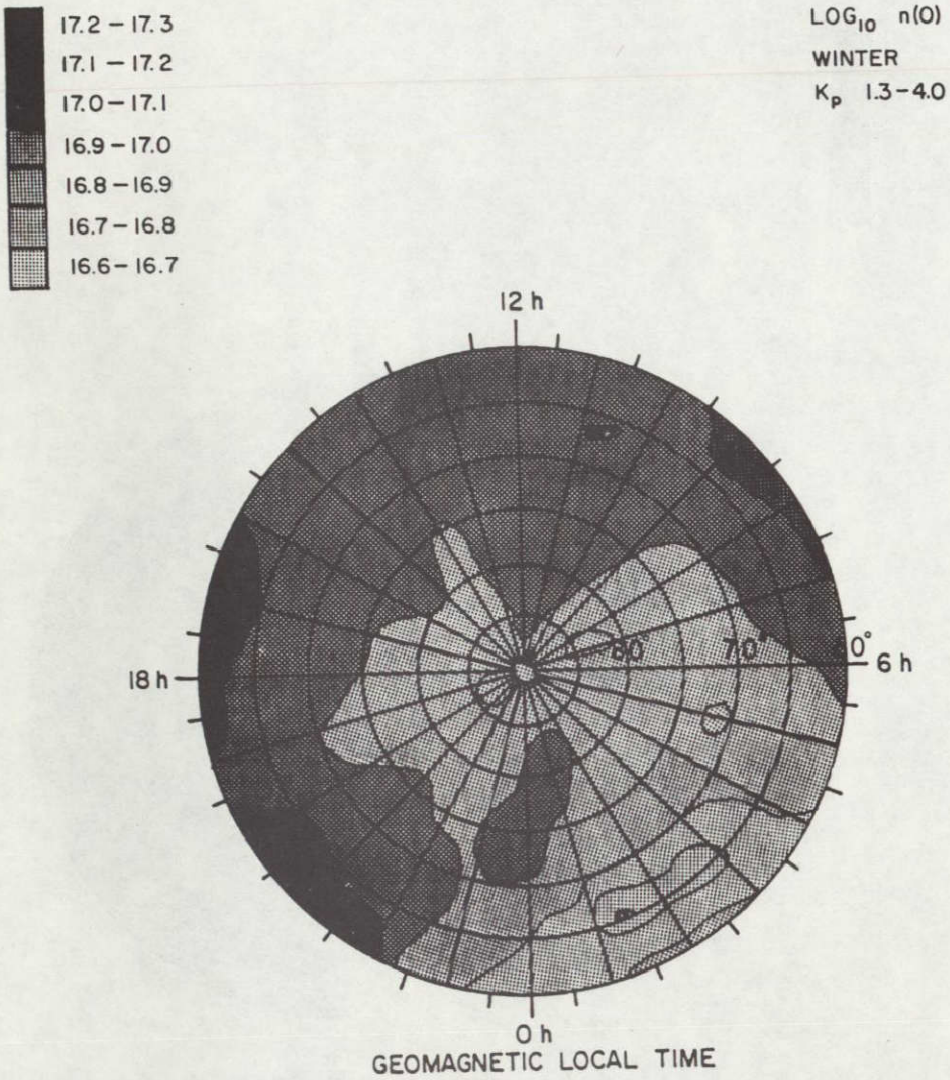

Figure 17: Atomic oxygen density at 120 km as a function of geomagnetic time and geomagnetic latitude for Kp range 1.3 to 4.0 for winter.

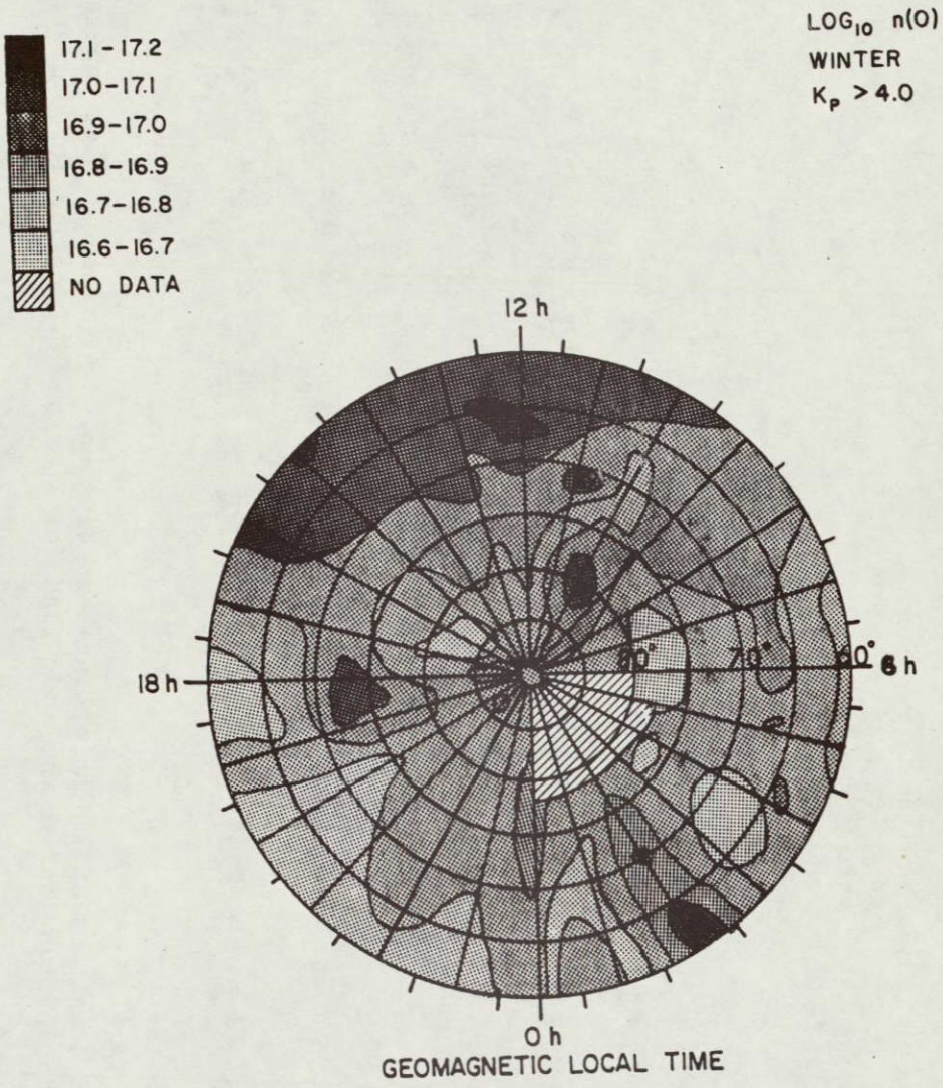

Figure 18: Atomic oxygen density at 120 km as a function of geomagnetic time and geomagnetic latitude for Kp range > 4.0 for winter.

$Log_{10}\ n(0)\ m^{-3}$

SUMMER

Kp = 0.0 - 1.3

Local Geomagnetic Time in Hours

Geomagnetic Latitude	1	2	3	4	5	6	7	8	9	10	11	12	13	14	15	16	17	18	19	20	21	22	23	24
85 - 90	16.61	16.57	16.68	16.64	16.57	16.57	16.59	16.57	16.58	16.56	16.55	16.60	16.61	16.56	16.62	16.62	16.62	16.60	16.59	16.57	16.57	16.56	16.55	16.65
	1	9	8	6	10	15	22	19	20	18	16	36	30	22	23	20	7	5	13	6	1	11	12	14
80 - 85	16.61	16.61	16.66	16.67	16.63	16.61	16.59	16.63	16.60	16.62	16.61	16.62	16.65	16.61	16.67	16.67	16.70	16.70	16.79	16.77	16.72	16.61	16.58	16.64
	31	48	95	67	69	65	99	129	107	105	140	126	136	90	123	142	96	81	25	26	29	15	25	20
75 - 80	16.69	16.66	16.62	16.63	16.64	16.54	16.63	16.69	16.68	16.66	16.74	16.75	16.72	16.67	16.65	16.67	16.67	16.72	16.74	16.75	16.73	16.74	16.64	16.63
	156	41	69	129	149	177	131	106	106	80	48	68	76	100	101	152	147	151	119	113	117	171	1	71
70 - 75	16.65	16.69	16.69	16.65	16.67	16.69	16.68	16.73	16.73	16.76	16.81	16.80	16.80	16.72	16.71	16.70	16.72	16.72	16.72	16.84	16.72	16.72	16.78	16.70
	73	168	175	183	186	187	169	117	127	93	118	87	94	131	170	176	191	162	171	121	204	222	102	1
65 - 70	16.77	16.75	16.68	16.68	16.67	16.67	16.70	16.72	16.76	16.80	16.80	16.83	16.83	16.77	16.73	16.71	16.73	16.74	16.76	16.75	16.73	16.70	16.81	16.79
	48	80	244	263	200	218	217	187	74	18	141	128	101	153	203	208	239	236	282	235	286	245	34	60
60 - 65	16.84	16.82	16.71	16.68	16.66	16.68	16.72	16.76	16.78	16.83	16.80	16.81	16.80	16.79	16.73	16.72	16.74	16.75	16.76	16.78	16.75	16.79	16.88	16.86
	1	1	131	227	188	212	262	200	183	173	214	223	210	215	259	264	260	242	280	295	173	74	50	1

Table 18: Atomic oxygen densities at 120 km and numbers of samples of averaged data tabulated by geomagnetic latitude and geomagnetic time for Kp range 0.0 to 1.3 for summer.

$\text{Log}_{10}\, n(O)m^{-3}$

SUMMER

Kp = 0.0-1.3

Coefficient	Geomagnetic Latitude 60-65	65-70	70-75	75-80	80-85	85-90
A_0	16.768	16.745	16.725	16.681	16.648	16.592
A_1	.010	-.020	-.026	-.011	.010	.006
B_1	-.017	-.017	-.024	-.032	-.047	0.000
A_2	.063	.050	.025	.010	-.036	-.004
B_2	-.024	-.015	-.031	-.026	-.004	.027
A_3	.018	-.001	-.021	-.024	-.030	.001
B_3	.015	.014	.000	.008	.016	.010
A_4	.014	.019	.006	.006	-.008	-.002
B_4	.012	.011	.002	.011	.013	0.000
A_5	.006	.009	-.004	-.010	.009	-.004
B_5	-.004	-.005	-.003	.004	.003	-.008

Table 19: Fourier coefficients for atomic oxygen densities at 120 km tabulated by geomagnetic latitude for Kp range 0.0 to 1.3 for summer.

$$\text{Log}_{10}\, n(O)m^{-3} = A_0 + \sum_{n=1}^{\infty} \left(A_n \cos \frac{2\pi nt}{T} + B_n \sin \frac{2\pi nt}{T}\right)$$

$\text{Log}_{10}\ n(0)m^{-3}$

SUMMER

Kp = 1 3 - 4 0

Local Geomagnetic Time in Hours

Geomagnetic Latitude	1	2	3	4	5	6	7	8	9	10	11	12	13	14	15	16	17	18	19	20	21	22	23	24
85 - 90	16 52	16 53	16 51	12 56	16 47	16 66	16 57	16 54	16 54	16 56	16 56	16 60	16 63	16 62	16 61	16 63	16 65	16 65	16 59	16.51	16.57	16 55	16.54	16.58
	22	28	26	34	28	38	27	21	23	42	35	33	65	31	38	43	71	39	26	14	16	19	20	33
80 - 85	16.61	16.57	16 61	16 57	16 60	16.59	16 57	16 57	16 58	16 59	16 60	16 57	16 60	16 65	16.63	16 62	16.65	16.69	16 72	16.68	16.63	16.56	16 66	16.59
	158	79	130	114	134	165	187	208	169	189	242	227	233	251	215	161	220	148	133	122	101	60	138	85
75 - 80	16.64	16 66	16 62	16 59	16.57	16 59	16 58	16 58	16 63	16 64	16 69	16 74	16 68	16 64	16 67	16 64	16 64	16 69	16.70	16 71	16 68	16 71	16 68	16.66
	302	276	286	276	215	269	330	251	173	215	198	130	140	148	227	210	234	270	249	189	229	272	253	326
70 - 75	16 63	16 56	16 64	16 58	16 55	16 56	16.57	16 60	16 64	16 64	16 76	16 77	16 71	16 68	16 73	16 69	16 68	16 68	16 73	16 71	16.71	16.69	16 70	16.67
	441	218	373	391	327	321	325	226	175	208	189	128	106	216	238	306	272	297	331	314	351	368	296	392
65 - 70	16 71	16 69	16 58	16 61	15.57	16 58	16 55	16 67	16 70	16 69	16 79	16 82	16 76	16.73	16 73	16 70	16 69	16 72	16 73	16 73	16.68	16.66	16 65	16.64
	130	166	545	454	472	493	362	284	251	191	236	160	185	229	277	310	381	422	433	443	419	452	565	531
60 - 65	16.74	16 72	16 74	16 59	16 58	16.57	16 60	16 70	16 74	16 76	16 79	16 79	16 79	16 73	16 75	16.74	16.72	16.72	16 77	16 75	16 72	16 74	16 71	16.81
	121	106	129	401	398	495	476	383	294	295	338	284	194	284	414	393	486	504	492	461	352	330	206	64

Table 20: Atomic oxygen densities at 120 km and numbers of samples of averaged data tabulated by geomagnetic latitude and geomagnetic time for Kp range 1.3 to 4.0 for summer.

$\text{Log}_{10}\, n(0)m^{-3}$

SUMMER

Kp = 1.3-4.0

Geomagnetic Latitude

Coefficient	60-65	65-70	70-75	75-80	80-85	85-90
A_0	16.718	16.684	16.661	16.652	16.613	16.572
A_1	-.016	-.045	-.025	0.000	.006	-.032
B_1	-.052	-.055	-.067	-.045	-.042	-.032
A_2	.057	.044	.036	.030	-.016	-.013
B_2	-.012	-.007	-.017	-.015	0.000	.014
A_3	.001	.017	-.017	-.018	-.007	.012
B_3	.034	.026	.003	.007	.009	-.008
A_4	-.007	.005	.004	.007	.008	.022
B_4	.011	.015	-.007	.001	.008	-.001
A_5	.001	-.001	-.002	-.007	.021	-.010
B_5	-.001	.008	0.000	.002	-.002	-.004

Table 21: Fourier coefficients for atomic oxygen densities at 120 km tabulated by geomagnetic latitude for Kp range 1.3 to 4.0 for summer.

$$\text{Log}_{10}\, n(0)m^{-3} = A_0 + \sum_{n=1}^{\infty} \left(A_n \cos \frac{2\pi nt}{T} + B_n \sin \frac{2\pi nt}{T}\right)$$

$\text{Log}_{10}\ n(O)m^{-3}$

SUMMER

Kp = > 4 0

Local Geomagnetic Time in Hours

Geomagnetic Latitude	1	2	3	4	5	6	7	8	9	10	11	12	13	14	15	16	17	18	19	20	21	22	23	24
85 - 90	0	16 61	0	0	0	[illegible]0	0	0	0	16 56	16.57	16 59	16 60	16 65	16 49	0	0	0	0	0	0	0	0	0
	0	1	0	0	0[illegible]	0	0	0	0	6	12	10	8	6	4	0	0	0	0	0	0	0	0	0
80 - 85	16.65	16.55	16 56	16 56	16.56	16 32	16.55	0	16.47	0	16 52	16.60	16 57	16 58	16.55	16 59	16 57	16 62	16 67	16 70	16.58	0	16.66	16.61
	12	7	5	5	5	2	8	0	24	0	13	26	31	47	29	20	28	13	8	22	7	0	13	8
75 - 80	16 46	0	16.63	16.66	0	16 66	16 42	16.40	16 48	16.50	0	16 59	16 58	16 70	16 67	16 58	16 54	16 57	0	16 84	0	0	0	0
	8	0	13	12	0	23	19	38	21	20	0	7	18	12	35	39	32	4	0	6	0	0	0	0
70 - 75	0	16.68	16 55	16.59	16 59	16.90	16 45	16 41	16 45	16 54	0	0	16 50	0	16 64	16 63	16 55	16.64	16 72	0	16.69	16 54	0	0
	0	14	8	14	24	4	37	43	18	18	0	0	8	0	44	8	23	12	21	0	9	8	0	0
65 - 70	0	0	16 58	16.56	16 59	16 53	16.40	16 53	16 55	16.68	0	0	16 43	16 56	16 68	16 69	16 63	16 73	0	0	16 82	16 61	0	0
	0	0	4	15	28	11	45	48	10	20	0	0	2	11	32	18	8	28	0	0	5	16	0	0
60 - 65	0	0	0	16 33	16.51	16 50	16 44	16 59	16 58	16.66	0	0	16 77	16 59	16.76	16 73	16 77	16 74	16 73	16 74	16 51	16 73	16.63	0
	0	0	0	3	11	18	60	38	4	18	0	0	4	11	13	33	11	12	38	40	19	37	12	0

Table 22: Atomic oxygen densities at 120 km and numbers of samples of averaged data tabulated by geomagnetic latitude and geomagnetic time for Kp range > 4.0 for summer.

Log_{10} n (O) m^{-3}

EQUINOX

Kp = 0 0 - 1.3

Local Geomagnetic Time in Hours

Geomagnetic Latitude	1	2	3	4	5	6	7	8	9	10	11	12	13	14	15	16	17	18	19	20	21	22	23	24
85 - 90	16 93	16 99	17 03	17 00	17.00	17.03	17 02	17 03	17 00	16 92	16 89	16 97	16 94	16.97	16 96	16 94	16.94	17 00	16.95	17 02	16 93	17 03	17 07	17 03
	7	22	29	31	24	24	15	25	17	15	14	25	15	13	27	19	17	13	10	11	19	17	19	19
80 - 85	16 99	16 98	16 98	16 96	16.97	16 95	17 00	16 99	17 02	17 00	16.95	16 96	17 02	17 04	17 08	17.02	17.04	16.99	17 02	17 02	17.05	16.98	16 97	16.98
	160	149	119	90	74	88	101	79	66	65	49	52	57	57	63	75	83	99	84	77	46	53	81	149
75 - 80	17 00	16 99	16.94	16 93	16 95	16 93	16 92	16.95	16.95	16 98	17 00	16 96	17.03	17.05	16 04	16 98	17 00	17 05	17 04	17 05	17 10	17.04	17 03	17 03
	127	73	54	61	51	56	92	113	92	111	127	120	133	135	196	127	138	121	112	96	65	57	127	179
70 - 75	17 00	16 91	16 83	16.87	16 94	16.90	16 87	16 97	16 99	17 00	17 02	17.04	17 04	17.09	17.09	17 02	17 03	17 07	17 05	17.13	17.11	17.06	17.06	17.05
	121	94	56	88	91	99	115	168	158	162	139	128	135	135	143	185	179	117	128	105	119	101	164	156
65 - 70	16.96	16 98	16.94	16 93	16 95	16 93	16 91	17.01	17.06	17 09	17.09	17 05	17 10	17 12	17 16	17.14	17.10	17.09	17.15	17 10	17 11	17 07	17 05	16 96
	31	65	112	142	140	100	150	189	119	108	158	126	146	146	188	245	194	227	150	193	153	156	152	54
60 - 65	16 92	16 90	16.92	16 94	16 95	16 87	16 91	17.02	17 13	17 18	17.10	17 08	17 10	17.16	17 16	17.09	17.08	17 07	17.13	17 16	17.14	17 12	17 10	17 01
	94	123	161	171	126	89	130	111	85	81	192	196	165	177	177	127	78	192	154	250	206	242	194	110

Table 23: Atomic oxygen densities at 120 km and numbers of samples of averaged data tabulated by geomagnetic latitude and geomagnetic time for Kp range 0.0 - 1.3 for equinox.

$\text{Log}_{10}\ n(O)m^{-3}$

EQUINOX

Kp = 0.0-1.3

Geomagnetic Latitude

Coefficient	60-65	65-70	70-75	75-80	80-85	85-90
A_0	17.051	17.045	17.005	16.997	16.998	16.980
A_1	-.054	-.047	-.014	.012	-.011	.030
B_1	-.094	-.089	-.092	-.054	-.028	.021
A_2	.029	.011	.029	.017	-.007	-.009
B_2	-.052	-.017	-.034	-.012	.003	-.009
A_3	-.009	-.004	.003	-.005	.010	.007
B_3	-.005	.004	-.016	-.008	-.004	-.023
A_4	-.038	-.024	.001	-.006	-.020	.001
B_4	-.018	-.007	.005	.009	.012	.006
A_5	.032	.012	.023	.011	.004	.004
B_5	-.011	.001	.008	.002	.003	-.026

Table 24: Fourier coefficients for atomic oxygen densities at 120 km tabulated by geomagnetic latitude for Kp range 0.0 to 1.3 for equinox.

$$\text{Log}_{10}\ n(O)m^{-3} = A_0 + \sum_{n=1}^{\infty} \left(A_n \cos \frac{2\pi nt}{T} + B_n \sin \frac{2\pi nt}{T}\right)$$

Log_{10} n(0) m^{-3}

EQUINOX

Kp = 1 3 - 4.0

Local Geomagnetic Time in Hours

Geomagnetic Latitude	1	2	3	4	5	6	7	8	9	10	11	12	13	14	15	16	17	18	19	20	21	22	23	24
85 - 90	16.84	16 83	16 85	16 87	16 90	16 90	16 89	16.89	16 91	16 86	16 88	16.83	16 94	16.94	16 95	16 98	16 98	16 95	16.93	16 89	16 92	16 93	16 93	16.90
	32	29	38	28	38	22	35	37	25	43	31	11	30	28	26	26	38	34	31	23	28	2	47	55
80 - 85	16 93	16.93	16 92	16.89	16 87	16 86	16 88	16.86	16 88	16 89	16 87	16.89	16 91	16 94	16 93	16 95	16 93	16 91	16 93	16 93	16 92	16 87	16.89	16 93
	155	155	121	130	144	153	126	91	138	138	102	111	108	141	166	203	182	160	126	115	113	112	157	170
75 - 80	16 92	16 93	16 89	16.91	16 85	16 83	16 82	16 85	16 87	16.85	16 89	16 91	16 96	16 94	16 94	16 95	16.94	16 91	16 95	17 01	16.98	16 91	16.91	16 95
	124	151	165	168	170	171	214	291	261	250	295	275	270	253	260	274	236	217	174	128	127	147	174	182
70 - 75	16 89	16 89	16 90	16 87	16 84	16 84	16 85	16 86	16 87	16.86	16 90	16 94	16 96	16 99	17 00	16 93	16.91	16 93	16 97	17.02	17.01	16 97	16 98	16.98
	140	144	201	239	268	198	264	330	392	345	355	405	421	351	329	339	328	330	222	188	155	217	234	198
65 - 70	16 91	16 82	16 86	16 86	16 85	16 87	16 88	16 92	16 96	16 97	16 95	16 99	17 00	17 04	17 04	17 02	16.99	17.01	17 04	17 02	17 05	17.04	17.01	16.94
	136	143	227	323	333	330	359	340	355	291	372	343	386	446	391	337	404	380	310	203	185	211	259	148
60 - 65	16 92	16.84	16 78	16 82	16 87	16 87	16.92	16 96	17 05	17 07	17 03	17 01	17 05	17 08	17 07	16 99	16 99	17 02	17 06	17 07	17 05	17 03	16 98	16.95
	208	231	189	389	301	307	251	182	183	248	332	434	411	359	328	272	259	326	383	355	297	240	217	198

Table 25: Atomic oxygen densities at 120 km and numbers of samples of averaged data tabulated by geomagnetic latitude and geomagnetic time for Kp range 1.3 to 4.0 for equinox.

$\text{Log}_{10}\ n(O)m^{-3}$

EQUINOX

Kp = 1.3-4.0

Coefficient	Geomagnetic Latitude 60-65	65-70	70-75	75-80	80-85	85-90
A_0	16.978	16.961	16.923	16.911	16.905	16.903
A_1	-.059	-.024	.011	.013	.004	-.011
B_1	-.082	-.086	-.066	-.052	-.026	-.040
A_2	.024	.013	.024	.015	.003	-.021
B_2	-.055	-.030	-.005	.010	.020	.002
A_3	.006	.004	-.011	-.015	.004	.018
B_3	-.011	-.019	-.023	.002	.009	-.018
A_4	-.011	-.010	-.012	-.011	-.007	.001
B_4	.009	-.004	.012	.012	.012	-.013
A_5	.027	.010	.008	.004	.004	.004
B_5	.004	-.008	-.003	.004	.005	-.012

Table 26: Fourier coefficients for atomic oxygen densities at 120 km tabulated by geomagnetic latitude for Kp range 1.3 to 4.0 for equinox.

$$\text{Log}_{10}\ n(O)m^{-3} = A_0 + \sum_{n=1}^{\infty} \left(A_n \cos \frac{2\pi nt}{T} + B_n \sin \frac{2\pi nt}{T}\right)$$

Log_{10} n $(O)_m^{-3}$

EQUINOX

Kp > 4 0

Local Geomagnetic Time in Hours

Geomagnetic Latitude	1	2	3	4	5	6	7	8	9	10	11	12	13	14	15	16	17	18	19	20	21	22	23	24
85 - 90	0 0	0 0	0 0	0 0	16 50 1	16 54 5	0 0	0 0	0 0	16 63 7	0 0	16 71 5	16 84 3	0 0	0 0	0 0	16 48 2	0 0	0 0	0 0	0 0	16 97 2	0 0	0 0
80 - 85	16 75 8	16 72 13	16.67 16	16.59 20	16 63 30	16 88 9	16 80 16	16 77 18	16.70 33	16 68 12	16 75 23	16.76 26	16.73 10	16 80 19	16 77 11	16 66 13	16 71 2	16.77 9	16 81 11	16 71 10	16.73 6	16.33 7	16.62 20	16 75 19
75 - 80	16.87 13	16 78 6	16 82 1	16 86 21	16 77 17	16 65 31	16 80 33	16.62 6	16 68 7	16.80 41	16 78 33	16.83 30	16 84 48	16.84 22	16 95 12	16 83 18	16 77 18	16.77 28	16 84 1	16.86 6	16.54 8	16 58 20	16.98 5	16 85 8
70 - 75	16.92 27	16 93 20	16 63 9	16 76 11	16 75 16	16.68 55	16.69 89	16.69 53	16 70 33	16 68 47	16 73 1	16 81 38	16 83 39	16 86 22	16 82 39	16 81 40	16 69 27	16.72 32	16 78 6	16 85 22	16 81 50	16 97 29	16 84 17	16.82 38
65 - 70	16 75 18	16.91 19	16.80 30	16 74 26	16 73 34	16 75 46	16 65 53	16 58 34	16 76 18	16.82 22	16 63 18	16 78 36	16 92 69	16.91 50	16 90 57	16 87 62	16 75 56	16.76 13	16 85 1	16.94 9	16.84 39	16 99 24	16.86 15	16 83 20
60 - 65	0 0	0 0	0 0	16 65 64	16.63 25	16 72 52	16.63 60	16 66 25	16 78 13	16 81 13	16.83 19	17 00 62	16 98 82	17 00 27	17.89 28	16 85 58	16 83 69	17.00 22	17 11 28	16.99 31	16 86 66	16.92 51	16 93 33	16 79 58

Table 27: Atomic oxygen densities at 120 km and numbers of samples of averaged data tabulated by geomagnetic latitude and geomagnetic time for Kp range > 4.0 for equinox.

$\text{Log}_{10}\, n(O)\, m^{-3}$

EQUINOX

Kp > 4.0

Geomagnetic Latitude

Coefficient	60-65	65-70	70-75	75-80	80-85	85-90
A_0	INSUFFICIENT DATA	16.805	16.783	16.789	16.712	INSUFFICIENT DATA
A_1		.031	.046	-.000	-.052	
B_1		-.080	-.047	-.024	.008	
A_2		.041	.063	.037	-.027	
B_2		.023	.013	.071	.015	
A_3		-.022	.000	.010	.011	
B_3		-.035	-.031	.016	.018	
A_4		-.041	-.006	.032	.046	
B_4		.008	.024	.005	.079	
A_5	———	.016	.001	.057	.020	
B_5		.001	.017	-.004	.038	

Table 28: Fourier coefficients for atomic oxygen densities at 120 km tabulated by geomagnetic latitude for Kp range > 4.0 for equinox.

$$\text{Log}_{10}\, n(O) = A_0 \sum_{n=1}^{\infty} \left(A_n \cos \frac{2\pi nt}{T} + B_n \sin \frac{2\pi nt}{T}\right)$$

Log_{10} n(0) m^{-3}

WINTER

Kp = 0 0 - 1 3

Local Geomagnetic Time in Hours

Geomagnetic Latitude	1	2	3	4	5	6	7	8	9	10	11	12	13	14	15	16	17	18	19	20	21	22	23	x
85 - 90	0	17 05	0	16 96	17 05	17 09	17 04	0	0	17 04	17 09	0	0	0	16 99	0	17 09	17 04	17 05	17 06	17 04	0	0	0
	0	6	0	1	3	2	1	0	0	4	3	0	0	0	6	0	1	1	2	3	3	0	0	0
80 - 85	17 05	17.02	17 05	17 06	17 02	16 96	17 03	16 87	17 02	17.09	17 09	17 10	17 14	17 11	17 10	17 12	17 10	17 06	17 10	17 08	17 13	17 05	17 12	17 10
	12	4	9	12	6	2	2	1	9	9	9	1	1	6	12	2	6	3	10	4	7	3	8	1
75 - 80	17 11	17 08	17 06	17 09	17 01	17 00	16.97	16 97	17 06	17.14	17 11	17 08	17 13	17.11	17 10	17.08	17.10	17 04	17 05	17 13	17 16	17 14	17 19	17.14
	4	10	16	15	5	10	4	5	11	10	16	28	7	15	10	12	27	13	9	10	9	2	4	15
70 - 75	0	16 98	17 06	16 97	16 94	17 02	16 99	17 00	17 04	17 12	17 08	17 11	17 14	17 13	17 09	17.13	17 14	17 17	17 16	17 21	17 18	0	0	0
	0	12	32	4	10	4	11	13	24	27	22	36	19	7	12	35	34	10	7	9	4	0	0	0
65 - 70	17 11	17 04	17 08	16 99	16 95	17 01	17 09	17.09	17.07	17.13	17.11	17.09	17.12	17 15	17 14	17 18	17 16	0	17.17	0	17 19	0	0	17 19
	1	5	20	7	12	19	12	21	26	41	39	43	30	17	32	33	13	0	7	0	24	0	0	1
60 - 65	0	0	0	17 03	17 01	17 11	17 15	17 16	17 11	17 15	17 10	17.10	17 10	17 17	17 15	17 15	17 23	17.25	0	0	0	0	0	0
	0	0	0	11	16	28	44	54	43	42	44	55	55	18	46	19	13	10	0	0	0	0	0	0

Table 29: Atomic oxygen densities at 120 km and numbers of samples of averaged data tabulated by geomagnetic latitude and geomagnetic time for Kp range 0.0 to 1.3 for winter.

$\text{Log}_{10}\, n(0)\, m^{-3}$

WINTER

Kp = 1.3 - 4 0

Local Geomagnetic Time in Hours

Geomagnetic Latitude	1	2	3	4	5	6	7	8	9	10	11	12	13	14	15	16	17	18	19	20	21	22	23	24
85 - 90	16 97	16 97	16 94	16 90	16 97	17 04	16 96	17 01	17 03	17 00	17 01	16 99	16.96	16 93	16 01	16 94	16 90	16.89	16 97	16 89	16.89	16 97	16.92	16 95
	5	1	6	5	2	1	1	3	2	3	6	3	4	2	6	6	3	6	4	5	3	6	7	7
80 - 85	16.99	17.16	16 93	16 98	16.96	16 97	16 93	16 89	16 85	16 92	16 96	17 03	17.03	17 04	16 88	16 97	16.96	16.99	16 94	16 92	16 93	16 89	16 98	16 94
	34	17	13	4	13	13	15	15	11	7	7	10	11	16	8	12	11	14	17	17	21	8	15	12
75 - 80	17.02	17.02	16 97	16 96	17.00	16 99	16 95	16 93	16 94	16 98	17 06	17 09	17 06	17 05	16 93	17 06	17.00	16.99	16 97	16 95	16 98	17 00	16 97	16 98
	28	42	24	22	14	19	16	21	19	37	17	10	34	21	16	33	27	25	32	37	32	18	5	23
70 - 75	17.00	16 92	17 03	16.93	16.90	16 92	16 88	16 93	16 99	17.00	17.04	17.06	17 07	17 04	17 02	17.04	17.06	17 03	17.03	16 99	17 00	17 03	17.00	17.03
	1	57	18	33	26	15	16	22	28	20	30	13	31	38	30	26	60	60	19	18	19	22	18	11
65 - 70	0	0	16.75	16 77	17.00	16 92	16 96	17 05	17.03	17 09	17 09	17 10	17 10	17.03	17.08	17.05	17.06	17.06	17.03	17 04	17 13	17.06	17 09	16.92
	0	0	49	27	18	29	13	35	56	46	32	38	40	60	42	66	54	5	15	32	17	19	16	6
60 - 65	0	0	16.95	16 90	16 83	16.98	17 02	17 08	17 14	17.11	17 09	17 07	17 09	17.10	17.06	17.07	17.09	17.28	17 13	0	0	17 21	0	0
	0	0	17	14	27	44	56	31	38	62	33	39	49	78	75	110	23	2	5	0	0	4	0	0

Table 30: Atomic oxygen densities at 120 km and numbers of samples of average data tabulated by geomagnetic latitude and geomagnetic time for Kp range 1.3 to 4.0 for winter.

$\text{Log}_{10}\, n(O)m^{-3}$

WINTER

Kp = 1.3-4.0

Geomagnetic Latitude

Coefficient		60-65	65-70	70-75	75-80	80-85	85-90
A_0			17.012	16.997	16.994	16.961	16.950
A_1			-.062	-.020	-.019	.008	-.036
B_1			-.074	-.053	-.011	-.001	.045
A_2			.025	.033	.028	.025	.014
B_2			-.064	.007	.021	.046	.002
A_3			.014	-.006	-.015	-.020	.020
B_3			-.022	.013	.000	.009	.001
A_4			.012	.003	.022	.028	.001
B_4			-.010	-.009	-.006	.019	.003
A_5			-.005	-.002	-.017	-.019	.005
B_5			.013	-.012	.011	.003	.020

INSUFFICIENT DATA

Table 31: Fourier coefficients for atomic oxygen densities at 120 km tabulated by geomagnetic latitude for Kp range 1.3 to 4.0 for winter.

$$\text{Log}_{10}\, n(O)m^{-3} = A_0 + \sum_{n=1}^{\infty} \left(A_n \cos \frac{2\pi nt}{T} + B_n \sin \frac{2\pi nt}{T}\right)$$

Log_{10} n(0) m^{-3}

WINTER

Kp > 4.0

Local Geomagnetic Time in Hours

Geomagnetic Latitude	1	2	3	4	5	6	7	8	9	10	11	12	13	14	15	16	17	18	19	20	21	22	23	24
85 - 90	0	0	0	0	0	16.79	0	0	0	16 94	16 93	0	0	0	0	0	0	16 89	0	0	0	0	0	0
	0	0	0	0	0	1	0	0	0	1	2	0	0	0	0	0	0	2	0	0	0	0	0	0
80 - 85	16 87	0	0	0	0	16 89	16.89	16 94	16 87	16 98	0	16 85	0	0	16.87	0	16 75	16 75	16.88	16 84	16 85	15.81	16 83	16 87
	2	0	0	0	0	4	3	4	8	1	0	2	0	0	5	0	1	1	4	6	4	3	2	1
75 - 80	16 96	0	0	0	16 92	16 74	16 74	16 74	16 78	16 89	17.12	16 86	16 91	0	16 98	16 86	16 87	16 81	16 90	16.98	16 79	16 86	16 89	16 84
	2	0	0	0	3	3	1	5	12	15	1	3	7	0	6	6	5	2	5	12	5	4	9	7
70 - 75	0	16 78	16 97	16.82	16 79	16.89	16 87	16 85	16 97	16.89	16 89	0	16 99	0	17 01	16 94	16 91	16 98	17.03	0	0	0	0	0
	0	11	6	6	9	5	15	10	5	2	13	0	8	0	8	7	8	16	6	0	0	0	0	0
65 - 70	0	16.69	17 06	16 76	0	16.87	16 93	16 92	16 94	17 00	16.83	17.03	17.16	17.06	17 01	17 08	17 03	16.91	16 79	0	0	0	0	0
	0	2	2	8	0	5	9	21	13	11	2	15	3	2	9	8	2	2	10	0	0	0	0	0
60 - 65	0	0	0	16.84	16.84	16.76	16 79	16 72	16 95	16 92	17.08	17 09	17.01	17.07	17 10	17 10	17 04	0	0	0	0	0	0	0
	0	0	0	18	5	20	22	33	28	13	26	27	3	5	13	10	5	0	0	0	0	0	0	0

Table 32: Atomic oxygen densities at 120 km and numbers of samples of averaged data tabulated by geomagnetic latitude and geomagnetic time for Kp range > 4.0 for winter.

Geographic Latitude	Atomic Oxygen Density (m^{-3}) Altitude 95 km	120 km	Difference
25^{o}	1.25×10^{17}	1.10×10^{17}	$.15 \times 10^{17}$
30^{o}	1.35×10^{17}	1.25×10^{17}	$.10 \times 10^{17}$
35^{o}	1.40×10^{17}	1.30×10^{17}	$.10 \times 10^{17}$
40^{o}	1.50×10^{17}	1.35×10^{17}	$.15 \times 10^{17}$
45^{o}	1.55×10^{17}	No Data	
50^{o}	1.55×10^{17}	No Data	
55^{o}	1.55×10^{17}	$.80 \times 10^{17}$	$.75 \times 10^{17}$
60^{o}	1.55×10^{17}	$.90 \times 10^{17}$	$.65 \times 10^{17}$

Table 33: Comparison of atomic oxygen densities at 95 km and 120 km as a function of geographic latitude for OGO-6 orbit #2176 day 307, 1969.

Geographic Latitude	Atomic Oxygen Density (m^{-3}) Altitude 95 km	120 km	Difference
-65^{o}	1.60×10^{17}	$.65 \times 10^{17}$	$.95 \times 10^{17}$
-70^{o}	2.00×10^{17}	$.62 \times 10^{17}$	1.38×10^{17}
-75^{o}	2.27×10^{17}	$.65 \times 10^{17}$	1.65×10^{17}
-80^{o}	1.87×10^{17}	$.70 \times 10^{17}$	1.17×10^{17}

Table 34: Comparison of atomic oxygen densities at 95 km and 120 km as a function of geographic altitude for OGO-6 orbit #1165 day 237, 1969.

Table 35: Data index for nitrogen "temperature", NT.

	Summer	Equinox	Winter
$0 < Kp < 1.3$	Tabulated Values: Table 36, p. 89	Tabulated Values: Table 41, p. 94	Tabulated Values: Table 47, p.100
	Graphical Analysis: Figure 19, p. 80	Graphical Analysis: Figure 22, p. 83	Graphical Analysis: Figure 25, p.86
	Fourier Analysis: Table 37, p. 90	Fourier Analysis: Table 42, p. 95	Fourier Analysis: Insufficient Data
$1.3 < Kp < 4.0$	Tabulated Values: Table 38, p. 91	Tabulated Values: Table 43, p. 96	Tabulated Values: Table 48, p.101
	Graphical Analysis: Figure 20, p. 81	Graphical Analysis: Figure 23, p. 84	Graphical Analysis: Figure 26, p.87
	Fourier Analysis: Table 39, p. 92	Fourier Analysis: Table 44, p. 97	Fourier Analysis: Insufficient Data
$Kp > 4.0$	Tabulated Values: Table 40, p. 93	Tabulated Values: Table 45, p. 98	Tabulated Values: Table 49, p.102
	Graphical Analysis: Figure 21, p. 82	Graphical Analysis: Figure 24, p. 85	Graphical Analysis: Figure 27, p.88
	Fourier Analysis: Insufficient Data	Fourier Analysis: Table 46, p. 99	Fourier Analysis: Insufficient Data

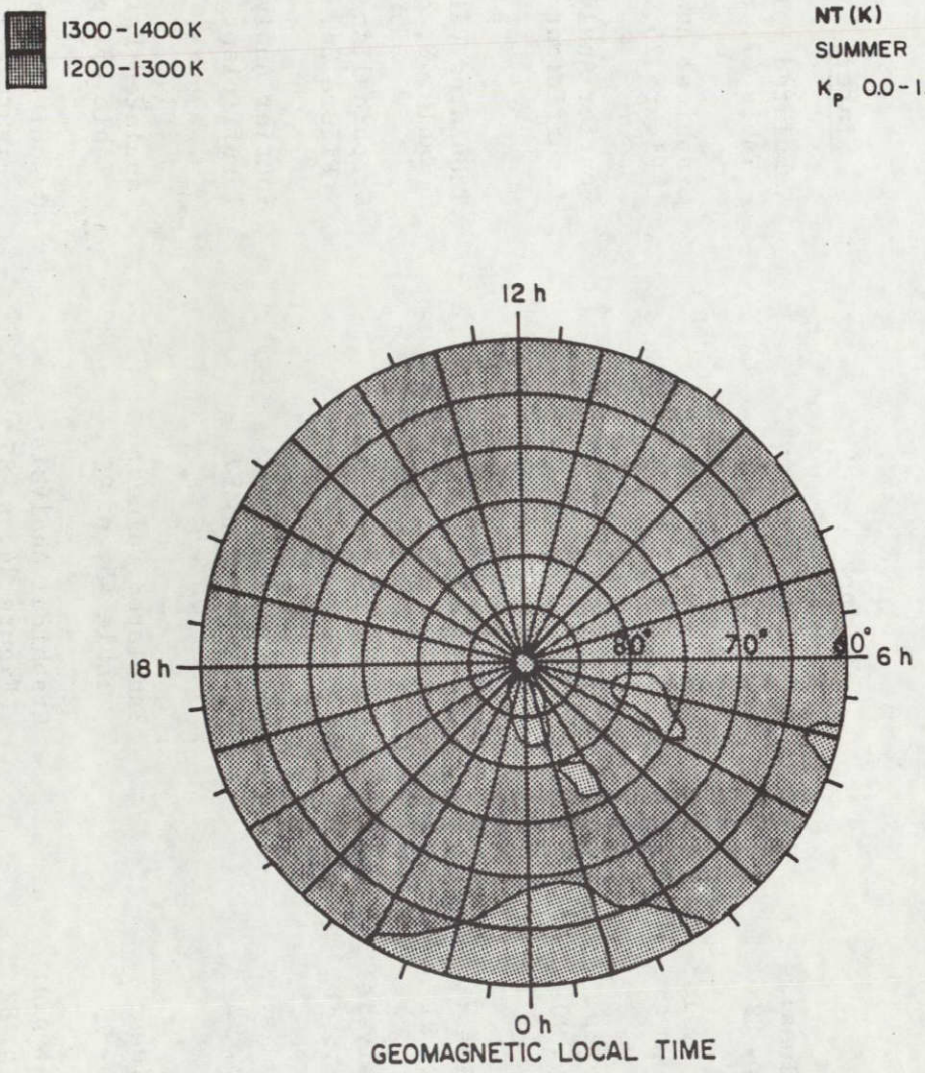

Figure 19: NT values as a function of geomagnetic time and geomagnetic latitude for Kp range 0.0 to 1.3 for summer.

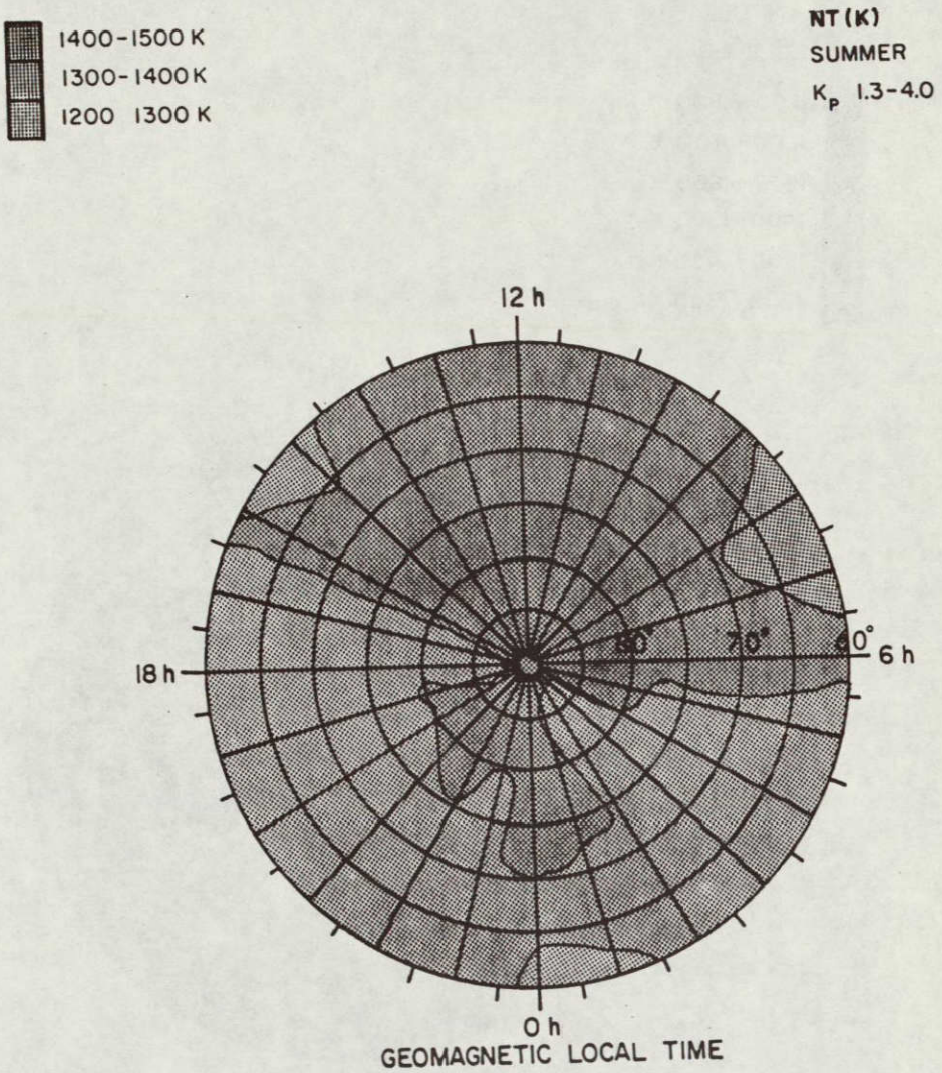

Figure 20: NT values as a function of geomagnetic time and geomagnetic latitude for Kp range 1.3 to 4.0 for summer.

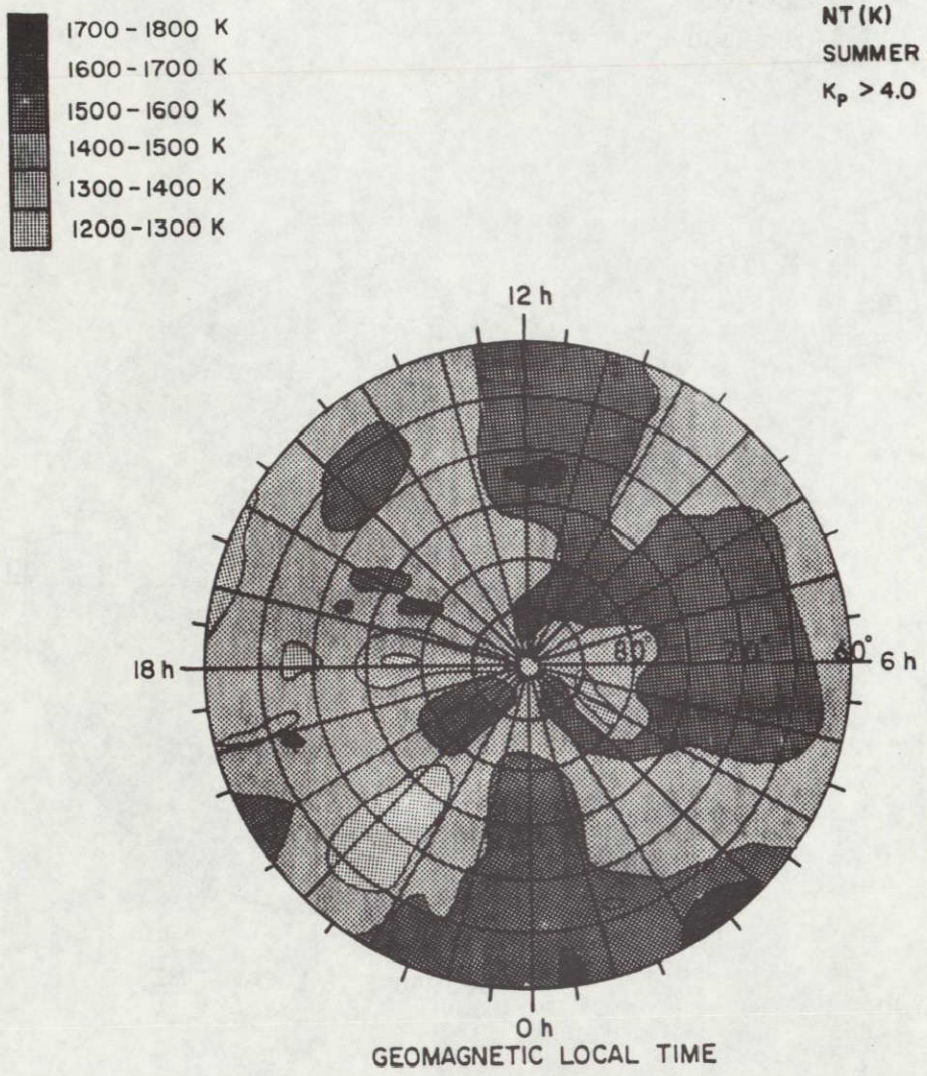

Figure 21: NT values as a function of geomagnetic time and geomagnetic latitude for Kp range > 4.0 for summer.

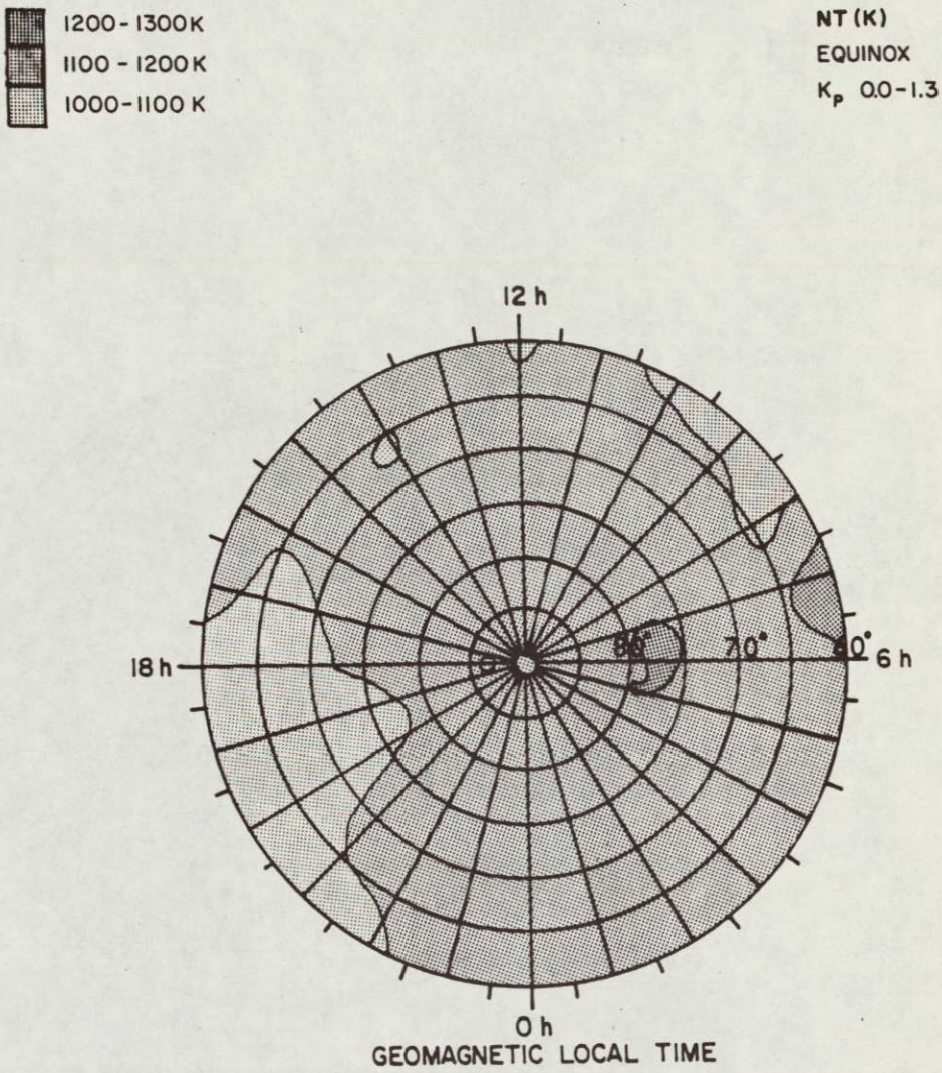

Figure 22: NT values as a function of geomagnetic time and geomagnetic latitude for Kp range 0.0 to 1.3 for equinox.

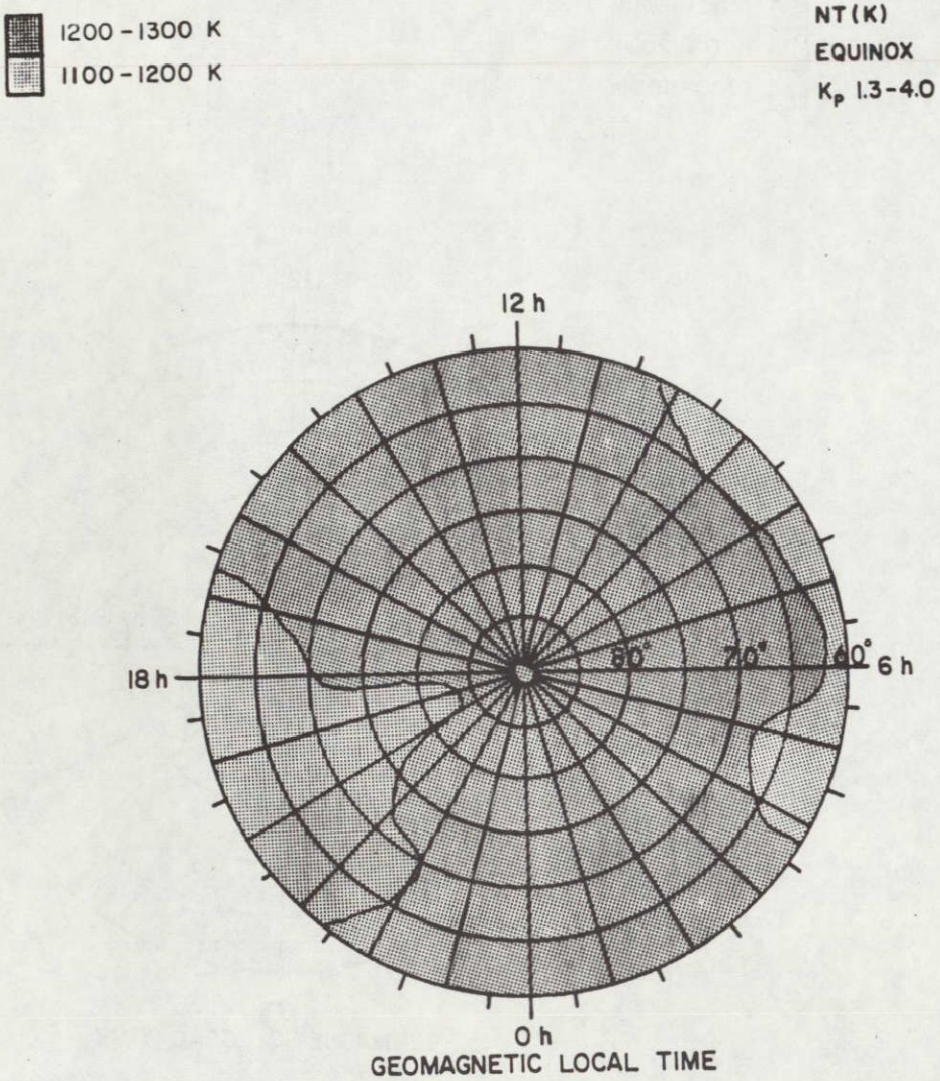

Figure 23: NT values as a function of geomagnetic time and geomagnetic latitude for Kp range 1.3 to 4.0 for equinox.

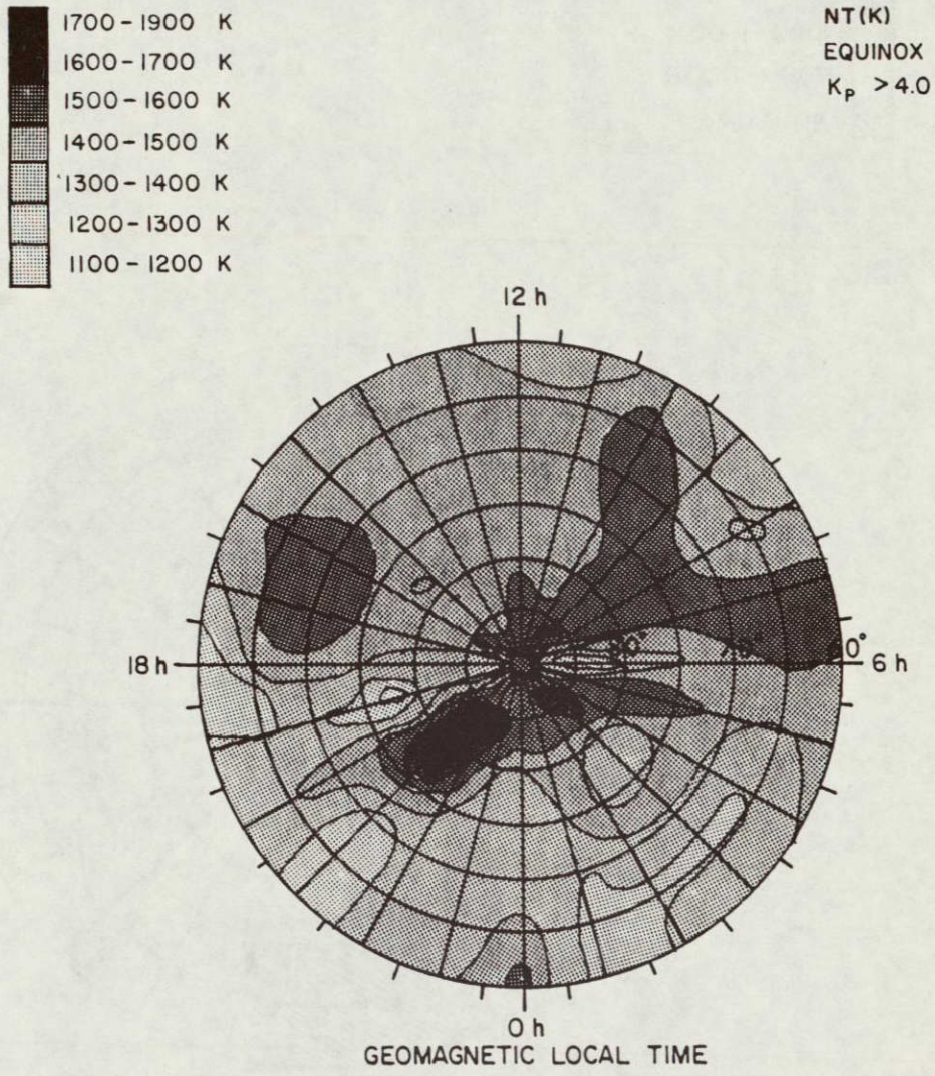

Figure 24: NT values as a function of geomagnetic time and geomagnetic latitude for Kp range > 4.0 for equinox.

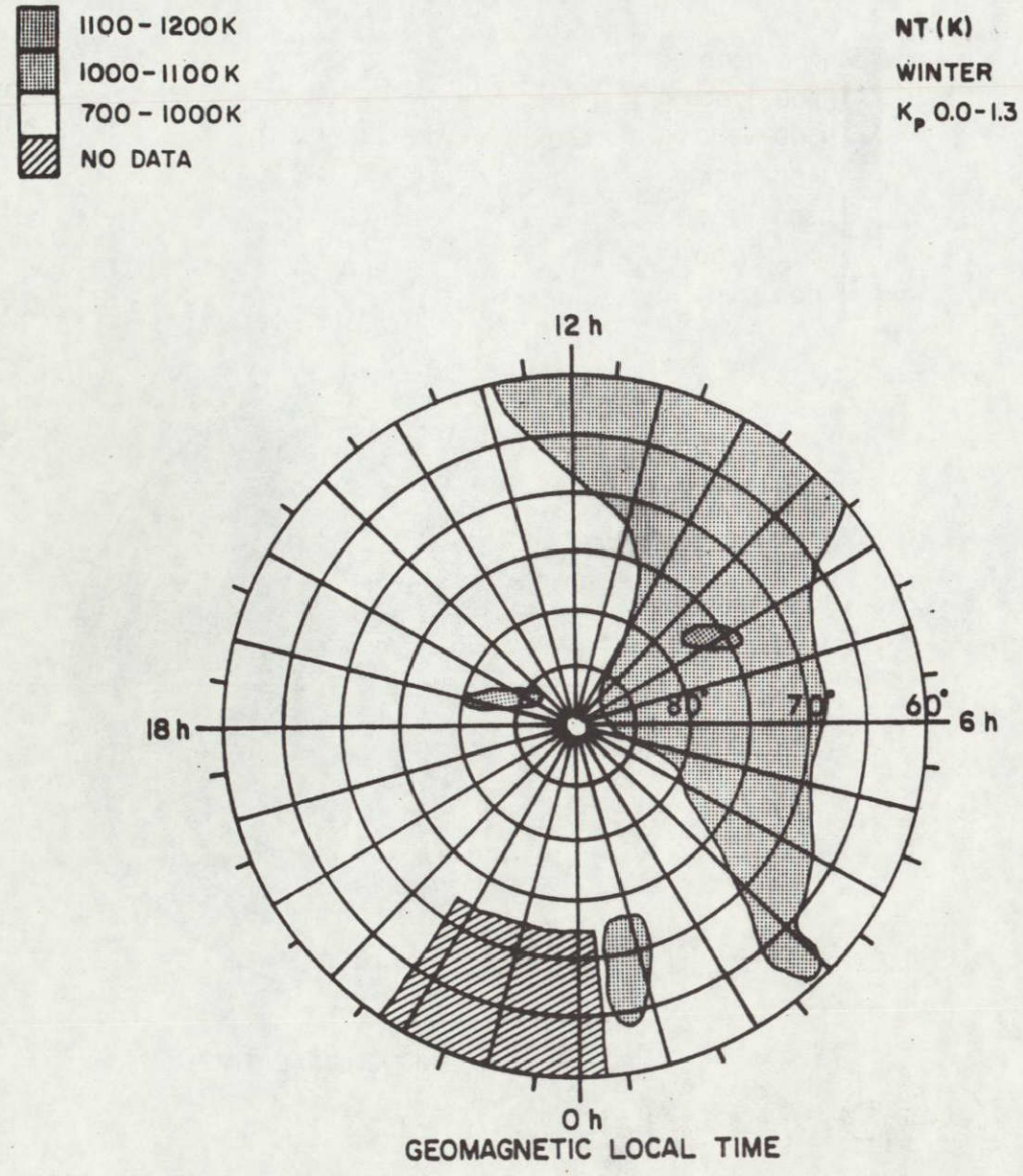

Figure 25: NT values as a function of geomagnetic time and geomagnetic latitude for Kp range 0.0 to 1.3 for winter.

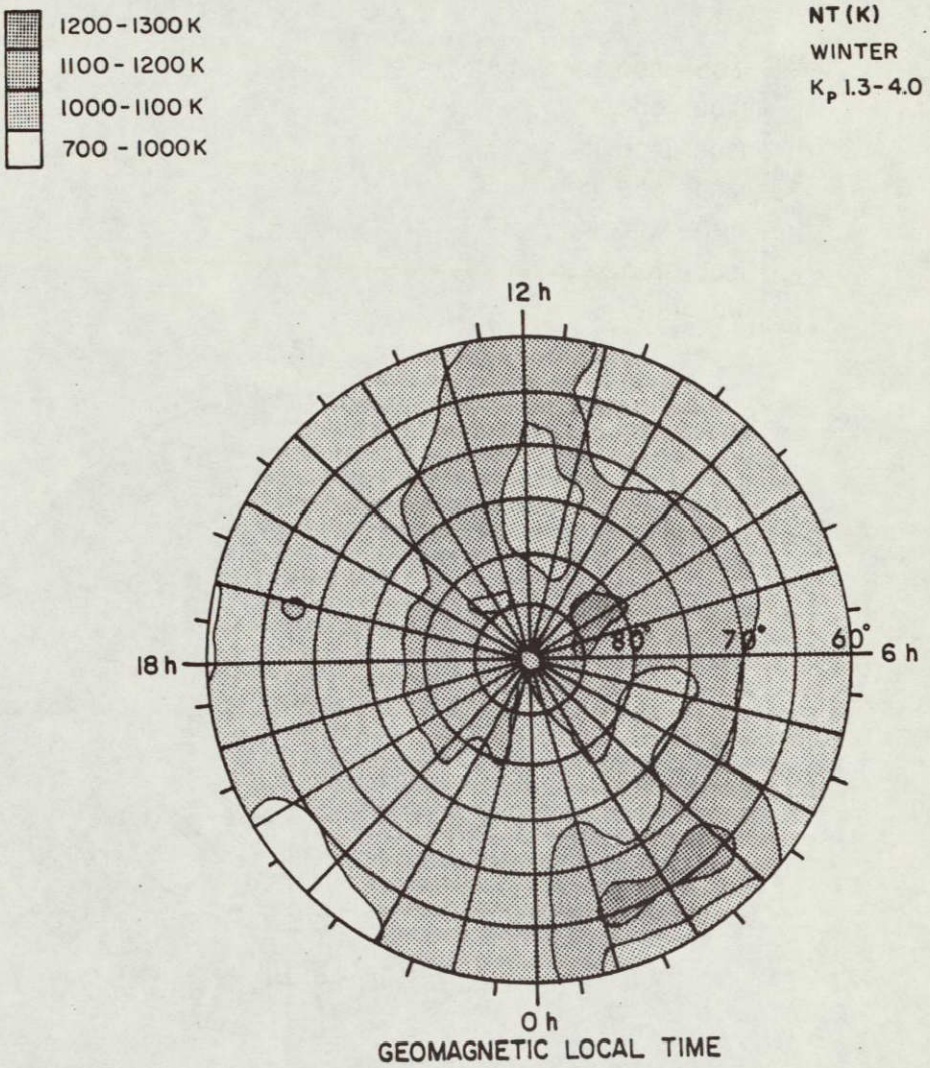

Figure 26: NT values as a function of geomagnetic time and geomagnetic latitude for Kp range 1.3 to 4.0 for winter.

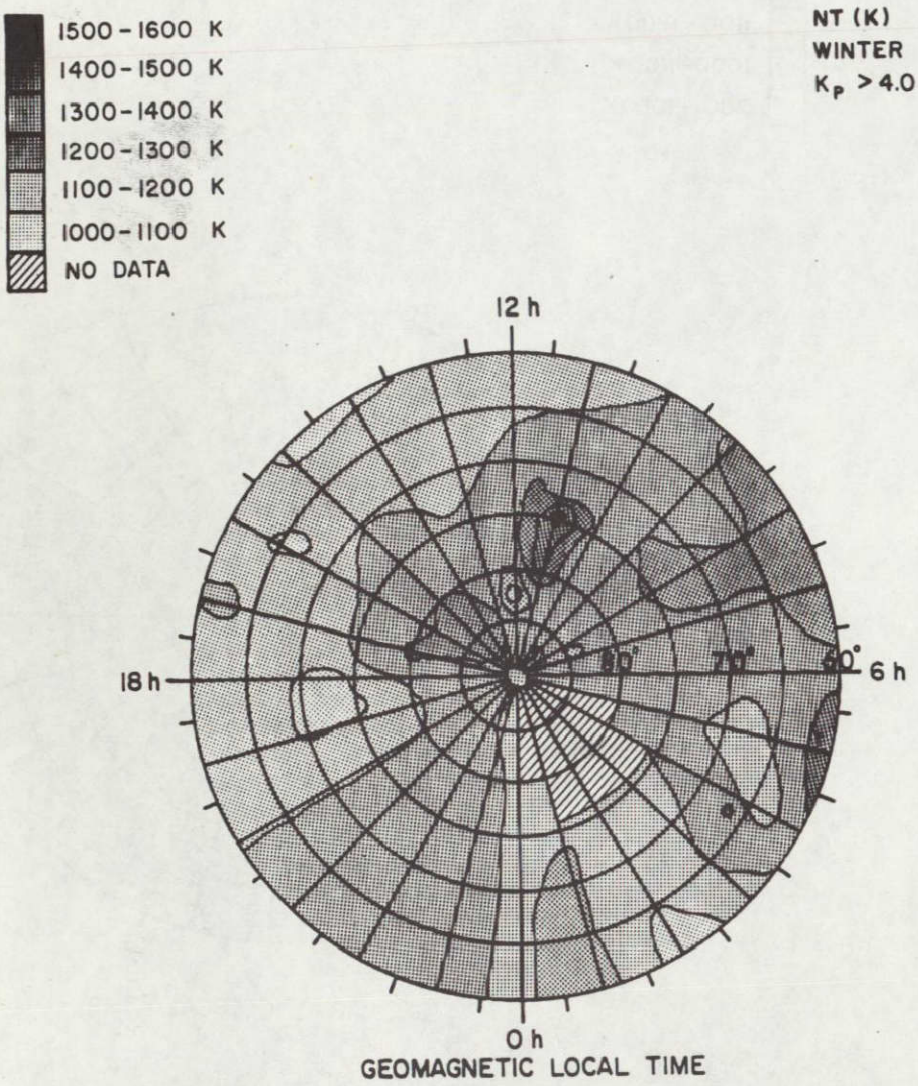

Figure 27: NT values as a function of geomagnetic time and geomagnetic latitude for Kp range > 4.0 for winter.

NT (K)

SUMMER

Kp = 0.0 - 1.3

Local Geomagnetic Time in Hours

Geomagnetic Latitude	1	2	3	4	5	6	7	8	9	10	11	12	13	14	15	16	17	18	19	20	21	22	23	24
85 - 90	1292	1299	1290	1331	1335	1292	1347	1341	1378	1355	1363	1353	1340	1346	1354	1344	1290	1327	1349	1321	1301	1295	1291	1285
	1	9	8	6	10	15	22	19	20	18	16	29	30	22	23	20	7	5	13	6	1	11	12	14
80 - 85	1283	1292	1329	1327	1321	1295	1316	1356	1340	1348	1350	1348	1370	1364	1372	1367	1344	1344	1389	1418	1360	1333	1323	1290
	31	48	105	67	69	65	99	129	107	105	140	126	136	91	123	142	96	81	25	26	29	15	25	20
75 - 80	1343	1297	1283	1329	1301	1293	1302	1343	1362	1369	1374	1389	1351	1371	1361	1349	1361	1332	1326	1347	1341	1349	1325	1331
	156	41	69	129	149	177	131	106	106	80	48	68	76	100	101	152	147	151	119	113	117	171	1	71
70 - 75	1331	1342	1320	1333	1298	1316	1336	1335	1321	1380	1367	1387	1377	1355	1352	1349	1362	1322	1333	1353	1359	1365	1336	1343
	74	168	175	183	186	187	169	117	127	93	118	87	95	131	170	176	191	162	171	122	204	222	102	1
65 - 70	1236	1278	1332	1325	1321	1306	1325	1336	1337	1335	1370	1362	1341	1362	1355	1338	1346	1330	1337	1332	1335	1335	1341	1312
	48	80	244	263	200	218	217	187	174	19	141	128	101	153	203	208	239	236	282	235	286	246	34	60
60 - 65	1260	1250	1277	1322	1318	1292	1325	1316	1322	1331	1365	1370	1383	1359	1363	1324	1333	1341	1324	1318	1322	1346	1279	1260
	1	1	131	227	188	212	262	200	183	173	214	223	211	215	259	264	260	242	280	295	173	74	50	1

Table 36: NT values and numbers of samples of averaged data tabulated by geomagnetic latitude and geomagnetic time for Kp range 0.0 to 1.3 for summer.

NT (K)

SUMMER

Kp = 0.0 - 1.3

Geomagnetic Latitude

Coefficient	60-65	65-70	70-75	75-80	80-85	85-90
A_0	1321	1330	1345	1339	1341	1326
A_1	-38.17	-24.07	-13.20	-23.27	-19.50	-31.62
B_1	-16.47	-12.08	-12.22	-16.42	-26.59	2.87
A_2	- .94	- 1.33	16.33	16.31	- 8.44	- 2.60
B_2	- 4.21	- 6.74	- 4.72	- 8.22	-10.07	- 6.21
A_3	-15.36	- 8.89	- 5.07	1.30	-14.65	- 4.33
B_3	-12.57	- 8.62	- 0.74	2.98	- 2.28	3.62
A_4	- 0.76	- 5.57	- 1.94	- 2.99	-14.41	- 6.34
B_4	- 5.77	-11.94	- 1.96	- 5.44	5.27	2.19
A_5	- 3.10	- 1.59	- 8.86	2.92	5.18	9.84
B_5	- 6.78	-10.41	3.50	1.34	- 2.20	- .76

Table 37: Fourier coefficients for NT values tabulated by geomagnetic latitude for Kp range 0.0 to 1.3 for summer.

$$T_{N2} = A_0 + \sum_{n=1}^{\infty} \left(A_n \cos \frac{2\pi nt}{T} + B_n \sin \frac{2\pi nt}{T}\right)$$

NT (K)

SUMMER

Kp = 1.3 - 4.0

Local Geomagnetic Time in Hours

Geomagnetic Latitude	1	2	3	4	5	6	7	8	9	10	11	12	13	14	15	16	17	18	19	20	21	22	23	24
85 - 90	1409	1392	1386	1402	1450	1420	1419	1393	1410	1393	1397	1394	1409	1428	1426	1399	1397	1411	1421	1439	1391	1412	1420	1442
	22	28	26	34	28	38	27	21	23	42	35	33	65	31	38	43	71	39	26	14	16	19	20	33
80 - 85	1423	1411	1384	1378	1386	1436	1421	1412	1397	1414	1418	1428	1422	1407	1408	1410	1403	1383	1367	1403	1411	1421	1405	1398
	158	179	130	114	134	165	187	208	169	189	242	227	233	251	215	161	220	148	133	122	101	60	138	85
75 - 80	1398	1403	1400	1385	1407	1389	1410	1434	1412	1397	1431	1450	1464	1445	1399	1418	1408	1378	1391	1398	1389	1406	1401	1399
	302	276	286	276	215	269	330	251	173	215	198	130	140	148	227	210	234	270	249	189	229	272	253	325
70 - 75	1420	1415	1395	1379	1397	1383	1430	1430	1399	1439	1445	1448	1463	1459	1438	1402	1401	1390	1383	1385	1397	1391	1398	1393
	441	219	373	391	327	321	325	226	175	208	189	128	106	216	238	306	272	297	331	314	351	368	296	392
65 - 70	1301	1325	1391	1378	1387	1374	1437	1396	1387	1428	1429	1428	1440	1447	1430	1404	1412	1387	1385	1386	1385	1384	1398	1388
	130	166	545	454	472	493	362	284	251	191	236	160	185	229	277	310	381	422	433	443	419	452	565	531
60 - 65	1279	1266	1314	1374	1352	1350	1415	1389	1381	1398	1418	1442	1448	1432	1431	1384	1400	1398	1367	1360	1372	1378	1374	1358
	121	106	129	401	398	495	476	383	294	295	338	284	194	284	414	393	486	504	492	461	352	330	206	64

Table 38: NT values and numbers of samples of averaged data tabulated by geomagnetic latitude and geomagnetic time for Kp range 1.3 to 4.0 for summer.

NT (K)

SUMMER

Kp = 1.3 - 4.0

Geomagnetic Latitude

Coefficient	60-65	65-70	70-75	75-80	80-85	85-90
A_0	1378	1396	1412	1409	1406	1411
A_1	-49.22	-35.44	-24.63	-18.87	- 6.20	3.86
B_1	-17.78	- 7.91	2.46	1.05	3.60	- 2.33
A_2	1.14	0.92	18.91	13.14	9.63	- 4.11
B_2	- 9.73	- 3.34	4.83	2.97	- 3.49	0.09
A_3	- 3.80	- 4.17	1.71	- 1.71	5.31	1.01
B_3	-21.87	-15.68	- 3.77	- 6.90	- 8.07	-10.84
A_4	6.45	- 0.41	0.61	2.13	3.61	6.62
B_4	- 8.77	- 7.56	9.41	6.50	2.21	2.88
A_5	- 0.51	- 0.91	- 3.75	- 6.93	- 9.63	14.66
B_5	-14.65	- 9.10	1.72	- 5.11	9.83	1.88

Table 39: Fourier coefficients for NT values tabulated by geomagnetic latitude for Kp range 1.3 to 4.0 for summer.

$$T_{N2} = A_O = \sum_{n=1}^{\infty} \left(A_n \cos \frac{2\pi nt}{T} + B_n \sin \frac{2\pi nt}{T}\right)$$

NT (K)

SUMMER

Kp > 4

Local Geomagnetic Time in Hours

Geomagnetic Latitude	1	2	3	4	5	6	7	8	9	10	11	12	13	14	15	16	17	18	19	20	21	22	23	24
85 - 90	0	1408	0	0	0	0	0	0	0	1424	1482	1484	1507	1425	1506	0	0	0	0	0	0	0	0	0
	0	1	0	0	0	0	0	0	0	4	12	10	8	6	4	0	0	0	0	0	0	0	0	0
80 - 85	1443	1451	1528	1567	1325	1427	1430	0	1493	0	1515	1502	1517	1524	1488	1451	1454	1380	1373	1455	1574	0	1477	1446
	12	7	5	5	5	2	8	0	24	0	13	26	31	47	29	20	28	13	8	22	7	0	13	8
75 - 80	1598	0	1456	1486	0	1562	1506	1504	1515	1530	0	1505	1448	1445	1467	1462	1526	1365	0	1460	0	0	0	0
	8	0	13	12	0	23	19	38	21	20	0	7	18	12	35	39	32	4	0	6	0	0	0	0
70 - 75	0	1503	1400	1402	1465	1562	1528	1559	1611	1472	0	0	1599	0	1474	1451	1505	1502	1422	0	1444	1391	0	0
	0	14	8	14	24	4	37	43	18	18	0	0	8	0	44	8	23	12	21	0	9	8	0	0
65 - 70	0	0	1529	1486	1464	1536	1505	1523	1496	1480	0	0	1555	1458	1500	1559	1448	1438	0	0	1508	1332	0	0
	0	0	4	15	28	11	45	48	10	20	0	0	2	11	32	18	8	28	0	0	5	16	0	0
60 - 65	0	0	0	1654	1419	1481	1484	1436	1491	1440	0	0	1545	1470	1487	1443	1402	1375	1414	1408	1551	1438	1518	0
	0	0	0	3	11	18	60	38	4	18	0	0	4	11	13	33	11	12	38	40	19	37	12	0

Table 40: NT values and numbers of samples of averaged data tabulated by geomagnetic latitude and geomagnetic time for Kp range > 4.0 for summer.

NT (K)

EQUINOX

Kp = 0.0 - 1.3

Local Geomagnetic Time in Hours

Geomagnetic Latitude	1	2	3	4	5	6	7	8	9	10	11	12	13	14	15	16	17	18	19	20	21	22	23	24
85 - 90	1147	1143	1113	1129	1136	1123	1128	1124	1126	1176	1194	1131	1148	1119	1156	1161	1137	1116	1133	1166	1172	1155	1098	1131
	24	22	29	31	24	24	15	25	17	15	14	25	15	13	27	19	17	13	10	11	19	17	26	19
80 - 85	1165	1152	1162	1168	1194	1203	1152	1150	1134	1143	1174	1175	1176	1152	1129	1149	1134	1130	1100	1114	1111	1155	1190	1172
	160	149	119	90	74	88	101	79	66	65	49	52	57	57	63	75	83	99	84	77	46	53	81	149
75 - 80	1137	1126	1124	1144	1104	1169	1209	1221	1164	1156	1155	1208	1163	1132	1145	1139	1149	1110	1122	1115	1092	1166	1179	1141
	127	73	54	61	51	56	92	113	92	111	127	120	133	135	196	127	138	121	112	96	65	57	127	179
70 - 75	1107	1179	1172	1155	1147	1207	1183	1167	1163	1156	1169	1165	1137	1134	1119	1134	1141	1112	1094	1035	1049	1135	1138	1100
	121	94	56	88	91	99	115	168	165	162	139	128	135	135	143	185	179	117	128	105	119	101	164	156
65 - 70	1124	1162	1169	1139	1145	1130	1172	1154	1096	1114	1104	1171	1099	1120	1094	1107	1101	1069	1043	1052	1058	1114	1096	1149
	31	65	112	142	140	100	150	189	119	108	158	126	146	146	188	245	194	227	150	193	153	156	152	54
60 - 65	1163	1113	1129	1127	1103	1139	1137	1325	1067	1087	1097	1112	1111	1116	1110	1186	1145	1132	1073	1024	1044	1069	1100	1115
	94	123	161	171	126	89	130	111	85	81	192	196	165	177	104	127	78	192	154	250	206	242	194	110

Table 41: NT values and numbers of samples of averaged data tabulated by geomagnetic latitude and geomagnetic time for Kp range 0.0 to 1.3 for equinox.

NT (K)

EQUINOX

Kp = 0.0-1.3

Geomagnetic Latitude

Coefficient	60-65	65-70	70-75	75-80	80-85	85-90
A_0	1118	1116	1138	1149	1154	1140
A_1	-13.84	-1.07	-18.30	-17.69	1.28	-7.37
B_1	24.10	38.11	39.17	17.63	21.11	-6.52
A_2	-13.61	8.47	-.65	8.26	11.42	6.01
B_2	18.23	18.03	12.15	-12.11	10.36	-6.76
A_3	40.38	7.02	8.94	16.31	.72	-7.16
B_3	4.72	-3.33	1.68	-8.84	-11.85	4.03
A_4	7.91	4.59	7.55	9.55	16.17	-7.73
B_4	10.60	.42	-9.93	2.18	-10.45	-5.51
A_5	-18.99	-16.46	-15.31	-14.49	-1.40	-2.00
B_5	-13.50	-2.70	-7.92	-9.47	-1.38	20.01

Table 42: Fourier coefficients for NT values tabulated by geomagnetic latitude for Kp range 0.0 to 1.3 for equinox.

$$T_{N2} = A_0 + \sum_{n=1}^{\infty} \left(A_n \cos \frac{2\pi nt}{T} + B_n \sin \frac{2\pi nt}{T}\right)$$

NT (K)

EQUINOX

Kp = 1.3 - 4.0

Local Geomagnetic Time in Hours

Geomagnetic Latitude	1	2	3	4	5	6	7	8	9	10	11	12	13	14	15	16	17	18	19	20	21	22	23	24
85 - 90	1268	1298	1281	1288	1246	1220	1217	1225	1208	1254	1235	1286	1215	1231	1207	1213	1225	1243	1260	1244	1239	1230	1228	1213
	32	29	38	28	38	22	35	37	25	43	31	11	30	28	26	26	38	34	31	23	28	2	47	55
80 - 85	1236	1228	1238	1228	1237	1256	1254	1269	1256	1257	1302	1273	1251	1220	1217	1216	1229	1210	1215	1175	1194	1245	1253	1256
	155	155	121	130	144	153	126	91	138	139	102	111	108	141	166	203	182	160	126	115	113	112	157	170
75 - 80	1212	1237	1214	1195	1223	1273	1277	1246	1263	1294	1285	1282	1240	1262	1246	1256	1228	1229	1194	1160	1173	1254	1264	1208
	124	151	165	168	170	171	214	291	261	250	295	275	270	253	260	274	236	217	174	128	127	147	174	182
70 - 75	1233	1240	1232	1226	1244	1214	1251	1244	1261	1271	1269	1275	1265	1235	1243	1268	1255	1240	1229	1143	1150	1206	1200	1207
	140	144	201	239	268	198	264	330	392	346	355	405	421	351	329	339	328	330	222	188	155	217	234	198
65 - 70	1278	1284	1238	1211	1199	1186	1229	1233	1222	1212	1231	1230	1248	1240	1226	1229	1230	1202	1150	1187	1156	1128	1196	1260
	136	143	227	323	333	330	359	340	355	291	372	343	386	446	391	337	404	380	310	203	185	211	259	148
60 - 65	1198	1245	1233	1224	1191	1179	1192	1167	1165	1144	1190	1219	1203	1220	1204	1204	1234	1181	1149	1133	1154	1175	1245	1229
	208	231	189	389	301	307	251	182	183	248	332	434	411	359	328	1265	259	326	383	355	297	240	217	198

Table 43: NT values and numbers of samples of averaged data tabulated by geomagnetic latitude and geomagnetic time for Kp range 1.3 to 4.0 for equinox.

NT (K)

EQUINOX

Kp = 1.3-4.0

Geomagnetic Latitude

Coefficient	60-65	65-70	70-75	75-80	80-85	85-90
A_0	1197	1217	1233	1248	1238	1241
A_1	5.01	-9.35	-31.80	-39.19	-13.59	12.63
B_1	-.10	15.95	12.72	32.37	21.57	7.88
A_2	12.03	18.77	4.52	3.48	15.41	5.24
B_2	35.93	27.94	14.91	-19.96	-6.48	9.52
A_3	13.82	16.68	9.50	35.14	5.74	-20.44
B_3	-1.64	17.47	15.35	-4.05	1.89	16.74
A_4	5.33	4.33	8.81	-.41	12.86	-.86
B_4	-11.78	15.20	-7.14	4.24	-8.52	2.76
A_5	-12.72	-3.14	-4.56	-17.00	-5.91	-4.62
B_5	-7.12	3.68	-5.95	-16.10	-3.87	-.31

Table 44: Fourier coefficients for NT values tabulated by geomagnetic latitude for Kp range 1.3 to 4.0 for equinox.

$$T_{N2} = A_0 + \sum_{n=1}^{\infty} \left(A_n \cos \frac{2\pi nt}{T} + B_n \sin \frac{2\pi nt}{T}\right)$$

NT (K)

EQUINOX

Kp > 4.0

Local Geomagnetic Time in Hours

Geomagnetic Latitude	1	2	3	4	5	6	7	8	9	10	11	12	13	14	15	16	17	18	19	20	21	22	23	24
85 - 90	0	0	0	0	1513	1493	0	0	0	1596	0	1554	1373	0	0	0	1821	0	0	0	0	1185	0	0
	0	0	0	0	1	5	0	0	0	7	0	5	3	0	0	0	2	0	0	0	0	2	0	0
80 - 85	1555	1552	1553	1660	1590	1387	1350	1458	1524	1597	1509	1522	1589	1445	1459	1489	1265	1370	1317	1501	1488	1752	1750	1573
	8	13	16	20	30	9	16	18	33	12	23	26	10	19	11	13	1	9	11	10	6	7	20	19
75 - 80	1309	1473	1380	1301	1378	1604	1377	1542	1592	1488	1487	1398	1403	1494	1458	1352	1416	1442	1230	1161	1488	1858	1420	1367
	13	6	1	21	17	31	33	6	7	41	33	30	48	22	12	18	18	28	1	6	8	20	5	8
70 - 75	1349	1335	1452	1459	1426	1487	1452	1532	1504	1429	1444	1414	1472	1431	1439	1501	1554	1544	1452	1298	1475	1265	1339	1394
	27	20	9	11	16	55	89	53	33	47	1	38	39	22	39	40	27	32	6	22	50	29	17	38
65 - 70	1456	1249	1265	1266	1277	1381	1519	1553	1387	1432	1585	1428	1437	1467	1401	1465	1514	1566	1360	1284	1413	1188	1389	1305
	18	19	30	26	34	46	53	34	18	22	18	36	69	50	57	62	56	13	1	9	39	24	15	20
60 - 65	1387	1388	1389	1390	1404	1450	1501	1520	1416	1335	1447	1330	1368	1421	1476	1487	1477	1315	1204	1328	1378	1279	1311	1386
	1	1	1	64	25	52	60	25	13	13	19	62	82	27	27	58	69	22	28	31	66	51	33	58

Table 45: NT values and numbers of samples of averaged data tabulated by geomagnetic latitude and geomagnetic time for Kp range > 4.0 for equinox.

NT (K)

EQUINOX

Kp > 4.0

Coefficient	Geomagnetic Latitude 60-65	65-70	70-75	75-80	80-85	85-90
A_0	1391	1401	1439	1433	1511	INSUFFICIENT DATA
A_1	-39.33	-88.50	-61.91	-25.16	60.12	
B_1	37.53	-20.40	7.81	30.73	39.04	
A_2	-22.54	-9.54	-48.99	30.05	103.12	
B_2	29.25	-18.90	4.84	-51.18	-8.83	
A_3	50.12	51.28	15.57	43.41	-20.40	
B_3	-16.10	25.24	27.54	-51.93	-35.13	
A_4	-17.13	46.75	2.54	-37.11	-34.41	
B_4	-.90	14.97	-13.99	-50.22	-60.18	
A_5	-25.40	-21.68	-1.93	-52.89	19.24	
B_5	24.62	5.67	-17.63	-26.51	-31.03	

Table 46: Fourier coefficients for NT values tabulated by geomagnetic latitude for Kp range > 4.0 for equinox.

$$T_{N2} = A_0 + \sum_{n=1}^{\infty} \left(A_n \cos \frac{2\pi nt}{T} + B_n \sin \frac{2\pi nt}{T}\right)$$

NT(K)

WINTER

Kp = 0.0 - 1.3

Local Geomagnetic Time in Hours

Geomagnetic Latitude	1	2	3	4	5	6	7	8	9	10	11	12	13	14	15	16	17	18	19	20	21	22	23	24
85 - 90	0	958	0	968	935	884	951	0	0	1106	1031	0	0	0	1033	0	964	1002	954	985	1000	0	0	0
	0	6	0	1	3	1	1	0	0	4	3	0	0	0	6	0	1	1	2	3	3	0	0	0
80 - 85	941	955	966	941	921	947	954	1106	1010	969	1101	972	881	959	984	975	982	984	916	934	899	965	948	0
	12	4	9	12	6	2	2	1	9	9	9	1	1	6	12	2	6	3	10	4	7	3	8	0
75 - 80	916	925	929	911	970	1058	1054	1106	1086	1127	1032	963	884	971	985	974	955	994	971	925	882	921	905	925
	4	10	16	14	5	10	4	1	11	10	16	28	7	15	10	14	27	13	9	10	9	2	4	15
70 - 75	0	1035	897	1005	1069	1003	1005	1046	1119	1063	1015	994	959	1011	969	945	941	933	921	853	878	0	0	0
	0	12	32	4	10	4	11	13	24	27	22	36	19	7	12	35	34	10	7	9	4	0	0	0
65 - 70	0	1000	889	1030	966	983	991	983	954	1063	1032	1021	1011	968	967	947	978	0	832	0	858	0	0	844
	0	5	20	7	12	19	12	21	26	41	38	43	39	17	32	33	13	0	7	0	24	0	0	1
60 - 65	0	0	0	992	976	929	926	929	962	1005	1035	1030	1031	977	972	986	871	871	0	0	0	0	0	0
	0	0	0	11	16	28	44	54	43	42	44	55	55	18	46	19	13	10	0	0	0	0	0	0

Table 47: NT values and numbers of samples of averaged data tabulated by geomagnetic latitude and geomagnetic time for Kp range 0.0 to 1.3 for winter.

NT (K)

WINTER

Kp = 1 3 - 4.0

Local Geomagnetic Time in Hours

Geomagnetic Latitude	1	2	3	4	5	6	7	8	9	10	11	12	13	14	15	16	17	18	19	20	21	22	23	24
85 - 90	1082	1112	1147	1201	1154	1105	1182	1139	1090	1060	1110	1182	1130	1137	1107	1129	1160	1191	1188	1174	1158	1168	1161	1104
	5	1	6	5	2	1	2	3	3	3	6	3	4	2	6	6	4	6	4	5	4	6	7	7
80 - 85	1079	1022	1134	1170	1151	1122	1174	1207	1247	1249	1167	1088	1156	1119	1089	1147	1139	1116	1146	1144	1128	1123	1084	1147
	34	18	13	5	13	13	15	15	11	7	8	10	11	16	9	12	12	14	17	17	21	9	15	12
75 - 80	1056	1051	1108	1076	1068	1067	1128	1142	1200	1149	1137	1078	1069	1118	1177	1084	1110	1098	1105	1107	1095	1108	1081	1080
	28	43	24	22	14	19	16	21	19	37	17	10	34	21	16	33	27	25	32	37	32	18	5	23
70 - 75	1051	1122	1055	1113	1145	1101	1112	1158	1112	1136	1094	1109	1089	1125	1125	1088	1065	1058	1046	1043	1075	1075	1054	1034
	1	57	18	33	26	15	16	22	28	20	30	13	31	38	30	26	60	60	19	19	19	22	18	11
65 - 70	1050	1050	1226	1265	1064	1081	1069	1066	1101	1069	1078	1099	1108	1121	1063	1075	1061	1134	1081	1075	1021	1051	1080	1048
	1	1	49	27	18	29	13	35	56	46	32	38	40	60	42	66	54	5	15	32	17	19	16	16
60 - 65	0	0	1025	1066	1086	1013	1007	989	1014	1075	1099	1093	1123	1083	1090	1060	1049	952	1017	0	0	902	0	0
	0	0	17	14	27	44	56	31	38	62	33	39	49	78	75	110	23	2	5	0	0	4	0	0

Table 48: NT values and numbers of samples of averaged data tabulated by geomagnetic latitude and geomagnetic time for Kp range 1.3 to 4.0 for winter.

NT (K)

WINTER

Kp = 1.3 - 4.0

Coefficient		Geomagnetic Latitude 60-65	65-70	70-75	75-80	80-85	85-90
A_0			1089	1091	1104	1139	1144
A_1	INSUFFICIENT DATA		- 1.23	-26.80	-26.95	-31.78	9.00
B_1			18.75	25.93	- 0.12	21.03	- 8.45
A_2			-10.19	- 4.69	- 5.00	-16.85	-27.62
B_2			30.90	3.83	-19.77	-33.52	- 4.84
A_3			-29.36	2.20	13.42	2.79	-16.47
B_3			11.13	- 9.08	6.10	9.62	-15.30
A_4			-11.06	-13.63	-24.64	-14.82	11.90
B_4			- 8.81	- 1.78	- 2.68	-12.80	5.44
A_5			5.72	0.37	9.12	17.21	-19.73
B_5			-37.58	0.98	- 4.44	-12.03	-19.60

Table 49: Fourier coefficients for NT values tabulated by geomagnetic latitude for Kp range 1.3 to 4.0 for winter.

$$T_{N2} = A_0 + \sum_{n=1}^{\infty} \left(A_n \cos \frac{2\pi nt}{T} + B_n \sin \frac{2\pi nt}{T}\right)$$

NT (K)

WINTER

Kp > 4

Local Geomagnetic Time in Hours

Geomagnetic Latitude	1	2	3	4	5	6	7	8	9	10	11	12	13	14	15	16	17	18	19	20	21	22	23	24
85 - 90	0	0	0	0	0	1423	0	0	0	1243	1221	0	0	0	0	0	0	1260	0	0	0	0	0	0
	0	0	0	0	0	1	0	0	0	1	2	0	0	0	0	0	0	2	0	0	0	0	0	0
80 - 85	1147	0	0	0	0	1208	1299	1299	1144	1345	0	1266	0	0	1350	0	1325	1306	1232	1246	1260	1240	1227	1270
	2	0	0	0	0	4	3	4	8	1	0	2	0	0	5	0	1	1	4	6	4	3	2	1
75 - 80	1141	0	0	0	1198	1283	1280	1283	1272	1271	1159	1497	1254	0	1252	1277	1243	1325	1189	1115	1206	1246	1220	1310
	2	0	0	0	3	3	1	5	12	15	1	3	7	0	6	6	5	2	5.	12	5	4	9	7
70 - 75	0	1215	1138	1097	1249	1196	1236	1265	1364	1273	1262	0	1234	0	1188	1238	1181	1160	1074	0	0	0	0	0
	0	11	6	6	9	5	15	10	5	2	13	0	8	0	8	7	8	16	6	0	0	0	0	0
65 - 70	0	1240	1074	1197	0	1157	1206	1304	1301	1230	1277	1202	1195	1165	1195	1124	1083	1200	1129	0	0	0	0	0
	0	2	2	8	0	5	9	21	13	11	2	15	3	2	9	8	2	2	10	0	0	0	0	0
60 - 65	0	0	0	1138	1269	1387	1289	1349	1316	1364	1179	1180	1192	1147	1069	1105	1117	0	0	0	0	0	0	0
	0	0	0	18	5	20	22	33	28	13	26	27	3	5	13	10	5	0	0	0	0	0	0	0

Table 50: NT values and numbers of samples of averaged data tabulated by geomagnetic latitude and geomagnetic time for Kp range > 4.0 for winter.

Table 51: Data index for helium density.

	Summer	Equinox	Winter
0 < Kp < 1.3	Tabulated Values: Table 52, p. 114	Tabulated Values: Table 57, p. 119	Tabulated Values: Table 63, p. 125
	Graphical Analysis: Figure 28, p. 105	Graphical Analysis: Figure 31, p. 108	Graphical Analysis: Figure 34, p. 111
	Fourier Analysis: Table 53, p. 115	Fourier Analysis: Table 58, p. 120	Fourier Analysis: Table 64, p. 126
1.3 < Kp < 4.0	Tabulated Values: Table 54, p. 116	Tabulated Values: Table 59, p. 121	Tabulated Values: Table 65, p. 127
	Graphical Analysis: Figure 29, p. 106	Graphical Analysis: Figure 32, p. 109	Graphical Analysis: Figure 35, p. 112
	Fourier Analysis: Table 55, p. 117	Fourier Analysis: Table 60, p. 122	Fourier Analysis: Table 66, p. 128
Kp > 4.0	Tabulated Values: Table 56, p. 118	Tabulated Values: Table 61, p. 123	Tabulated Values: Table 67, p. 129
	Graphical Analysis: Figure 30, p. 107	Graphical Analysis: Figure 33, p. 110	Graphical Analysis: Figure 36, p. 113
	Fourier Analysis: Insufficient Data	Fourier Analysis: Table 62, p. 124	Fourier Analysis: Insufficient Data

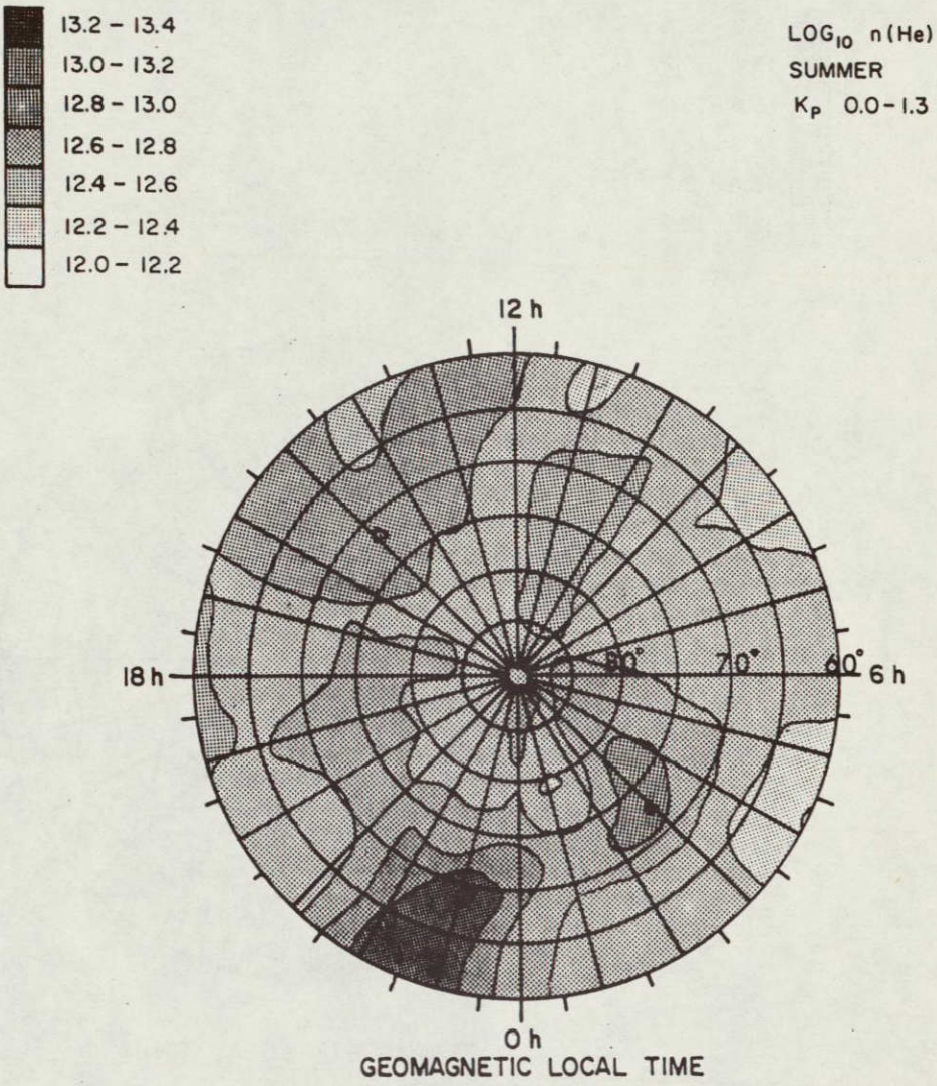

Figure 28: Helium density at 300 km as a function of geomagnetic time and geomagnetic latitude for Kp range 0.0 to 1.3 for summer.

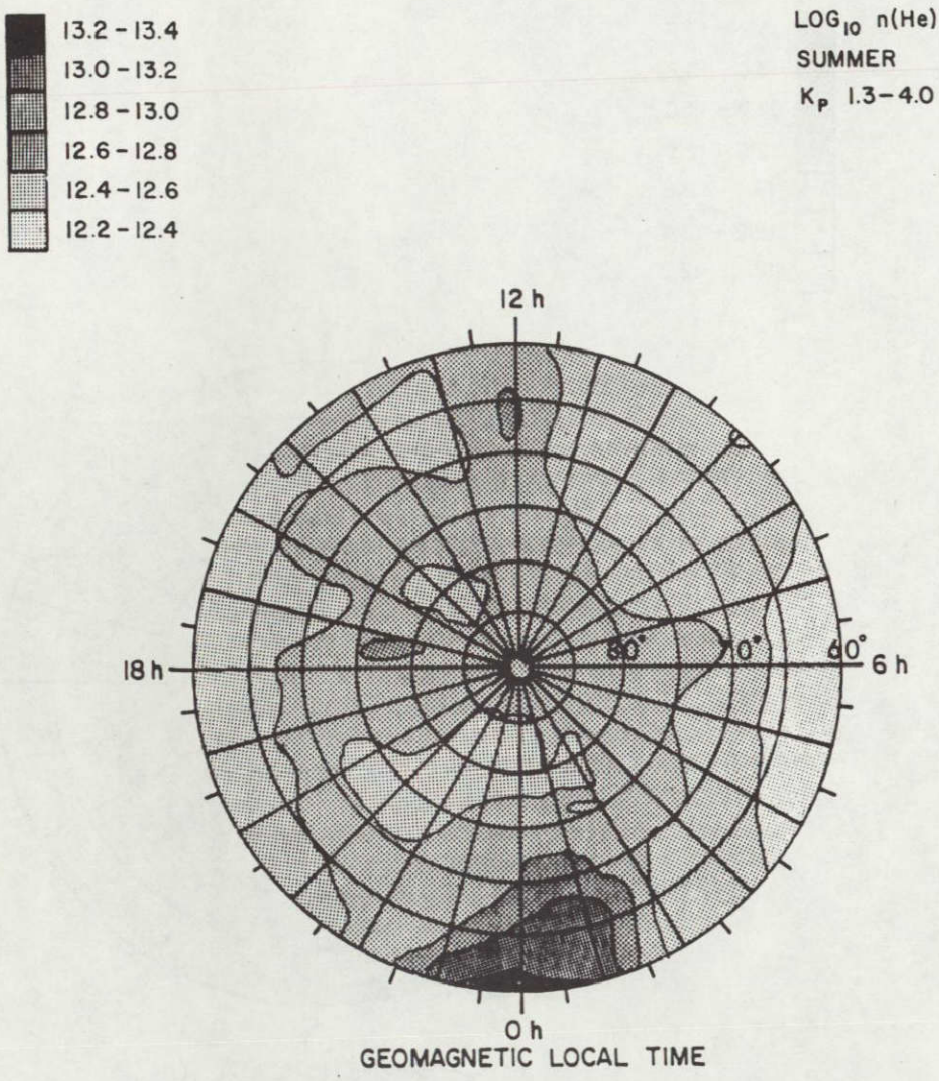

Figure 29: Helium density at 300 km as a function of geomagnetic time and geomagnetic latitude for Kp range 1.3 to 4.0 for summer.

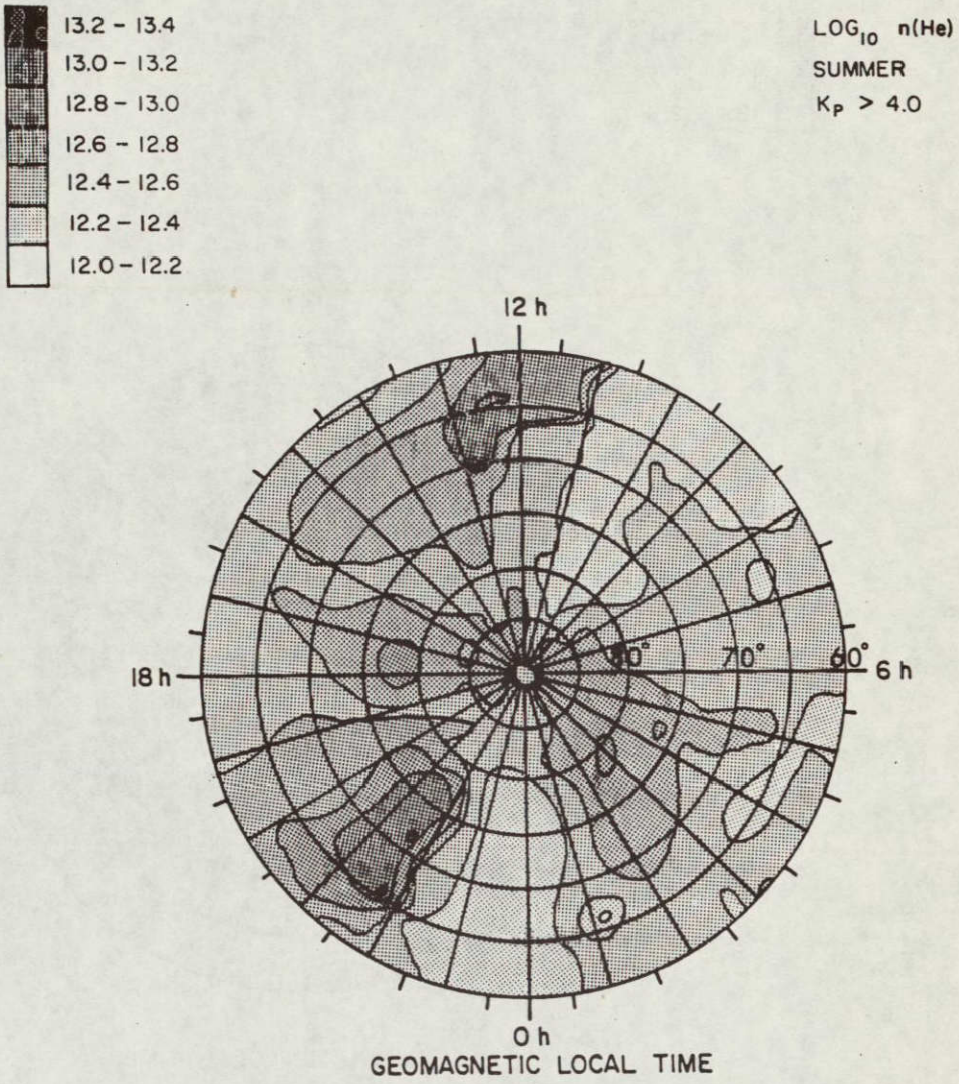

Figure 30: Helium density at 300 km as a function of geomagnetic time and geomagnetic latitude for Kp range > 4.0 for summer.

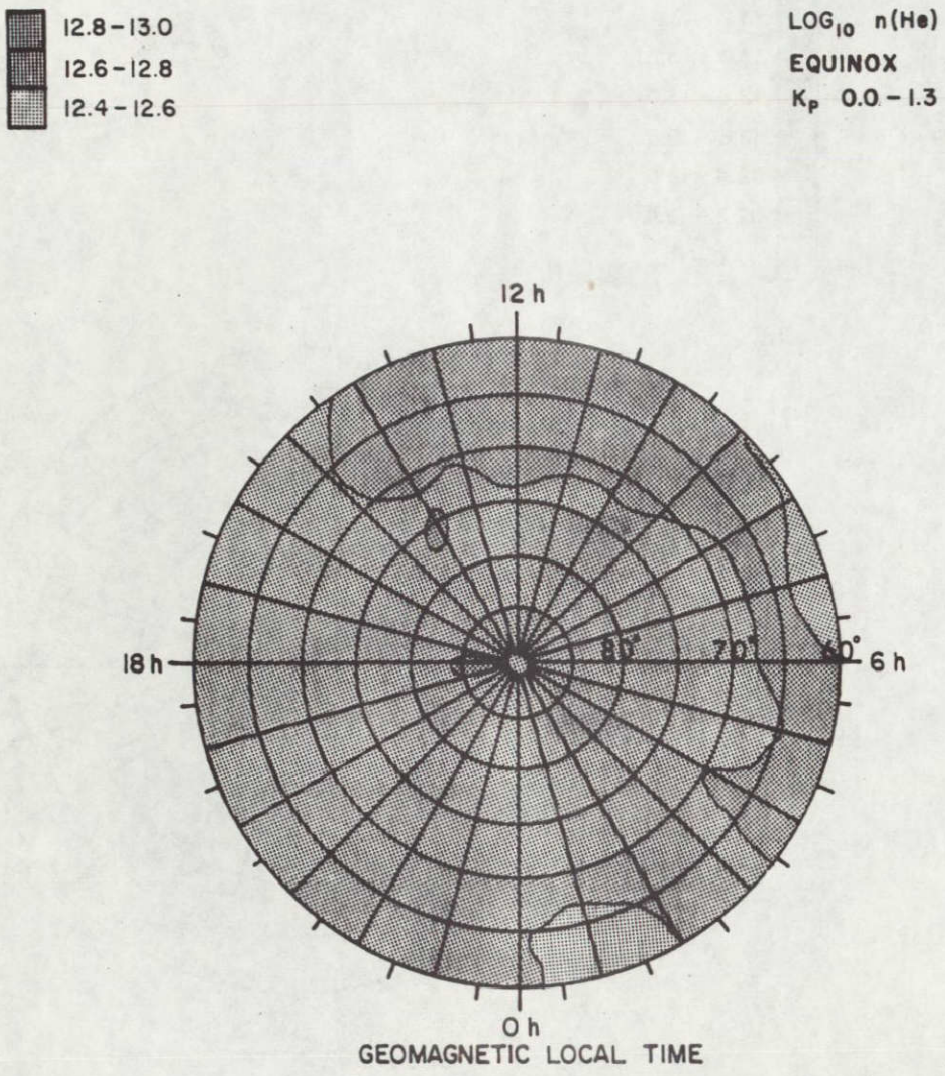

Figure 31: Helium density at 300 km as a function of geomagnetic time and geomagnetic latitude for Kp range 0.0 to 1.3 for equinox.

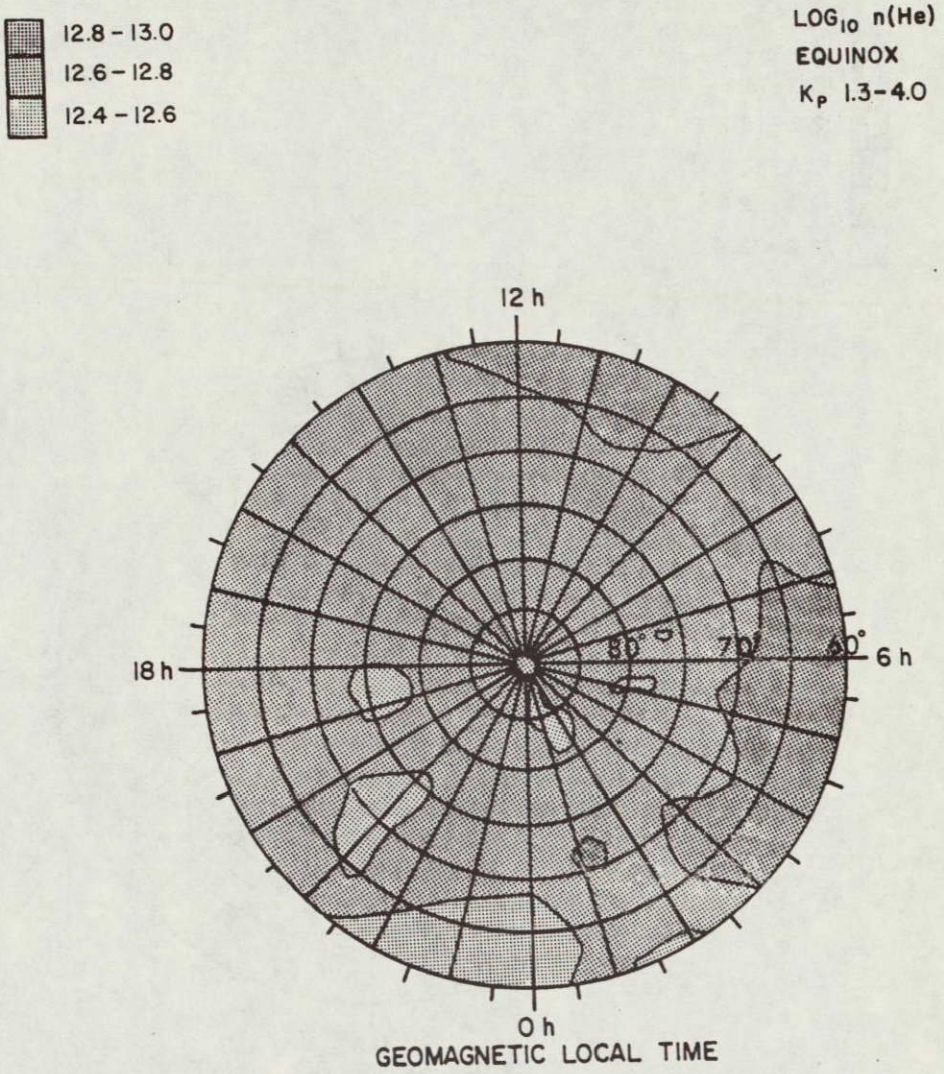

Figure 32: Helium density at 300 km as a function of geomagnetic time and geomagnetic latitude for Kp range 1.3 to 4.0 for equinox.

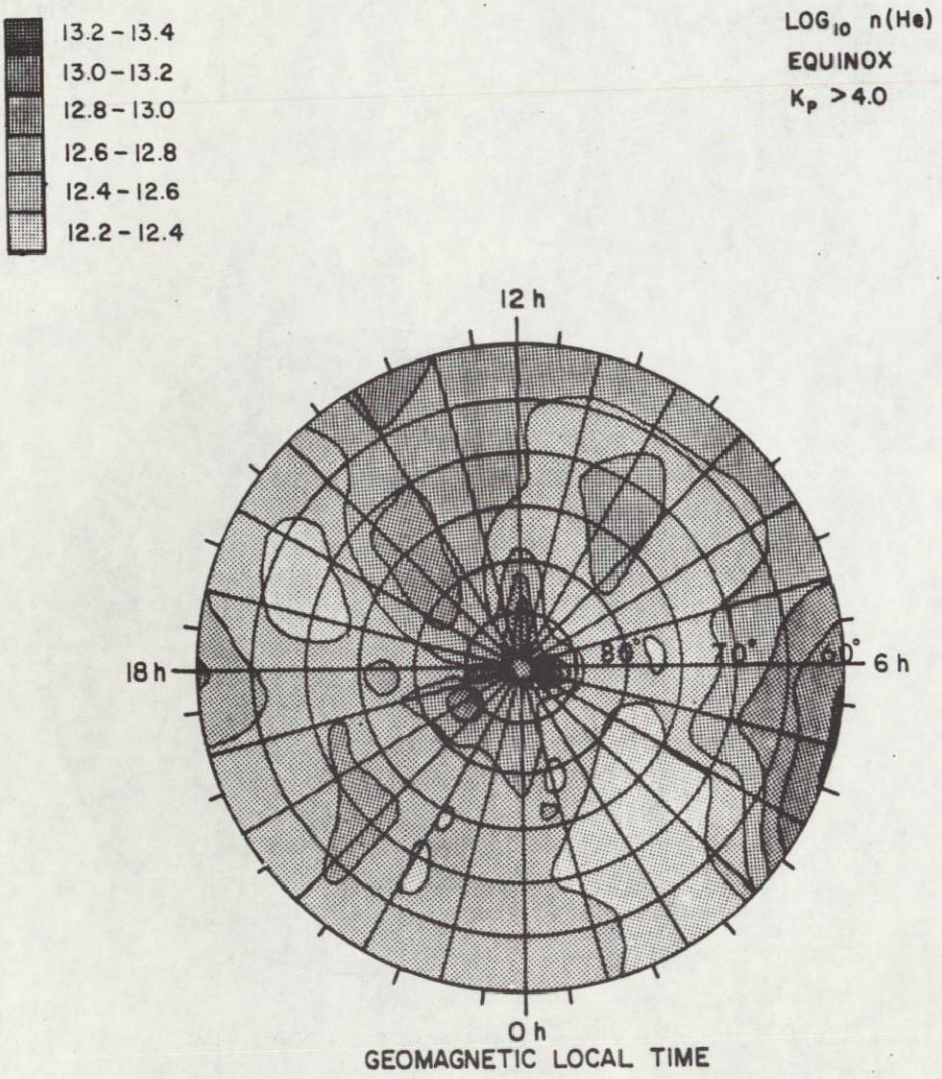

Figure 33: Helium density at 300 km as a function of geomagnetic time and geomagnetic latitude for Kp range > 4.0 for equinox.

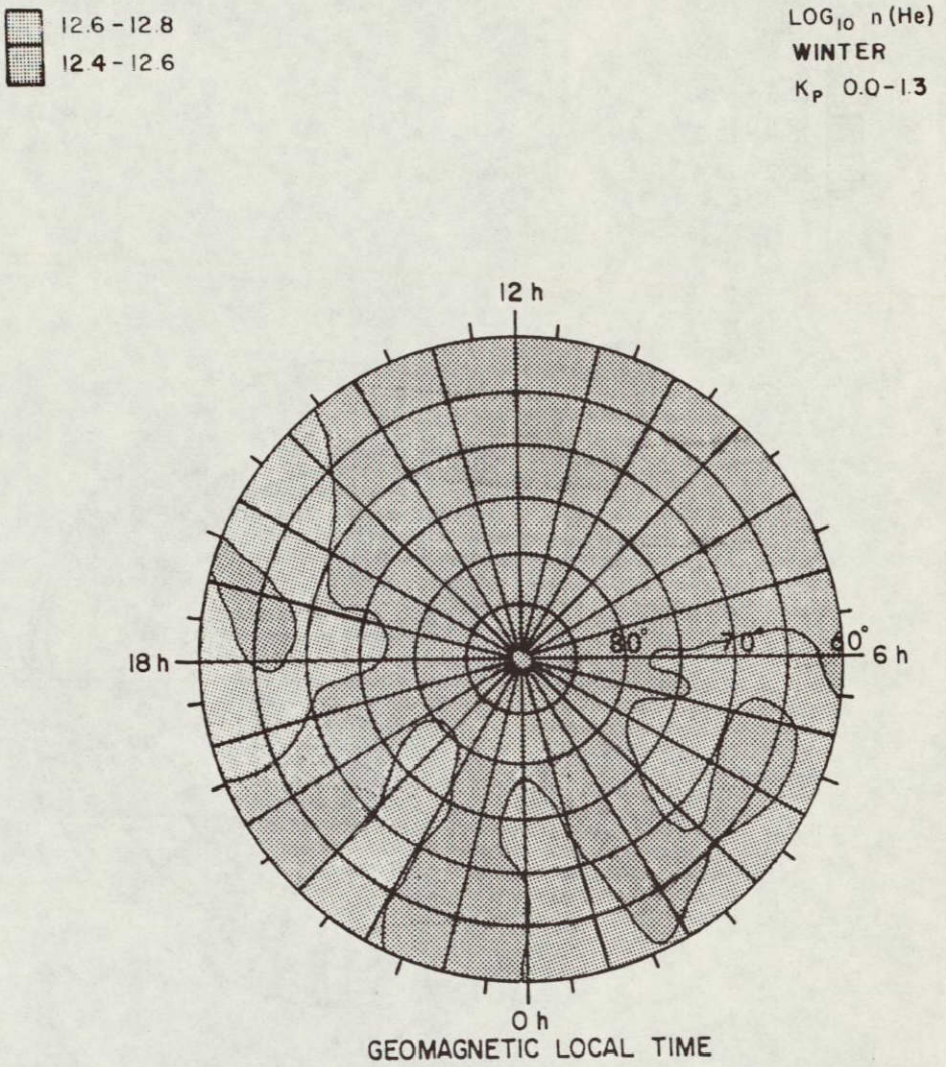

Figure 34: Helium density at 300 km as a function of geomagnetic time and geomagnetic latitude for Kp range 0.0 to 1.3 for winter.

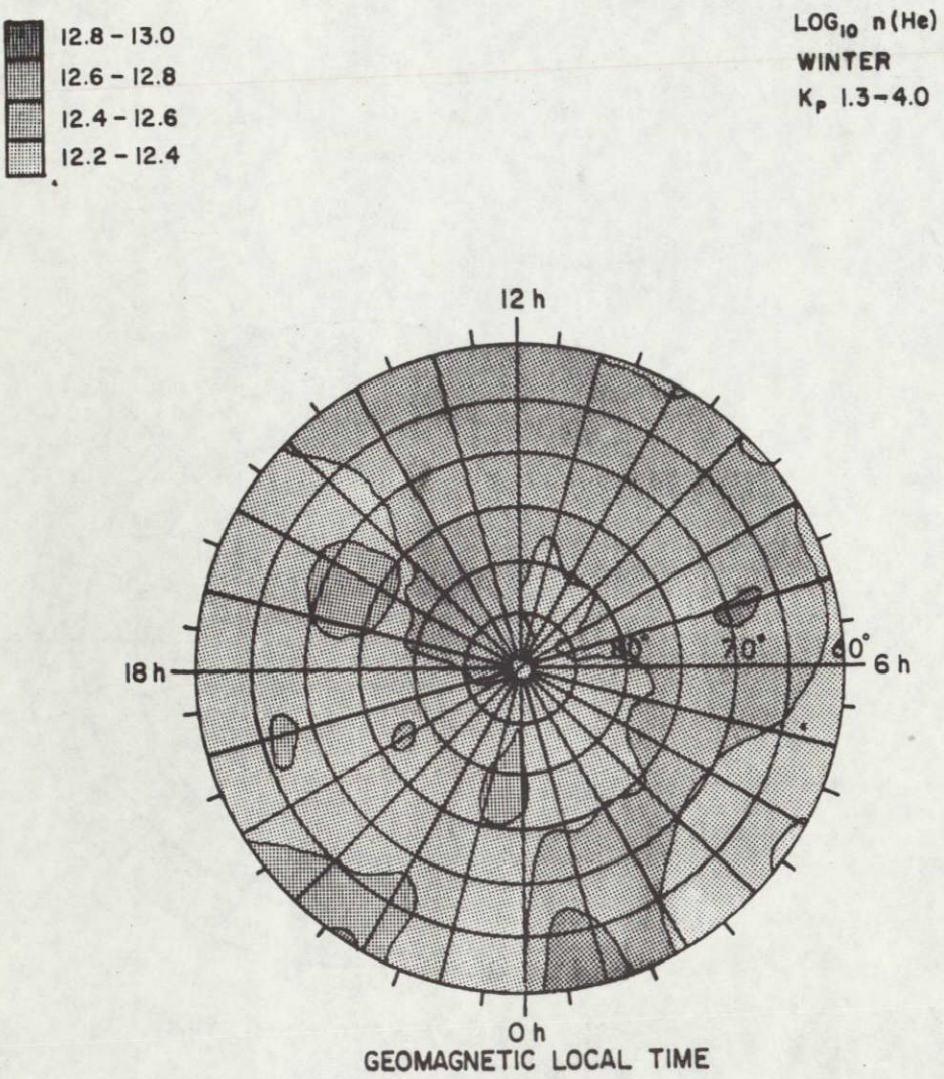

Figure 35: Helium density at 300 km as a function of geomagnetic time and geomagnetic latitude for Kp range 1.3 to 4.0 for winter.

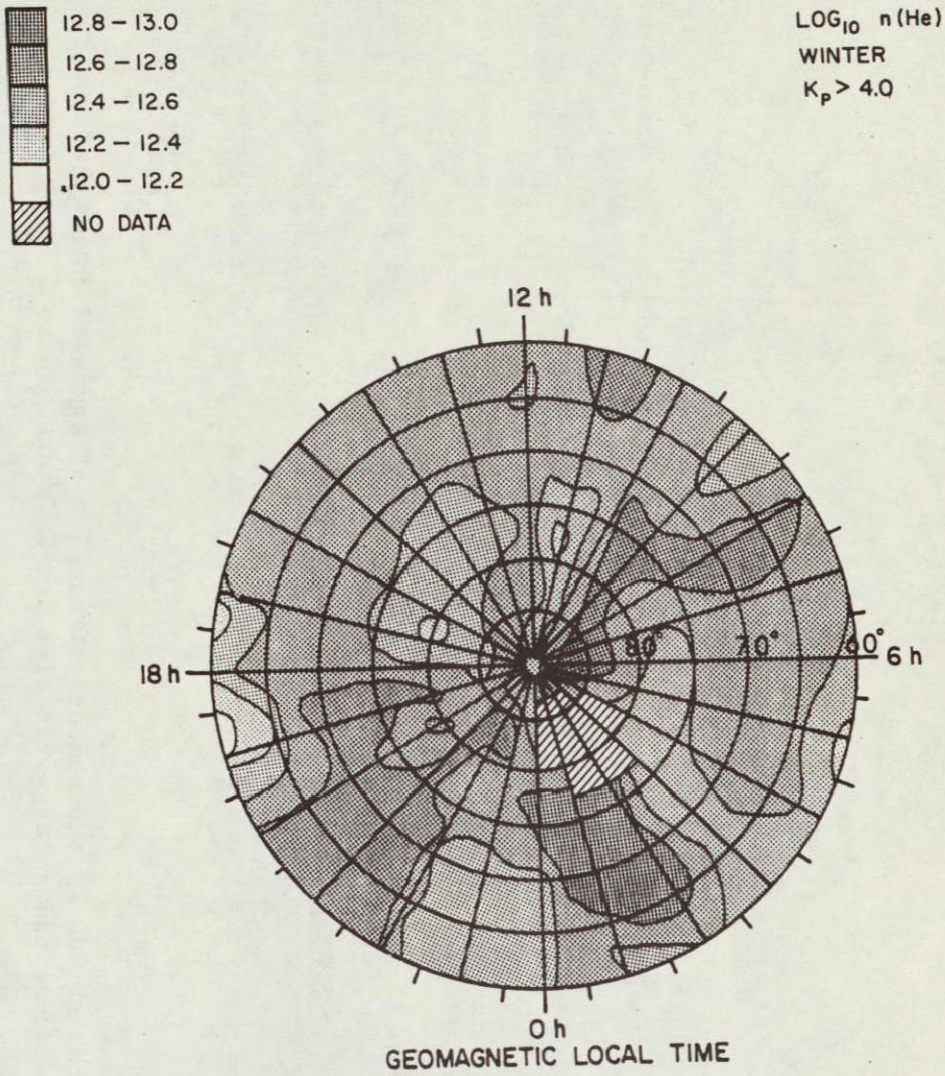

Figure 36: Helium density at 300 km as a function of geomagnetic time and geomagnetic latitude for Kp range > 4.0 for winter.

$\text{Log}_{10}\, n(He)\, m^{-3}$

SUMMER

Kp = 0.0 - 1.3

Local Geomagnetic Time in Hours

Geomagnetic Latitude	1	2	3	4	5	6	7	8	9	10	11	12	13	14	15	16	17	18	19	20	21	22	23	24
85 - 90	0	0	12.40	12.65	12.59	12.49	0	12.33	12.43	12.38	12.45	12.50	12.43	12.51	12.52	12.48	12.60	12.45	12.59	12.65	0	12.55	12.53	12.59
	0	0	1	5	3	3	0	1	4	2	2	5	8	4	6	7	3	7	5	3	0	4	2	1
80 - 85	12.66	12.43	12.53	12.54	12.57	12.85	12.69	12.52	12.61	12.63	12.78	12.78	12.53	12.49	12.64	12.51	12.56	12.66	12.50	12.35	12.52	12.44	12.44	12.52
	5	8	25	30	21	19	17	21	21	23	12	24	10	19	12	27	32	33	3	2	10	4	11	166
75 - 80	12.58	12.36	12.41	12.96	12.90	12.65	12.55	12.55	12.41	12.44	12.58	12.68	12.53	12.64	12.49	12.64	12.54	12.60	12.71	12.59	12.66	12.54	12.54	12.54
	35	12	23	20	39	17	14	21	12	20	2	20	19	24	8	36	45	40	25	13	12	18	1	7
70 - 75	12.95	12.69	12.86	12.89	12.77	12.67	12.49	12.42	12.55	12.41	12.73	12.84	12.41	12.56	12.69	12.80	12.60	12.63	12.57	12.75	12.64	12.65	12.86	12.74
	11	26	29	44	45	42	36	17	26	10	26	18	7	8	15	47	43	41	45	7	39	45	5	1
65 - 70	12.70	12.49	12.45	12.47	12.36	12.45	12.39	12.49	12.42	12.38	12.64	12.29	12.61	12.77	12.61	12.58	12.69	12.54	12.50	12.60	12.49	12.51	13.03	13.14
	5	4	24	32	15	28	25	32	25	6	25	3	8	15	27	40	40	64	79	57	41	39	13	29
60 - 65	0	0	12.41	12.49	12.24	12.23	12.55	12.45	12.32	12.42	12.50	12.36	12.65	12.60	12.54	12.68	12.61	12.61	12.65	12.64	12.37	12.54	13.10	0
	0	0	62	42	13	29	50	42	12	21	33	17	23	29	61	54	57	71	35	26	21	29	20	0

Table 52: Helium densities at 300 km and numbers of samples of averaged data tabulated by geomagnetic latitude and geomagnetic time for Kp range 0.0 to 1.3 for summer.

$\text{Log}_{10}\ n(\text{He})\,m^{-3}$

SUMMER

Kp = 0.0-1.3

Geomagnetic Latitude

Coefficient		60-65	65-70	70-75	75-80	80-85	85-90
A_0			12.565	12.676	12.293	12.574	
A_1	INSUFFICIENT DATA		.084	.115	.167	-.078	
B_1			-.096	.003	-.560	.061	
A_2			.109	.043	.442	-.007	
B_2			.027	.084	.322	.002	
A_3			.114	-.028	-.492	.002	
B_3			-.033	.011	.351	.011	
A_4			.061	-.024	-.237	.078	
B_4			-.009	-.062	-.544	-.020	
A_5			.074	.005	.591	-.016	
B_5			-.027	.045	-.145	.048	

Table 53: Fourier coefficients for helium densities at 300 km tabulated by geomagnetic latitude for Kp range 0.0 to 1.3 for summer.

$$\text{Log}_{10}\ n(\text{He})m^{-3} = A_0 + \sum_{n=1}^{\infty} \left(A_n \cos \frac{2\pi nt}{T} + B_n \sin \frac{2\pi nt}{T}\right)$$

$Log_{10}\ N(HE)_m^{-3}$

SUMMER

Kp = 1.3 - 4.0

Local Geomagnetic Time in Hours

Geomagnetic Latitude	1	2	3	4	5	6	7	8	9	10	11	12	13	14	15	16	17	18	19	20	21	22	23	24
85 - 90	12.86	12 43	12 73	12 43	12 56	12 72	12 81	12 85	12.69	12 67	12 63	12 75	12.60	12 82	12 67	12 89	12 65	12.66	12 70	12 68	12.71	12.58	12 65	12 70
	3	8	10	1	9	15	9	10	7	17	8	5	14	11	16	11	8	11	12	7	11	7	5	2
80 - 85	12.59	12 59	12 64	12.60	12 73	12 82	12 76	12 87	12 74	12.84	12 81	12 68	12 64	12 54	12 64	12 45	12 56	12 70	12 66	12 61	12.64	12 64	12 62	12.58
	42	33	48	27	98	17	103	63	58	58	48	66	68	64	58	43	57	33	22	37	38	41	44	36
75 - 80	12 49	12 64	12 54	12.75	12.69	12.70	12 78	12 57	12.50	12.50	11 63	12 69	12.82	12 69	12.64	12 66	12 57	12 68	12 89	12 67	12 63	12.61	12.54	12.56
	50	73	119	179	153	69	27	34	34	21	18	12	51	57	39	57	59	52	49	57	62	85	81	87
70 - 75	12 79	12.62	12.64	12.71	12.57	12 53	12 69	12 53	12 46	12 55	12 42	12.60	12 70	12 55	12 66	12 66	12 68	12 53	12 67	12 66	12 58	12 59	12 56	12 69
	134	70	162	137	72	43	59	49	29	22	17	14	15	71	50	70	97	71	72	50	66	94	90	125
65 - 70	12 90	13.15	12.58	12 53	12.45	12 40	12 33	12 43	12.57	12 44	12 52	12 46	12.98	12 58	12.55	12 60	12 62	12 60	12 57	12 59	12 62	12 66	12 64	12.61
	25	18	102	131	64	45	30	49	45	40	55	16	11	63	99	103	118	145	164	192	146	153	146	149
60 - 65	13 24	13 09	12 30	12 50	12 27	12 21	12.23	12 29	12 43	12.40	12 48	12 51	12 59	12 62	12 68	12 62	12 57	12 58	12.62	12 53	12.47	12 53	12 65	13.19
	20	17	5	68	50	48	70	48	55	93	63	46	34	77	168	150	136	167	159	69	62	105	111	6

Table 54: Helium densities at 300 km and numbers of samples of averaged data tabulated by geomagnetic latitude and geomagnetic time for Kp range 1.3 to 4.0 for summer.

$\text{Log}_{10}\ n(He)m^{-3}$

SUMMER

Kp = 1.3-4.0

Geomagnetic Latitude

Coefficient	60-65	65-70	70-75	75-80	80-85	85-90
A_0	12.565	12.600	12.609	12.642	12.664	12.687
A_1	.148	.085	.045	-.027	-.046	-.039
B_1	-.113	-.057	-.022	-.024	.080	-.018
A_2	.193	.114	-.002	-.055	-.022	-.005
B_2	.115	.086	.055	.020	-.079	-.019
A_3	.104	.001	.008	-.069	-.011	.074
B_3	.103	.056	-.003	-.043	.009	-.015
A_4	.048	-.017	.009	.037	.019	.010
B_4	.085	.076	.034	.042	.001	.050
A_5	.057	-.036	-.004	-.002	.004	-.008
B_5	.057	-.008	.009	-.010	.024	.031

Table 55: Fourier coefficients for helium densities at 300 km tabulated by geomagnetic latitude for Kp range 1.3 to 4.0 for summer.

$$\text{Log}_{10}\ n(He)m^{-3} = A_0 + \sum_{n=1}^{\infty} \left(A_n \cos \frac{2\pi nt}{T} + B_n \sin \frac{2\pi nt}{T}\right)$$

$\text{Log}_{10}\ n(He)m^{-3}$

SUMMER

Kp > 4.0

Local Geomagnetic Time in Hours

Geomagnetic Latitude	1	2	3	4	5	6	7	8	9	10	11	12	13	14	15	16	17	18	19	20	21	22	23	24
85 - 90	0	0	0	0	12.53	12 43	0	0	0	12 53	12.42	0	12 37	12.47	12 49	0	0	0	0	0	0	0	0	0
	0	0	0	0	1	1	0	0	0	2	2	0	2	1	1	0	0	0	0	0	0	0	0	0
80 - 85	12 53	12 58	0	12 75	12 75	12 74	12 67	0	12 73	0	12.35	12 32	12 72	12 57	12 51	12 76	12 55	12 58	12.60	12 52	12 62	0	12 56	12 41
	3	4	0	14	20	3	9	0	18	0	5	3	4	6	2	10	14	10	3	12	9	0	7	3
75 - 80	12 27	0	12 70	12 85	0	12.67	12 66	12 39	12.41	12 30	0	0	12.48	12 66	0	12 47	12.66	12.89	0	12 56	0	0	0	0
	2	0	16	18	0	10	9	10	8	1	0	0	8	5	0	12	24	6	0	15	0	0	0	0
70 - 75	0	12 42	12 85	12 67	12.53	12.75	12 38	12 52	12 53	12 44	0	0	0	0	12 69	12 65	12 56	12 63	12 59	12 54	12 82	13.11	0	0
	0	6	24	17	2	7	9	17	13	1	0	0	0	0	24	7	9	5	10	3	2	11	0	0
65 - 70	0	0	12 55	12 40	12 30	0	12.45	12 37	0	0	0	0	0	12 83	12 77	12 77	12 61	12 60	12 41	12.71	12 50	13.18	0	0
	0	0	8	2	1	0	12	3	0	0	0	0	0	2	18	36	11	44	4	7	1	12	0	0
60 - 65	0	0	0	0	12.52	0	12 36	12 58	0	12 27	0	0	12 99	12 50	12 38	12 47	12 51	12.55	12.43	12.44	12 80	12 59	12.41	0
	0	0	0	0	2	0	3	22	0	5	0	0	14	7	16	17	13	11	25	5	23	20	2	0

Table 56: Helium densities at 300 km and numbers of samples of averaged data tabulated by geomagnetic latitude and geomagnetic time for Kp range > 4.0 for summer.

Log_{10} n(He)

EQUINOX

Kp = 0 0 - 1 3

Local Geomagnetic Time in Hours

Geomagnetic Latitude	1	2	3	4	5	6	7	8	9	10	11	12	13	14	15	16	17	18	19	20	21	22	23	24
85 - 90	12 45 15	12 70 37	12 67 38	16 63 50	12 69 47	12 66 36	12 71 30	12 76 36	12 73 25	12 75 22	12 73 21	12 75 33	12 72 18	12 69 24	12 77 44	12 71 33	12 71 36	12 78 34	12 80 32	12 81 30	12 73 49	12.67 41	12 79 25	12 73 35
80 - 85	12 72 227	12 69 196	12 68 191	12 64 143	12 65 117	12 70 155	12 75 144	12 78 121	12 77 107	12 77 101	12 72 93	12 74 91	12 70 95	12 79 115	12 78 114	12 83 124	12 80 144	12 82 196	12 80 183	12 78 161	12 81 121	12 80 119	12 82 160	12 70 215
75 - 80	12 76 208	12 74 198	12 67 107	12 62 101	12 66 134	12 64 142	12 63 160	12 72 167	12 71 168	12 72 217	12 71 228	12 67 212	12 73 247	12 78 241	12 82 333	12 78 257	12 75 260	12 74 202	12 70 158	12 66 144	12 68 116	12 68 82	12 67 176	12 70 220
70 - 75	12 69 209	12 71 176	12 61 109	12 72 211	12 81 179	12 63 224	12 71 243	12 70 288	12 70 265	12 80 330	12 82 240	12 80 320	12 81 290	12 79 319	12 79 306	12 77 343	12 79 252	12 71 207	12 66 221	12 70 203	12 66 175	12 67 160	12 66 208	12 75 228
65 - 70	12 62 111	12 55 131	12 63 263	12 76 306	12 85 319	12 76 281	12 86 381	12 84 551	12 86 391	12 86 368	12.84 395	12 86 293	12 86 403	12 87 303	12 87 324	12 79 442	12 78 259	12 75 313	12 74 225	12 71 297	12 69 299	12.61 266	12 63 238	12.60 139
60 - 65	12 61 188	12 57 226	12 56 266	12 78 408	12 83 371	12 87 294	12 82 368	12 74 289	12 82 298	12 80 289	12 87 411	12 88 374	12 87 414	12 87 360	12 83 248	12 75 238	12 63 130	12 65 256	12 72 241	12 77 362	12 72 374	12 67 486	12 65 360	12 65 210

Table 57: Helium densities at 300 km and numbers of samples of averaged data tabulated by geomagnetic latitude and geomagnetic time for Kp range 0.0 to 1.3 for equinox.

$\text{Log}_{10}\ n(\text{He})\ m^{-3}$

EQUINOX

Kp = 0.0-1.3

Geomagnetic Latitude

Coefficient	60-65	65-70	70-75	75-80	80-85	85-90
A_0	12.747	12.758	12.726	12.705	12.753	12.712
A_1	-.106	-.130	-.059	-.024	-.011	-.032
B_1	.024	.015	-.009	-.034	-.054	-.037
A_2	-.005	-.032	.020	.016	-.006	-.020
B_2	-.017	-.006	.023	.027	-.033	-.040
A_3	-.036	-.006	-.004	.032	.032	-.012
B_3	-.063	-.024	.001	.016	-.002	-.003
A_4	.011	.001	.012	-.014	-.009	-.005
B_4	-.001	-.006	-.019	.008	-.002	-.004
A_5	.032	.022	.013	.007	-.007	.007
B_5	.023	-.003	.011	.008	-.004	-.020

Table 58: Fourier coefficients for helium densities at 300 km tabulated by geomagnetic latitude for Kp range 0.0 to 1.3 for equinox.

$$\text{Log}_{10}\ n(\text{He})m^{-3} = A_0 + \sum_{n=1}^{\infty} \left(A_n \cos \frac{2\pi nt}{T} + B_n \sin \frac{2\pi nt}{T}\right)$$

$Log_{10}\ n(he)\ m^{-3}$

EQUINOX

Kp = 1 3 - 4 0

Local Geomagnetic Time in Hours

Geomagnetic Latitude	1	2	3	4	5	6	7	8	9	10	11	12	13	14	15	16	17	18	19	20	21	22	23	24
85 - 90	12 58 54	12 52 44	12 58 44	12 68 41	12 69 51	12 68 38	12 69 58	12 71 57	12.69 67	12 65 51	12 79 39	12 38 11	12 58 36	12 68 34	12 72 43	12 72 49	12 67 62	12 72 82	12 71 72	12 74 62	12 70 66	12 68 2	12 73 79	12 69 67
80 - 85	12 62 178	12 55 190	12 57 156	12 66 181	12 62 185	12 65 219	12 75 173	12 78 174	12 72 227	12 69 181	12 66 146	12 64 151	12 71 171	12 63 215	12 68 316	12 72 373	12 77 362	12 76 319	12 72 270	12 72 251	12 o9 243	12 73 272	12 72 256	12 72 211
75 - 80	12 66 206	12 71 191	12 66 223	12 70 257	12 74 256	12 59 246	12 58 283	12 63 404	12 66 381	12 63 336	12 68 335	12 68 376	12 70 431	12 70 507	12 71 510	12 71 450	12 78 442	12 66 356	12 57 243	12 59 218	12 66 183	12 60 193	12 66 219	12 69 263
70 - 75	12.63 197	12 90 254	12 74 340	12 85 368	12 69 354	12 86 328	12 81 436	12 63 529	12 67 568	12 69 565	12 73 580	12 72 611	12 73 673	12 74 626	12 72 561	12 74 514	12 69 426	12 62 468	12 63 408	12 60 361	12 61 265	12 58 272	12 67 313	12 69 268
65 - 70	12 55 183	12 61 184	12 74 414	12 88 493	12 86 545	12 83 674	12 84 782	12 85 741	12 77 822	12 82 712	12 81 751	12 85 682	12 74 731	12 74 819	12 72 583	12 70 499	12 70 605	12 64 514	12 65 486	12 63 467	12 61 429	12 60 343	12 62 387	12 56 220
60 - 65	12 56 328	12 66 287	12 49 261	12 81 713	12 93 722	12 82 579	12 89 472	12 76 416	12 75 552	12 80 576	12 85 756	12 82 839	12 88 822	12 79 739	12 74 559	12 70 442	12 64 444	12 65 552	12 68 637	12 68 682	12 66 577	12 62 503	12 57 421	12 57 367

Table 59: Helium densities at 300 km and numbers of samples of averaged data tabulated by geomagnetic latitude and geomagnetic time for Kp range 1.3 to 4.0 for equinox.

$\text{Log}_{10}\ n(He)m^{-3}$

EQUINOX

Kp = 1.3-4.0

Coefficient	Geomagnetic Latitude 60-65	65-70	70-75	75-80	80-85	85-90
A_0	12.721	12.722	12.705	12.664	12.687	12.666
A_1	-.108	-.091	-.016	-.012	-.017	.003
B_1	.059	.088	.059	-.007	-.032	-.025
A_2	-.032	-.040	-.005	.011	-.026	-.048
B_2	-.009	.005	.062	.047	-.045	-.037
A_3	-.043	-.033	-.007	.008	.033	.030
B_3	-.050	-.018	-.006	.007	-.008	-.019
A_4	.025	0.000	.005	-.001	.011	-.016
B_4	-.001	-.027	.002	-.025	-.007	-.028
A_5	.015	-.002	-.020	-.004	-.002	.042
B_5	.018	-.012	.016	-.004	-.023	.006

Table 60: Fourier coefficients for helium densities at 300 km tabulated by geomagnetic latitude for Kp range 1.3 to 4.0 for equinox.

$$\text{Log}_{10}\ n(He)m^{-3} = A_0 + \sum_{n=1}^{\infty} \left(A_n \cos \frac{2\pi nt}{T} + B_n \sin \frac{2\pi nt}{T}\right)$$

$Log_{10}\ n(He)_m^{-3}$

EQUINOX

Kp > 4 0

Local Geomagnetic Time in Hours

Geomagnetic Latitude	1	2	3	4	5	6	7	8	9	10	11	12	13	14	15	16	17	18	19	20	21	22	23	24
85 - 90	0 0	12 35 1	12 33 3	0 0	0 0	0 0	0 0	13 49 3	13 65 2	12 73 2	0 0	12 64 1	0 0	0 0	0 0	0 0	12 71 2	0 0	0 0	0 0	0 0	12 61 4	0 0	12 61 4
80 - 85	12 78 1	12 36 4	12 61 4	12 49 6	12 50 7	12 54 8	12 55 9	12 58 7	12 44 10	12 59 4	12 41 9	12 72 17	13 16 9	12 34 3	12 68 27	12 69 15	12 81 21	12 70 20	12 55 10	12 89 15	12.98 17	12 71 20	12 69 10	12 64 9
75 - 80	12 67 3	12 57 1	12 45 1	12.32 6	12 33 2	12 33 4	12 41 15	12 32 3	12.50 7	12 62 16	12 67 10	12 37 13	12 56 35	12 53 10	12 82 23	12 99 35	12 81 25	12 50 12	12 56 1	12 58 8	12 34 10	12 60 3	12 39 5	12 47 4
70 - 75	12 36 14	12 38 10	12 29 3	12 32 1	12 26 2	12 80 25	12.55 35	12 56 24	12.49 11	12 59 33	12 71 4	12 59 25	12 58 18	12 73 20	12 77 52	12 97 45	12 34 5	12 36 7	12 57 2	12 57 14	12 68 28	12 64 29	12 34 14	12 56 23
65 - 70	12.46 16	12 43 12	12.37 22	12 40 10	12.53 7	12 92 42	12.89 58	12 80 43	12 41 22	12 59 32	12 58 23	12 52 33	12 63 71	12 60 43	12 79 74	12 46 38	12 32 20	12 32 11	12.32 1	12 51 13	12 47 29	12 68 18	12 38 20	12 49 27
60 - 65	0 0	0 0	0 0	12 36 4	13 33 43	13 10 43	13 32 35	12 67 13	12 74 14	12 69 40	12 65 28	12 71 90	12 70 113	12 84 39	12 93 84	12 42 31	12 50 65	12.59 32	12.84 29	12 56 33	12 48 60	12 56 42	12 57 31	12 46 40

Table 61: Helium densities at 300 km and numbers of samples of averaged data tabulated by geomagnetic latitude and geomagnetic time for Kp range > 4.0 for equinox.

$\text{Log}_{10}\ n(\text{He})_m^{-3}$

EQUINOX

Kp > 4.0

Geomagnetic Latitude

Coefficient	60-65	65-70	70-75	75-80	80-85	85-90
A_0	INSUFFICIENT DATA	12.535	12.540	12.530	12.644	INSUFFICIENT DATA
A_1		-.084	-.122	-.058	.024	
B_1		.092	-.073	-.134	-.130	
A_2		-.018	.009	.020	.033	
B_2		-.037	-.032	.071	-.030	
A_3		.045	.032	.083	-.027	
B_3		-.143	-.093	.068	-.051	
A_4		.001	-.041	-.040	.027	
B_4		.051	.009	-.037	.022	
A_5		-.029	-.012	-.009	-.062	
B_5		.069	.113	.083	-.003	

Table 62: Fourier coefficients for helium densities at 300 km tabulated by geomagnetic latitude for Kp range > 4.0 for equinox.

$$\text{Log}_{10}\ n(\text{He})m^{-3} = A_0 + \sum_{n=1}^{\infty} \left(A_n \cos \frac{2\pi nt}{T} + B_n \sin \frac{2\pi nt}{T}\right)$$

Log_{10} N(He) m^{-3}

WINTER

Kp = 0 0 - 1 3

Local Geomagnetic Time in Hours

Geomagnetic Latitude	1	2	3	4	5	6	7	8	9	10	11	12	13	14	15	16	17	18	19	20	21	22	23	24
85 - 90	12 48	12 66	12 63	12 81	12 62	12 70	12 59	12 51	12 58	12 59	12.58	12 69	12 70	12 78	12.74	12 71	12 76	12 69	12 71	12 63	12 66	12 60	12.48	12.36
	1	20	14	9	16	18	7	16	10	13	22	1	1	10	24	12	14	15	6	8	9	9	1	6
80 - 85	12 81	12 64	12.64	12 65	12 69	12 60	12.64	12 56	12 73	12 67	12 65	12 71	12 67	12 71	12.68	12 63	12 59	12 63	12.70	12 61	12.71	12 66	12 68	12 61
	24	48	63	69	62	51	46	32	54	60	28	21	60	69	71	61	57	15	77	29	59	23	28	8
75 - 80	12 55	12 67	12 68	12 63	12 56	12 62	12.61	12 61	12 60	12 65	12.73	12 73	12 75	12 74	12 71	12 74	12 73	12 60	12.60	12 63	12 64	12 51	12 59	12.73
	42	87	113	94	84	117	118	76	94	93	84	171	86	51	54	65	82	54	85	119	140	27	26	70
70 - 75	12 55	12 55	12 67	12 57	12 56	12 61	12 59	12 63	12 60	12 59	12 74	12 73	12 73	12 67	12 82	12 74	12 66	12.62	12 63	12 66	12 62	12 51	12 59	12 73
	42	27	142	41	89	118	116	91	89	92	101	201	79	45	60	76	89	79	90	99	127	27	26	41
65 - 70	12 57	12 52	12.68	12 62	12.68	12 60	12 60	12 61	12 67	12 71	12 62	12 74	12 70	12 68	12 64	12 61	12 51	12.65	12 64	12 50	12 68	12 57	12 60	12 63
	1	35	162	116	106	113	139	135	209	197	224	204	160	130	166	186	168	153	147	28	142	1	1	51
60 - 65	0	0	0	12 50	12 50	12.58	12.61	12 68	12 72	12 71	12 62	12 68	12 68	12 65	12 66	12 56	12.60	12 60	12 55	12 51	0	0	0	0
	0	0	0	32	63	194	262	209	234	311	283	270	222	147	253	201	161	113	35	31	0	0	0	0

Table 63: Helium densities at 300 km and numbers of samples of averaged data tabulated by geomagnetic latitude and geomagnetic time for Kp range 0.0 to 1.3 for winter.

$\text{Log}_{10}\ \bar{n}(\text{He})\text{m}^{-3}$

WINTER

Kp = 0.0-1.3

Geomagnetic Latitude

Coefficient	60-65	65-70	70-75	75-80	80-85	85-90
A_0	INSUFFICIENT DATA	12.626	12.639	12.648	12.662	12.635
A_1		-.041	-.059	-.054	.008	-.052
B_1		.013	-.039	-.024	-.003	-.040
A_2		.020	.016	.022	.035	-.060
B_2		000	.030	.042	.003	.064
A_3		-.026	.000	-.005	-.007	-.061
B_3		-.010	-.006	.005	.002	-.015
A_4		.001	.002	.000	-.002	-.027
B_4		-.008	.004	.001	.011	-.007
A_5	———	.017	.001	-.014	.022	-.015
B_5		-.019	.015	.009	.008	-.007

Table 64: Fourier coefficients for helium densities at 300 km tabulated by geomagnetic latitude for Kp range 0.0 to 1.3 for winter.

$$\text{Log}_{10}\ n(\text{He})\text{m}^{-3} = A_0 + \sum_{n=1}^{\infty} \left(A_n \cos \frac{2\pi nt}{T} + B_n \sin \frac{2\pi nt}{T}\right)$$

$\text{Log}_{10}\, n(He)m^{-3}$

WINTER

Kp = 1 3 - 4 0

Local Geomagnetic Time in Hours

Geomagnetic Latitude	1	2	3	4	5	6	7	8	9	10	11	12	13	14	15	16	17	18	19	20	21	22	23	24
85 - 90	12 55	12 50	12 58	12 51	12.53	12 59	12 52	12 52	12 57	12 75	12 61	12 60	12 84	12 75	12.78	12 71	12 65	12 74	12 68	12 59	12 59	12.64	12 67	12 53
	17	13	10	36	28	24	26	32	37	32	19	29	18	24	16	29	22	21	25	22	14	23	22	25
80 - 85	12 62	12 54	12 58	12 53	12 49	12 57	12 55	12 58	12 69	12 50	12 54	12 59	12 55	12 61	12 67	12 67	12 66	12.64	12 59	12 59	12 57	12.52	12 57	12 59
	101	108	129	130	119	85	86	67	92	96	78	105	139	123	109	107	43	100	109	129	120	71	90	111
75 - 80	12 61	12 57	12 58	12.55	12 63	12 63	12 58	12 70	12.70	12 65	12 67	12 55	12 69	12.67	12 61	12 62	12 58	12 60	12 55	12.58	12 62	12 59	12 56	12 62
	228	312	262	235	180	174	127	107	92	108	145	190	191	184	174	175	145	147	163	221	147	211	161	206
70 - 75	12 62	12 60	12 64	12 61	12 64	12 62	12 74	12 82	12 63	12 70	12 59	12 67	12 68	12 62	12 65	12 58	12 65	12 62	12 56	12 59	12 56	12 56	12 58	12.57
	1	251	287	233	176	221	222	253	208	161	247	185	228	234	161	158	251	196	195	222	180	137	178	155
65 - 70	12 71	12.88	12 62	12 58	12 51	12 62	12 68	12 82	12.72	12 65	12 64	12.68	12 68	12 67	12 65	12.58	12 58	12.56	12 59	12.62	12 59	12 55	12 63	12.56
	1	68	220	225	203	202	235	302	311	293	265	303	220	246	261	331	247	333	288	212	155	155	177	101
60 - 65	0	0	12 62	12 39	12 39	12 50	12 55	12 56	12 62	12 62	12.61	12 60	12 64	12 66	12 62	12.63	12 55	12 51	12 49	12 48	12 49	12 75	0	0
	0	0	38	85	282	254	267	379	492	367	367	410	323	387	384	475	342	211	100	59	41	114	0	0

Table 65: Helium densities at 300 km and numbers of samples of averaged data tabulated by geomagnetic latitude and geomagnetic time for Kp range 1.3 to 4.0 for winter.

$\text{Log}_{10}\, n\,(\text{He})\, m^{-3}$

WINTER

Kp = 1.3-4.0

Geomagnetic Latitude

Coefficient		60-65	65-70	70-75	75-80	80-85	85-90
A_0			12.641	12,629	12.613	12.584	12.626
A_1	INSUFFICIENT DATA		-.020	-.041	-.035	-.017	-.063
B_1			.040	.041	.015	-.036	-.082
A_2			.034	-.013	.009	-.009	.020
B_2			-.002	-.006	-.013	.014	.018
A_3			.027	.020	.016	.036	.001
B_3			.028	.001	-.006	.015	-.014
A_4			-.024	-.001	-.012	-.008	-.001
B_4			.066	.023	.008	.011	-.008
A_5			-.025	-.016	.013	.001	.024
B_5			.001	-.017	-.001	-.001	-.020

Table 66: Fourier coefficients for helium densities at 300 km tabulated by geomagnetic latitude for Kp range 1.3 to 4.0 for winter.

$$\text{Log}_{10}\, n(\text{He})m^{-3} = A_0 + \sum_{n=1}^{\infty} \left(A_n \cos \frac{2\pi nt}{T} + B_n \sin \frac{2\pi nt}{T}\right)$$

Log_{10} n(He) m^{-3}

WINTER

Kp > 4.0

Local Geomagnetic Time in Hours

Geomagnetic Latitude	1	2	3	4	5	6	7	8	9	10	11	12	13	14	15	16	17	18	19	20	21	22	23	24
85 - 90	12 30 7	0 0	0 0	12.75 1	0 0	0 0	0 0	0 0	0 0	0 0	12 69 1	0 0	0 0	12 29 1	0 0	12 65 2	0 0	12 73 1	0 0	0 0	0 0	0 0	0 0	0 0
80 - 85	12 37 8	0 0	0 0	0 0	0 0	12.70 5	12 91 5	12 92 4	12 84 13	12.76 3	12 58 4	12 58 4	0 0	12 91 6	12 66 14	0 0	12 57 11	12 47 9	12 52 7	12.81 8	12 60 7	12 67 4	12.97 7	12 76 4
75 - 80	12.82 45	0 0	0 0	0 0	12.51 10	12 54 3	12.50 1	12 52 6	12 69 23	12.89 11	12 95 6	12 35 4	12 57 20	12 56 8	12 52 27	12 49 19	12.41 7	12 33 7	12.71 16	12.84 31	12 49 13	12 91 22	12 62 23	12 79 25
70 - 75	0 0	12 98 27	12 88 20	12.41 19	12 64 29	12 69 16	12.69 12	12 76 10	12 87 27	12 80 28	12.79 24	12 27 1	12.75 30	12 61 21	12 60 31	12 62 21	12 75 19	12 67 31	12.64 7	12 98 14	12.80 18	12.94 20	0 0	0 0
65 - 70	12.63 1	12.77 10	13 01 14	12 53 20	12 63 1	12 72 12	12.78 16	12 69 27	12.97 27	12 50 41	12.73 26	12 85 33	12 57 40	12.64 21	12 61 19	12 69 36	12 59 13	12 63 25	12 87 27	12.30 1	12 86 8	12 68 1	12.68 1	12.49 17
60 - 65	0 0	0 0	12 65 17	12 45 16	12.52 12	12 32 3	12.48 17	12 69 24	12.79 67	12 52 44	12 77 73	12 85 36	12 64 20	12 64 26	12.77 31	12 65 35	12 66 8	12 56 1	12 46 3	0 0	0 0	0 0	0 0	0 0

Table 67: Helium densities at 300 km and numbers of samples of averaged data tabulated by geomagnetic latitude and geomagnetic time for Kp range > 4.0 for winter.

CHAPTER IV

SUMMARY AND CONCLUSIONS

4.1 Summary of the Structure and Variability of the Airglow Temperature and Densities of O, N_2 and He in the Polar Thermosphere

The 630 nm airglow temperatures have been shown to be much higher in summer than in winter and they are also much higher at high magnetic activity. The temperatures peak over the pole in winter and peak at lower latitudes in summer. Daily, there is a temperature maximum in the pre-midnight sector and minimum temperatures occur in the magnetic noon sector.

The atomic oxygen densities at 120 km have been shown to be higher in winter than summer and also show marked decreases with increased magnetic activity. The densities decrease with increasing latitude, the difference in densities between the pole and lower latitudes being greatest in summer and least at equinox. The densities are definitely low in the post midnight sector and high near magnetic noon.

The nitrogen "equivalent temperature" NT values have been shown to be higher in summer than in winter and to increase with magnetic activity. These values peak near the pole in winter with higher values occurring at lower latitudes in summer. The difference in NT values between the pole and lower latitudes is greater in winter than in summer. The values also appear to peak in the morning hours and in the pre-midnight sector.

The helium densities at 300 km show considerable variability in horizontal distribution which may be due, in part, to fewer observations. The densities peak at equinox and are low during high magnetic activity. There does not appear to be a persistent dependence of the density on latitude. The densities generally show a minimum in the post midnight sector hours and maxima during the magnetic noon and the pre-midnight sectors.

4.2 Physical Implications of the Results

With the concepts presented in Chapter I and observations discussed in Chapter III of the variations with magnetic time, qualitative discussion of possible physical causes of the observations may be made. It is convenient to discuss the magnetic local time dependence of the results as displayed in Figures 1 through 36.

The hours around magnetic noon are characterized by low temperatures, high atomic oxygen and helium densities and median NT values. The work of Nisbet and Glenar (1976) shows a possible energy input near the noon sector due to convergent winds. This convergence could explain the high densities. The temperatures are low due to low particle energy inputs in the noon sector.

The pre-midnight hours are characterized by high temperature, high He density, low NT values and median oxygen densities. Again there is an indication of thermospheric wind convergence in the high He densities. This convergence plus the auroral particle inputs and electric fields which exist at night could explain the high temperatures. The low NT values could be due to the thermospheric wind

convergence and Joule heating changing the temperature gradients around the 120 km altitude level.

The post midnight sector is characterized by low atomic oxygen and helium densities, median temperatures and high NT values. The low densities are due to divergence of the thermospheric wind field which requires upward diffusion of atomic oxygen in the region. The high NT values are presumably caused by the changes produced in the temperature profile by the divergence of the horizontal wind velocity at around 120 km.

It is apparent from the above discussion that the true state of the polar thermosphere is very different from that presented previously. For example, the model of Mayr and Volland (1974) shows upward vertical velocity everywhere over the pole. The results presented here indicate that the upward velocity is concentrated in the post magnetic midnight sector.

Maeda (1976) has modeled the neutral and ion drifts in the polar ionosphere under the influence of a convection electric field. His results agree with the observations of Brekke et al., (1974) for daytime, but not for nighttime. Maeda's model has not, however, shown the divergence of the winds which can influence the energy balance and distribution of all thermospheric constituents as shown by the results discussed in section 4.2.

Taeusch and Hinton (1975) have used the OGO-6 N_2 density measurements to imply a very different distribution of temperature than is shown in Chapter III. This difference is because the N_2

density is not a true indicator of temperature, i.e. high N_2 density does not necessarily imply a high temperature again because the effect of variations in the temperature gradients in the lower thermosphere on thermospheric densities were not taken into account.

Because the polar thermosphere has been shown to be more complex than has been shown previously it will take a more complex dynamical model to explain the detailed structure of energy and transport indicated by these observations.

4.3 Recommendations for Future Work

This study has also pointed out five areas which require further effort:

1) More data is required in order to get a more complete picture of the polar thermosphere. In particular more information is needed about molecular oxygen, helium and argon.
2) The measured airglow temperatures presented in this paper were not coincident in latitude and longitude with the measured densities. This circumstance complicates intercomparisons of these quantities on time scales which are shorter than those used in this study. Simultaneous measurements would be much more useful in this kind of analysis.
3) Direct 557.7 nm airglow measurements over the pole would be helpful in developing a better understanding of the behavior of atomic oxygen in the lower thermosphere if the effects of high energy particle input can be accounted for.

4) Theoretical models need to be developed which incorporate much more complicated vertical and longitudinal structure than has been incorporated to date.

5) This study has provided background measurements of temperatures and densities in the polar thermosphere. Atmospheric Explorer satellites now provide more accurate data and these should be used to study more constituents so that specific conditions of the polar thermosphere can be studied in detail. In particular individual magnetic storms should be studied based on the departures from the gross morphology presented in the present work.

REFERENCES

Agy, V., Geomagnetic coordinates and geomagnetic time, NBS Report No. 8789, 1965.

Bailey, G. J. and R. J. Moffett, The influence of vertical motions on the diurnal variations of temperature and density in the thermosphere, Planetary Space Sci., 20, 1085-1094, 1972.

Barlier, F., P. Bauer, C. Jaeck, G. Thullier and G. Kockarts, North-south asymmetries in the thermosphere during the last maximum of the solar cycle, J. Geophys. Res., 79, 5273-5285, 1974.

Blamont, J. E. and J. M. Luton, Geomagnetic effect on the neutral temperature of the F region during the magnetic storm of September 1969, J. Geophys. Res., 77, 3534-3556, 1972.

Blum, P. W. and I. Harris, Full non-linear treatment of the global thermospheric wind system-I Mathematical method and analysis of forces, J. Atmos. Terr. Phys., 37, 193-212, 1975a.

Blum, P. W. and I. Harris, Full non-linear treatment of the global thermospheric wind system-II Results and comparison with observation, J. Atmos. Terr. Phys., 37, 213-235, 1975b.

Blum, P. W. and I. Harris, The global wind system in the thermosphere, in: Rycroft, M. J. and Runcorn, S. K. (Eds.), Space Research XIII, Proceedings of the Fifteenth Plenary Meeting of COSPAR, Madrid, 1972, Volume 1, Akademia-Verlag, Berlin, 369-377, 1973.

Brekke, A., J. R. Doupnik and P. M. Banks, Observations of neutral winds in auroral E region during magnetospheric storm of August 3-9, 1972, J. Geophys. Res., 79, 2448-2456, 1974.

Burge, J. D., D. Eccles, J. W. King and R. Ruster, The effects of thermospheric winds on the ionosphere at low and middle latitudes during magnetic disturbances, J. Atmos. Terr. Phys., 35, 617-623, 1973.

Carignan, G. R., Thermospheric composition, Rev. of Geophys. Sp. Phys., 13, 885-887, 1975.

Carignan, G. R. and W. H. Pinkus, OGO-FØ4 experiment description, Technical Note 08041-31T, University of Michigan, Ann Arbor, Michigan, 1968.

Carignan, G. R. and C. A. Reber, The neutral atmosphere response to the large magnetic storm of 8 March, 1970, EOS, 52, 571, 1971.

Champion, K. S. W., Dynamics and structure of the quiet thermosphere, J. Atmos. Terr. Phys., 37, 915-926, 1975.

CIRA 1972, COSPAR International Reference Atmosphere, Akademie-Verlag, Berlin, 1972.

Cole, K. D., Energy deposition in the thermosphere caused by the solar wind, J. Atmos. Terr. Phys., 37, 939-949, 1975.

Creekmore, S. P., J. M. Strauss, R. M. Harris, B. K. Ching and Y. T. Chiu, A global model of thermospheric dynamics-I. Wind density fields derived from a phenomenological temperature, J. Atmos. Terr. Phys., 37, 491-515, 1975.

DeVries, L. L., Structure and motion of the thermosphere shown by density data from the low-G accelerometer calibration system (LOGACS), in: Bowhill, S. A., Jaffee, L. D. and Rycroft, M. J. (Eds.), Space Research XII, Proceedings of the Fourteenth Plenary Meeting of COSPAR, Seattle, Washington, U.S.A., 1971, Volume 2, Akademie-Verlag, Berlin, 867-879, 1972.

Donahue, T. M., B. Guenther and R. J. Thomas, Spatial and temporal behavior of atomic oxygen determined by OGO-6 airglow observations, J. Geophys. Res., 79, 1959-1964, 1974.

Forbes, J. M. and F. A. Marcos, Thermospheric density variations associated with auroral electrojet activity, J. Geophys. Res., 78, 3841-3847, 1973.

Hays, P. B., R. A. Jones and M. H. Rees, Auroral heating and the composition of the neutral atmosphere, Planetary Space Sci., 21, 559-573, 1973.

Hedin, A. E., H. G. Mayr, C. A. Reber, N. W. Spencer and G. R. Carignan, Empirical model of global thermospheric temperature and composition based on data from the OGO-6 quadrupole mass spectrometer, J. Geophys. Res., 79, 215-225, 1974.

Hedin, A. E. and C. A. Reber, Longitudinal variations of thermospheric composition indicating magnetic control of polar heat input, J. Geophys. Res., 77, 2871-2879, 1972.

Jacchia, L. G., Two atmospheric effects in the orbital acceleration of artificial satellites, Nature, 183, 526-627, 1959a.

Jacchia, L. G., Corpuscular radiation and the acceleration of artificial satellites, Nature, 183, 1662, 1959b.

Jacchia, L. G., Static diffusion models of the upper atmosphere with empirical temperature profiles, Smithsonian Astrophysical Observatory Special Report No. 170, 1964.

Jacchia, L. G., Static diffusion models of the upper atmosphere with empirical temperature profiles, Smithsonian Contrib. Astrophysical, 8, 215, 1965.

Jacchia, L. G., New static models of the thermosphere and exosphere with empirical temperature profiles, Smithsonian Astrophysical Observatory Special Report No. 313, 1970.

Jacchia, L. G., Revised static models of the thermosphere and exosphere with empirical temperature profiles, Smithsonian Astrophysical Observatory Special Report No. 332, 1971.

Jacchia, L. G., Variations in thermospheric composition: A model based on mass spectrometer and satellite drag data, J. Geophys. Res., 13, 1923-1927, 1974.

Johnson, F. S., Horizontal variations in thermospheric composition, Rev. of Geophys. Space Phys., 11, 741-754, 1973.

Johnson, F. S., Energy input to the lower thermosphere, J. Atmos. Terr. Phys., 36, 1707-1713, 1974.

Johnson, F. S. and B. Gottlieb, Atomic oxygen transport in the thermosphere, Planetary Space Sci., 21, 1001-1009, 1973.

Kasprzak, W. T. and G. P. Newton, Comparison of the San Marcos 3 Nace neutral composition data with the extrapolated OGO-6 empirical model, J. Geophys. Res., 81, 1404-1406, 1976.

Kohl, H. and J. W. King, Atmospheric winds between 100 and 700 km and their effects on the ionosphere, J. Atmos. Terr. Phys., 29, 1045-1062, 1967.

Maeda, H., Neutral winds and ion drifts in the polar ionosphere caused by convection electric fields-1, J. Atmos. Terr. Phys., 38, 197-205, 1976.

Mayr, H. G. and H. Volland, Magnetic storm effects in the neutral composition, Planetary Space Sci., 20, 379-393, 1972.

Mayr, H. G. and H. Volland, Magnetic storm characteristics of the thermosphere, J. Atmos. Terr. Phys., 36, 2025-2036, 1974.

Moffett, R. J., On the diurnal variations of total mass density, number density and temperature in the upper atmosphere, Planetary Space Sci., 21, 1457-1459, 1973.

Newton, G. P., Latitudinal dependence of the diurnal density variation, J. Geophys. Res., 75, 5510-5516, 1970.

Nicolet, M., Structure of the thermosphere, Planetary Space Sci., 5, 1-32, 1961.

Nisbet, J. S., Geomagnetic coordinates, Ionosphere Research Laboratory Internal Report No. 58, The Pennsylvania State University, University Park, Pennsylvania, 1976.

Nisbet, J. S., On the construction and use of a simple ionospheric model, Ionosphere Research Laboratory Scientific Report No. 355, The Pennsylvania State University, University Park, Pennsylvania, 1970.

Nisbet, J. S. and D. A. Glenar, Thermospheric meridional winds and atomic oxygen depletion at high latitudes, submitted to J. Geophys. Res., 1976.

Nisbet, J. S., B. J. Wydra, C. A. Reber and J. M. Luton, Global exospheric temperatures and densities under active solar conditions, Planetary Space Sci., 25, 59-69, 1977.

Philbrick, C. R., Satellite measurements of neutral atmospheric composition in the altitude range 150 to 450 km in: Rycroft, M. J. and Reasenberg, R. D. (Eds), Space Research XIV, Proceedings of the Sixteenth Plenary Meeting of COSPAR, Constance, F.R.G., 1973, 151-155, 1974.

Prölss, G. W. and U. von Zahn, Large and small scale changes in the disturbed upper atmosphere, J. Atmos. Terr. Phys., 38, 655-659, 1976.

Reber, C. A., D. N. Harpold, R. Horowitz and A. E. Hedin, Horizontal distribution of helium in the earth's upper atmosphere, J. Geophys. Res., 76, 1845-1848, 1971.

Reber, C. A. and P. B. Hays, Thermospheric wind effects on the distribution of helium and argon in the earth's upper atmosphere, J. Geophys. Res., 78, 2977-2991, 1973.

Reber, C. A. and A. E. Hedin, Heating of the high-latitude thermosphere during magnetically quiet periods, J. Geophys. Res., 79, 2457-2461, 1974.

Reber, C. A., A. E. Hedin and S. Chandra, Equatorial phenomena in neutral thermospheric composition, J. Atmos. Terr. Phys., 35, 1223-1228, 1973.

Rishbeth, H., Structure of the F region and global thermospheric winds, in: Verniani, F. (Ed.), Developments in Atmospheric Science 1, Structure and Dynamics of the Upper Atmosphere, 435-479, 1974.

Roemer, M., Geomagnetic activity effect on atmospheric density in the 250 to 800 km altitude region, in: Kondratyev, K. Ya, Rycroft, M. J. and Sagan, C. (Eds.), Space Research XI, Proceedings of the Thirteenth Plenary Meeting of COSPAR, Leningrad, 1970, 2, 965-974, 1971.

Strauss, J. M., S. P. Creekmore, R. M. Harris, B. K. Ching and Y. T. Chiu, A global model of thermospheric dynamics-II. Wind, density and temperature fields generated by EUV heating, J. Atmos. Terr. Phys., 37, 1245-1253, 1975.

Taeusch, D. R., G. R. Carignan and C. A. Reber, Neutral composition variation above 400 kilometers during a magnetic storm, J. Geophys. Res., 76, 8318-8325, 1971.

Taeusch, D. R. and B. B. Hinton, Structure of electrodynamic and particle heating in the undisturbed polar thermosphere, J. Geophys. Res., 80, 4346-4350, 1975.

Thuillier, G., J. L. Falin and C. Wachtel, Experimental global model of the exospheric temperature based on measurements from the Fabry-Perot interferometer on board the OGO-6 satellite, in Program/Abstracts of Nineteenth Plenary Meeting of COSPAR, Philadelphia, Pennsylvania, 250, 1976.

Truttse, Ye. L., Upper atmosphere during geomagnetic disturbances III. Some regularities in density variations, Planetary Space Sci., 17, 181-187, 1969.

von Zahn, U., Composition studies in the thermosphere by means of mass spectrometers, in: Verniani, F. (Ed.), Developments in Atmospheric Science 1, Structure and Dynamics of the Upper Atmosphere, 435-479, 1974.

Wydra, B. J., Global exospheric temperatures and densities under active solar conditions, Ionosphere Research Laboratory Scientific Report No. 436, The Pennsylvania State University, University Park, Pennsylvania, 1975.

Zimmerman, S. P. and T. J. Keneshea, The thermosphere in motion, J. Geophys. Res., 81, 3187-3197, 1976.

Gardner, Larry J , Densities and Temperatures in the Polar Thermosphere, The Ionosphere Research Laboratory, Electrical Engineering East University Park, Pennsylvania, 16802, 1977

PSU-IRL-SCI-455

Classification Numbers

1 9 3 Heterosphere

The importance of the polar thermosphere has been well documented For the first time, data from the OGO-6 satellite has made it possible to separate a number of temperature effects from those based on density and thus the morphology of the high-latitude thermosphere can be studied in some detail Specifically the atomic oxygen density at 120 km, the 630 nm airglow temperature the helium density at 300 km and the molecular nitrogen density near 400 km have been examined as functions of geomagnetic latitude, geomagnetic time, season and magnetic activity level The long-term averages of these quantities have been examined so as to provide a baseline of these thermospheric parameters from which future studies may be made for comparison

The hours around magnetic noon are characterized by low temperatures high O and He densities, and median nitrogen densities The pre-midnight hours exhibit high temperatures, high He density, low nitrogen density and median O densities The post-midnight sector shows low O and He densities median temperatures and high nitrogen densities These results are compared to recent models and observations and are discussed with respect to their causes due to divergence of the wind field and energy deposition in the thermosphere

Gardner, Larry J , Densities and Temperatures in the Polar Thermosphere The Ionosphere Research Laboratory, Electrical Engineering East University Park, Pennsylvania, 16802, 1977

PSU-IRL-SCI-455

Classification Numbers

1 9 3 Heterosphere

The importance of the polar thermosphere has been well documented For the first time, data from the OGO-6 satellite has made it possible to separate a number of temperature effects from those based on density and thus the morphology of the high-latitude thermosphere can be studied in some detail Specifically, the atomic oxygen density at 120 km, the 630 nm airglow temperature, the helium density at 300 km and the molecular nitrogen density near 400 km have been examined as functions of geomagnetic latitude, geomagnetic time, season and magnetic activity level The long-term averages of these quantities have been examined so as to provide a baseline of these thermospheric parameters from which future studies may be made for comparison

The hours around magnetic noon are characterized by low temperatures, high O and He densities, and median nitrogen densities The pre-midnight hours exhibit high temperatures, high He density, low nitrogen density and median O densities The post-midnight sector shows low O and He densities, median temperatures and high nitrogen densities These results are compared to recent models and observations and are discussed with respect to their causes due to divergence of the wind field and energy deposition in the thermosphere

Gardner, Larry J , Densities and Temperatures in the Polar Thermosphere The Ionosphere Research Laboratory, Electrical Engineering East University Park, Pennsylvania, 16802 1977

PSU-IRL-SCI-455

Classification Numbers

1 9 3 Heterosphere

The importance of the polar thermosphere has been well documented For the first time, data from the OGO-6 satellite has made it possible to separate a number of temperature effects from those based on density and thus the morphology of the high-latitude thermosphere can be studied in some detail Specifically the atomic oxygen density at 120 km the 630 nm airglow temperature the helium density at 300 km and the molecular nitrogen density near 400 km have been examined as functions of geomagnetic latitude, geomagnetic time, season and magnetic activity level The long-term averages of these quantities have been examined so as to provide a baseline of these thermospheric parameters from which future studies may be made for comparison

The hours around magnetic noon are characterized by low temperatures high O and He densities, and median nitrogen densities The pre-midnight hours exhibit high temperatures, high He density, low nitrogen density and median O densities The post-midnight sector shows low O and He densities median temperatures and high nitrogen densities These results are compared to recent models and observations and are discussed with respect to their causes due to divergence of the wind field and energy deposition in the thermosphere

Gardner, Larry J , Densities and Temperatures in the Polar Thermosphere The Ionosphere Research Laboratory, Electrical Engineering East, University Park, Pennsylvania, 16802 1977

PSU-IRL-SCI-455

Classification Numbers

1 9 3 Heterosphere

The importance of the polar thermosphere has been well documented For the first time, data from the OGO-6 satellite has made it possible to separate a number of temperature effects from those based on density and thus the morphology of the high-latitude thermosphere can be studied in some detail Specifically, the atomic oxygen density at 120 km, the 630 nm airglow temperature the helium density at 300 km and the molecular nitrogen density near 400 km have been examined as functions of geomagnetic latitude geomagnetic time, season and magnetic activity level The long-term averages of these quantities have been examined so as to provide a baseline of these thermospheric parameters from which future studies may be made for comparison

The hours around magnetic noon are characterized by low temperatures, high O and He densities, and median nitrogen densities The pre-midnight hours exhibit high temperatures, high He density, low nitrogen density and median O densities The post-midnight sector shows low O and He densities median temperatures and high nitrogen densities These results are compared to recent models and observations and are discussed with respect to their causes due to divergence of the wind field and energy deposition in the thermosphere

Gardner, Larry J , Densities and Temperatures in the Polar Thermosphere, The Ionosphere Research Laboratory, Electrical Engineering East University Park, Pennsylvania, 16802, 1977

PSU-IRL-SCI-455

Classification Numbers

1 9 3 Heterosphere

The importance of the polar thermosphere has been well documented For the first time, data from the OGO-6 satellite has made it possible to separate a number of temperature effects from those based on density and thus the morphology of the high-latitude thermosphere can be studied in some detail Specifically the atomic oxygen density at 120 km the 630 nm airglow temperature the helium density at 300 km and the molecular nitrogen density near 400 km have been examined as functions of geomagnetic latitude, geomagnetic time, season and magnetic activity level The long-term averages of these quantities have been examined so as to provide a baseline of these thermospheric parameters from which future studies may be made for comparison

The hours around magnetic noon are characterized by low temperatures high O and He densities, and median nitrogen densities The pre-midnight hours exhibit high temperatures, high He density, low nitrogen density and median O densities The post-midnight sector shows low O and He densities median temperatures and high nitrogen densities These results are compared to recent models and observations and are discussed with respect to their causes due to divergence of the wind field and energy deposition in the thermosphere

Gardner, Larry J , Densities and Temperatures in the Polar Thermosphere The Ionosphere Research Laboratory, Electrical Engineering East University Park, Pennsylvania, 16802, 1977

PSU-IRL-SCI-455

Classification Numbers

1 9 3 Heterosphere

The importance of the polar thermosphere has been well documented For the first time, data from the OGO-6 satellite has made it possible to separate a number of temperature effects from those based on density and thus the morphology of the high-latitude thermosphere can be studied in some detail Specifically, the atomic oxygen density at 120 km, the 630 nm airglow temperature the helium density at 300 km and the molecular nitrogen density near 400 km have been examined as functions of geomagnetic latitude geomagnetic time, season and magnetic activity level The long-term averages of these quantities have been examined so as to provide a baseline of these thermospheric parameters from which future studies may be made for comparison

The hours around magnetic noon are characterized by low temperatures, high O and He densities, and median nitrogen densities The pre-midnight hours exhibit high temperatures, high He density, low nitrogen density and median O densities The post-midnight sector shows low O and He densities, median temperatures and high nitrogen densities These results are compared to recent models and observations and are discussed with respect to their causes due to divergence of the wind field and energy deposition in the thermosphere

Gardner, Larry J Densities and Temperatures in the Polar Thermosphere, The Ionosphere Research Laboratory, Electrical Engineering East University Park, Pennsylvania, 16802 1977

PSU-IRL-SCI-455

Classification Numbers

1 9 3 Heterosphere

The importance of the polar thermosphere has been well documented For the first time data from the OGO-6 satellite has made it possible to separate a number of temperature effects from those based on density and thus the morphology of the high-latitude thermosphere can be studied in some detail Specifically, the atomic oxygen density at 120 km the 630 nm airglow temperature the helium density at 300 km and the molecular nitrogen density near 400 km have been examined as functions of geomagnetic latitude, geomagnetic time, season and magnetic activity level The long-term averages of these quantities have been examined so as to provide a baseline of these thermospheric parameters from which future studies may be made for comparison

The hours around magnetic noon are characterized by low temperatures high O and He densities, and median nitrogen densities The pre-midnight hours exhibit high temperatures, high He density, low nitrogen density and median O densities The post-midnight sector shows low O and He densities, median temperatures and high nitrogen densities These results are compared to recent models and observations and are discussed with respect to their causes due to divergence of the wind field and energy deposition in the thermosphere

Gardner, Larry J , Densities and Temperatures in the Polar Thermosphere The Ionosphere Research Laboratory, Electrical Engineering East, University Park, Pennsylvania, 16802, 1977

PSU-IRL-SCI-455

Classification Numbers

1 9 3 Heterosphere

The importance of the polar thermosphere has been well documented For the first time, data from the OGO-6 satellite has made it possible to separate a number of temperature effects from those based on density and thus the morphology of the high-latitude thermosphere can be studied in some detail Specifically, the atomic oxygen density at 120 km, the 630 nm airglow temperature the helium density at 300 km and the molecular nitrogen density near 400 km have been examined as functions of geomagnetic latitude geomagnetic time, season and magnetic activity level The long-term averages of these quantities have been examined so as to provide a baseline of these thermospheric parameters from which future studies may be made for comparison

The hours around magnetic noon are characterized by low temperatures, high O and He densities, and median nitrogen densities The pre-midnight hours exhibit high temperatures, high He density, low nitrogen density and median O densities The post-midnight sector shows low O and He densities median temperatures and high nitrogen densities These results are compared to recent models and observations and are discussed with respect to their causes due to divergence of the wind field and energy deposition in the thermosphere